DISLOCATIONS IN SOLIDS, VOLUME 15

J. Hirth and L. Kubin Eds.

Dislocations in Minerals (2.10.2009)

David J. Barber
Physics Centre, University of Essex, Colchester CO4 3SQ and Wolfson Centre for Materials Processing, Brunel University, Uxbridge, Middlesex UB8 3PH, U.K.

Hans-Rudolf Wenk
Department of Earth and Planetary Science, University of California, Berkeley CA 94720, USA

Greg Hirth
Department of Geological Sciences, Brown University, Providence RI 02912, USA

David L. Kohlstedt
Department of Geology and Geophysics, University of Minnesota, Minneapolis MN 55455, USA

Abstract

Dislocations in minerals have a long history: The first images of dislocations ever seen were obtained by Seidentopf in 1905 on rocksalt (halite) with an optical microscope. Since then, and particularly after the development of ion thinning techniques in the early nineteen sixties, dislocations in minerals have been studied in great detail by transmission electron microscopy. While diffraction contrast images of dislocations are similar in metals and minerals, the structures of most minerals are very complex and of low symmetry, which leads to their having a great variety of slip systems that change with temperature-pressure-strain rate conditions. Thus the identification of dislocations in rock-forming minerals and the analysis of their characteristics can be used to infer geological conditions during deformation. Recently much emphasis has been placed on the nature of dislocations in high pressure phases that occur deep in the Earth. Here findings from transmission electron microscopy are combined with atomic scale modeling. This chapter provides an overview of early and modern work on dislocations in minerals and discusses applications to different mineral groups and their geologic significance.

Contents

1. Introduction

Minerals are naturally occurring, macroscopically homogeneous chemical compounds with a regular crystal structure that form by a geological process. There are over 4000 different mineral species. In about 100 of these dislocation structures have been studied in some detail. Minerals compose rocks. They also are synthesized for industrial applications. Dislocations and microstructures constitute a record of the various processes that formed and modified rocks and other geological materials. Study of the constituent minerals by geologists can constrain the conditions that have been experienced, e.g. pressure, temperature, stresses. Understanding the rheology of crustal rocks is dependent on knowledge of the deformation behavior of their minerals. Correspondingly, the rheology of the zones in the mantle is strongly dependent on the plasticity of the high pressure minerals in them [1, 2]. In both cases the chemical environment (especially water content) has an important influence on deformation behaviour and anisotropy, e.g. fabric development.

Owing to space limitations, what follows is not a comprehensive review of what is known about dislocations in minerals; we are obliged to be selective and to feature mainly highlights. We also assume that readers will consult suitable texts concerning both the theory of dislocations (e.g. [3], [4] for a more advanced treatment) and their characterization (e.g. [5], [6]).

The strain and contrast associated with large numbers of dislocations causes tell-tale broadening of X-ray diffraction peaks (see section 5 in [7]) but techniques of much greater resolution are needed to image dislocations and microstructures directly. Probably the first images of dislocations ever obtained were from a geological material - the mineral, halite (NaCl). These were obtained in 1905 when Seidentopf [8] examined naturally-coloured rocksalt with an optical microscope. His observations (of dislocations decorated with sodium metal) pre-dated the theoretical concept of a dislocation in an elastic medium [9] and the ideas that dislocations might play an important role in plastic deformation [10, 11, 12, 13]. Thus the significance of Seidentopf's results was not recognized. Much later, Rexer [14] inadvertently decorated dislocation lines in rocksalt crystals with colloidal sodium. His work gave rise to the decoration methods used successfully to study dislocation behaviour in alkali halides [15, 16]). Fig. 1a shows an extensive decorated network. Decoration methods are of limited value in revealing dislocation microstructures, however, because a thermal treatment is usually required and this causes recovery. Exceptions are the print-out effect in silver halides [17], the first direct observation of dislocations where they were properly identified, and olivine [18, 19, 20]. Olivine requires heat for the dislocations to become decorated but apparently at temperatures and times for which climb (see section 2.4) is minimal. For an excellent report of early work on dislocations in many materials, including some minerals, see Amelinckx [5].

Growth twins in minerals, e.g. in calcite, have been known for centuries; observation of mechanical twinning also has a long history. But the dislocations often associated with both types of twinning remained undiscovered. The link between twinning and dislocations only emerged in the 1950s, after thin metal foils were first examined in the transmission electron microscope (TEM) by Hirsch et al. [21] and Bollmann [22]. Thereafter the association was found in minerals that are well known for their twinning, like calcite (e.g. [23]).

Although results from TEM studies on metals forged ahead of those from minerals prior to the widespread adoption of the ion-milling method [24, 25], mineral crystals played key roles in earlier work. For example Griffin [26] recognized groups of monomolecular surface steps on beryl crystals as indicative of the emergence of screw dislocations (Fig. 1b). Some 20 years earlier, Honess [27] described various surface features that we now recognize as associated with

dislocations, e.g. tails or "beaks" extending from etch pits into the interiors of many mineral crystals (caused by dissolution following impurity atmospheres or decorating particles along dislocations). Dislocations in minerals can be preserved and locked against movement through geological times by the pinning of impurities or the segregation of a second phase [28]. In general new dislocations must be nucleated for plastic deformation to proceed.

The study of dislocations by etch pitting was useful in early studies of plastic deformation. One of the best illustrations is the work of Gilman and Johnston [29] on synthetic lithium fluoride. Successful etch-pitting reagents were also devised for other minerals, such as halite [30] and olivine [31], but by then X-ray topography [32] and TEM had emerged as preferable techniques because of their potential for obtaining images capable of providing 3-D information.

The first TEM studies of defects in minerals were mostly carried out on layer-structured crystals that could easily be cleaved to electron transparent thicknesses. These included mica [33], graphite [34], molybdenite [35, 36] and talc [37]. The study of dislocation networks in talc [38] is an early milestone in dislocation analysis. Thereafter, the ion-milling method (and, more recently, the FIB (focused ion beam) technique) made it possible to investigate dislocations and other defects in a wide range of minerals, crustal rocks and extraterrestrial materials.

The lunar samples returned by the Apollo 11 mission first demonstrated the value of ion-milling in TEM investigations of minerals. The resulting investigations helped convince geologists of the importance of detailed studies of microstructures and dislocations for the interpretation of the deformational and thermal history of geological materials. Various studies on lunar rock specimens (e.g. [39], [40], [41], [42]) made geologists, who already used SEM and EPMA, suddenly aware of the power of the TEM to analyse mineral microstructures, cosmic ray tracks, etc., leading to the acquisition of ion-milling equipment and TEMs by numerous laboratories. There followed a very active period during which many TEM papers were published detailing the relationships between microstructures, macroscopic properties and mineral behaviour. Although much progress was made [6], the boom in such studies was soon over and today only a few earth science laboratories work with the TEM, perhaps a reflection of the time-consuming nature of specimen preparation and the rigorous analytical approach required. There remains some interest in high-resolution imaging (HRTEM). Although the latter supplies valuable information about stacking disorder, grain boundary structure, polytypism and phase transformations [43], it seldom informs about dislocation behaviour.

2. Dislocation microstructures in different environments:

2.1 Dislocations and other defects introduced during growth and crystallization

Minerals form by various processes, embracing a wide range of temperatures. Those of sedimentary and low temperature (LT) origin tend to start as poorly crystalline and often disordered solids. Unsurprisingly, dislocations are not usually observed in minerals in this state (e.g. geologically young dolomites). More equilibrated LT minerals such as clays often show stacking defects but in general are not noted for significant numbers of dislocations. However, ancient calcian dolomites and other rhombohedral carbonates that exhibit compositional fluctuations producing lattice strain often contain collections of dislocations.

Minerals grains formed at higher temperatures (HT) by crystallization from melts, by phase transformations, or by reactions, generally contain "grown in" dislocations. The densities of such dislocations are typically low to moderate (i.e. below about 10^4 cm^{-2}), unless special factors apply. Recrystallized grains are often dislocation-free. Most HT minerals have cooled over

geologic times, enabling equilibration, which favours low dislocation densities in the absence of subsequent deformation. An additional source of dislocations in any mineral that has cooled very rapidly can be the collapse of the lattice around clusters of point defects, especially vacancies.

Many minerals have ordered structures and they may exist in both ordered and disordered states. Ordering can occur when two different atomic species A and B utilize the same lattice sites and order is achieved when the two types of atoms occupy alternate adjacent sites, i.e. ABABABA. Typically at high temperatures the site occupancy is random; ordering commences as the mineral cools. Because the ordering usually starts at many places simultaneously antiphase boundaries frequently occur where ordered domains impinge, e.g. ABABA|ABABA (e.g. p.211 in [44]). Igneous rocks generally contain ordered minerals, whereas unmetamorphosed sedimentary rocks tend to contain disordered minerals. Generally speaking, order-disorder transitions do not appear to cause changes in the numbers of dislocations. Ordered structures, however, allow for a new type of dislocation, a superdislocation, which is a line defect of the both the A and B sublattices. Superdislocations in some structures are able to dissociate into super-partials.

An antiphase boundary is a type of stacking fault. Stacking faults also occur in materials that do not order, the simplest example being a fault in the normal close-packed layering in face-centred cubic metals, like copper, represented by CABCAB|ABCABC. Stacking faults, formed during crystal growth or as a result of deformation (slip), are bounded by partial dislocations.

2.2 Deformation, slip, slip system analysis, Burgers vector

Deformation is the main source of dislocations in rocks and minerals, although what is observed may have been modified subsequently. If the original deformation is brittle in nature there will be much cataclasis, but this may also generates dislocation because of the high stresses present at advancing crack tips. The detailed analysis of such cataclastic materials can be difficult even if subsequent annealing has occurred. Laboratory deformation of single crystal minerals has often been used to elucidate slip systems. The results must be applied with care when interpreting natural rock deformation because normally this has taken place at strain rates several orders of magnitude below those obtainable experimentally. Other considerations apply when interpreting natural shock deformation but here too laboratory experiments have played a useful role. Shock deformation effects in terrestrial and meteoritic minerals have been reviewed [45, 46].

Plastic deformation creates many dislocations, possibly accompanied by effects such as twinning and kinking, grain boundary sliding and competition from climb (see below). The first two processes can themselves add to the production of dislocations. Depending on the symmetry of the mineral, slip may proceed on one or on several planes. The slip planes in simple structures are close-packed planes or, in more complex structures, planes for which the breaking of bonds is relatively easy and/or does not bring oppositely charged ions into closer proximity. The choice of slip direction is also governed by several structural considerations. In any case, too much energy is required for slip to occur simultaneously over a large area of slip plane and so instantaneously the slip is of limited extent - the boundary between slipped and unslipped material defines a dislocation in the atomic structure [44]. Slip occurs incrementally by the glide of dislocations across the slip planes. The motion of a dislocation out of its original slip plane can occur either by cross-slip onto an intersecting slip plane (provided there is a common slip direction) or by climb (if the diffusion of point defects is possible). Dislocations are typically

curved, not straight, expanding from a small source under the action of applied stress. Where a dislocation is perpendicular to the direction of slip it is said to have edge character, where it is parallel it is screw-like (see, e.g. [3] for an explanation); where it is neither, the dislocation is of mixed character. A slip system is specified in terms of a slip plane {hkl} and either a slip direction <uvw> or the associated Burgers vector, if it is known. Table 1 lists the slip data for many important minerals and they will be discussed in later sections.

A dislocation is characterized by its Burgers vector, **b**. This is a measure of the local displacement of the lattice after a dislocation has passed through it. The Burgers vector is a translation vector of the unit cell. It determines whether, or how, a dislocation will interact with other dislocations. To analyse microstructures, to understand how they have formed and how they relate to macroscopic properties like texture, strength, etc., it is crucial to have complete information about dislocations (and other defects), slip systems and Burgers vectors. Diffraction methods enable dislocations to be imaged, their properties identified and their Burgers vectors determined. X-ray topography and TEM are both suitable for this work; by comparing the visibility of dislocations in images recorded using several Bragg reflections in turn, one can ascertain Burgers vectors. TEM is the more widely applicable diffraction contrast method [47]: the conditions $\mathbf{g}.\mathbf{b} = 0$ and $\mathbf{g}.\mathbf{b} \times \mathbf{u} = 0$, where **g** is the diffraction vector and **u** is the direction of the dislocation, apply when a dislocation becomes invisible. Fig. 2 shows darkfield images of quartz with some dislocations in and out of contrast, depending on which **g** is used [48]. Analysing dislocation strain fields by this method is dependent upon setting up "two beam conditions" for imaging. This requires that there is only one strong electron reflection (only one reciprocal lattice vector **g** operating). Achieving and/or recognizing out-of-contrast conditions for a dislocation in a mineral is often not straightforward because i) anisotropy in elastic properties may forbid complete invisibility and give residual contrast; ii) crystal symmetry considerations can make it impossible to achieve two-beam conditions in certain crystal orientations with respect to the electron beam; iii) radiation damage may decorate dislocations and this effect will be seen even when the dislocation's strain field does not interact with the electron beam (Fig. 2b) . Less widely used TEM technique for characterizing Burgers vectors without any *a priori* assumptions are Large Angle Convergent Beam Electron Diffraction (LACBED), as first demonstrated by Carpenter and Spence [49] and Ishida fringes [6].

The characteristics of stacking faults and other defects can also be found using both diffraction contrast [6] and convergent beam techniques [50]. Simple stacking faults and other, more complex, planar faults commonly occur as a result of slip in minerals. Because the strain energy of a dislocation is proportional to $|\mathbf{b}|^2$, it can be energetically favourable for a dislocation to dissociate into two partials, $\mathbf{b}_1$ and $\mathbf{b}_2$, separated by a ribbon of stacking fault. Dissociation is favoured in minerals where cations in identical sites have large separations. Fig. 3a illustrates this behavior in experimentally deformed dolomite slipping on the basal plane, according to

$\frac{1}{3}\langle 2\bar{1}\bar{1}0\rangle \rightarrow \frac{1}{3}\langle 1\bar{1}00\rangle + \frac{1}{3}\langle 10\bar{1}0\rangle$.

In addition to slip, mechanical twinning may occur as a deformation mechanism. Twin boundaries are often decorated with dislocations to relieve local strain (Fig. 3b).

2.3 Hardening

Much less is known about the hardening of minerals caused by plastic deformation than is the case for metals and alloys [51]. This is attributable to i) the long-standing importance of understanding and optimizing the mechanical properties of metals, ii) the poorly known and complex geological settings and conditions that pertained when rocks were deformed, and iii) the

comparatively few laboratory studies of mineral deformation. Nonetheless, we know from the stress-strain curves of minerals and rocks plastically deformed at low-to-moderate temperatures to moderate strains that the effect of strain is to increase resistance to further deformation, i.e. to strengthen and harden the material. This hardening is largely due to a) increased dislocation densities, formation of tangles of dislocations, etc., making the passage of newly nucleated dislocations more difficult and b) a lack of activatable slip planes and slip systems. In the more ductile minerals strained to a few percent, cellular dislocation microstructures can develop that are similar to those seen in the stage III work hardening of metals (see p.167 and figs. 11b, 12b in [52]). Thus there are similarities in behaviour, so mineralogists and geologists can look to the large literature on metals for help in understanding the microscopic behaviour of minerals and rocks. Complications arise with minerals, however, because of the inability of many minerals to conform to the von Mises [53] criterion because of a symmetry-related lack of slip systems and hence their tendency to fracture. Nicolas and Poirier [54] give a good description of various hardening mechanisms and the role of climb and other processes in softening minerals, together with a discussion on how dislocation substructures relate to applied stress. Note that flow laws and hardening behaviour have been quantified for only a few minerals.

2.4 Climb and recovery

Below temperatures where point defects are mobile, an edge dislocation and a mixed dislocation with an edge component are unable to move out of their glide planes (screws have no glide plane and so are not similarly confined). Interactions are therefore limited, being restricted to dislocations in a given glide plane unless a process like cross-slip is possible. But if point defects are mobile they can interact with a dislocation and gradually change its position: edges may move out of their glide plane; screws may become helices. Such effects are manifestations of a process called climb. Climb is the rearrangement and interaction of dislocations to reduce the stored elastic energy – i.e. it is partial equilibration. Climb only occurs at temperatures above $\sim 0.5T_m$, where T_m is the melting point in degrees Kelvin. Climb is only possible if all the relevant point defect species are mobile.

Annealing allows high energy configurations of dislocations created by deformation to reduce their energies – by mutual annihilation, reactions and climb. The dislocation density is reduced but all the dislocations are not eliminated; many will persist in the form of networks and other types of low energy sub-boundaries dislocation arrays. Fig. 4a) illustrates the effect of climb in quartz.

2.5 Recrystallization

Recrystallization implies that a crystal or an existing grain structure is replaced with another. It is a solid state process, driven by a need to reduce energy stored in the assembly and so it can proceed by more than one mechanism. The strain energy is directly proportional to the dislocation density [55, 56]. Recrystallization occurs during diagenesis and metamorphism (a reduction of chemical free energy). The replacement of heavily deformed grains by new undeformed grains of the same type (giving a reduction of strain energy) is also known as recrystallization - short for strain-induced recrystallization. This process is a more drastic equilibration than can be achieved by climb. A wave of atomic rearrangement passes systematically through each heavily deformed grain, sweeping out any dislocations and generally leaving most grains free of dislocations and other extensive defects. Where a completely new grain structure is formed the grain boundaries are almost all high angle (>10°).

Static recrystallization is triggered when a heavily strained material is rapidly raised to a critical temperature. New dislocation-free grains are nucleated and swiftly grow by consuming heavily deformed material until they impinge on their neighbours. The resulting grainsize depends on the relative successes of the two competing mechanisms, nucleation and growth. The equilibration to a new grain structure is catastrophic and primary recrystallization, the initial stage of generating the new grain structure, is complete within seconds if all the material is at the same temperature. Grain growth and secondary recrystallization take the form of some grain enlargement at the expense of much smaller grains, thus reducing total grain boundary area (and energy), together with some grain boundary flattening, equilibration at triple junctions, etc.

Although massive submicroscopic rearrangement has occurred, the macroscopic process described above is called static recrystallization, to distinguish it from dynamic recrystallization. The latter occurs while a material is under stress and being deformed at an elevated temperature, one such that point defects are mobile and usually other stress-reducing mechanisms are also active (e.g. cross-slip, grain boundary sliding). Dynamic recrystallization causes some softening to mitigate the effects of the hardening that usually accompanies plastic deformation. It does so by providing new grains with relatively low defect densities [54]. In metals, these are often elongate in the direction of the macroscopic deformation [57]; the same effect is seen in ductile minerals, e.g. halite and calcitic marbles. Fig. 4b illustrates nucleation in regions of high dislocation densities in quartz [58]. The degree of softening during dynamic recrystallization is dependent on the strain rate and other factors because the new grains deform and acquire dislocations as they grow (e.g. see the case of olivine: [59, 60]).

2.5 Preferred Orientation

The macroscopic effects of the processes of pervasive deformation (and recrystallization) are the development of anisotropy in properties, due to preferred orientation or texture. Clearly texture development is closely linked to movement of dislocations on slip planes and Taylor [61] introduced the first comprehensive theory to model texture development by slip that is still widely used. Interestingly there is no mention of dislocations or slip systems in Sander's [62] famous treatise on fabric analysis. It was only through the classical "Yule marble studies" of Griggs and Turner that metallurgical concepts to link microscopic mechanisms with macroscopic properties, i.e. the linkage of dislocations and texture patterns, became accepted in structural geology and has played a dominant role ever since (e.g. [63, 64]). The role of this micro-macro linkage is twofold: Firstly, if slip systems of constituent minerals in rocks are known, we can predict the evolution of texture patterns during tectonic deformation in the crust (e.g. [65]) or convection in the mantle (e.g. [66, 67]) and then use texture to interpret geological history or seismic anisotropy. Secondly, if slip systems are not known, for example because ultrahigh pressure phases cannot be quenched and studied by TEM, experimental texture patterns recorded *in situ* at highest pressures with diamond anvil cells can be used to infer slip systems (e.g. [68]). Not just deformation textures but also recrystallization textures can be related to dislocation structures, in terms of individual grain deformation that controls nucleation and growth [69]. There is no space here to discuss preferred orientation in minerals and several reviews exist [42, 70, 71]. In the next sections we will look at dislocation in a variety of mineral systems and their variation with physical conditions, mainly temperature, strain rate and pressure.

3. Dislocations in various minerals

Dislocations have been studied in many minerals of both geological and materials science interest. We review investigations on some mineral systems in considerable detail, without trying to achieve completeness. Slip systems and Burgers vectors of important minerals are summarized in Table 1. Many advances have been made since earlier reviews by Christie and Ardell [72] and McLaren [6]. Minerals are discussed in order of chemical groups, except for high pressure minerals relevant for the deep earth; these are the subject of the last section. We must mention briefly results that have relevance in other disciplines. For example, diamond and other various forms of carbon are very important technologically; a concise summary of relevant findings is given by Bernaerts and Amelinckx [73]. Ceramic materials are polymineralic and the microstructures of the constituent grains can strongly influence bulk properties [74]. Extraterrestrial materials, especially meteorites, embrace a wide range of minerals, sometimes with unique or unusual microstructures [75]. Recently considerable attention has been given to dislocation structures in ice [76].

3.1 Halides

The susceptibility of halides to radiation damage and, for some also, to atmospheric attack, has meant that there are few direct observations of dislocations within them. Much of our knowledge comes from optical observations of surface slip traces, etch pits and decorated dislocations. For a review of plastic deformation and dislocations in ionic crystals see Castaing [77]. The highly ionic nature of halides imbues them with the interesting possibility of their dislocations being charged. Despite this, there has not been much research into the subject of charged dislocations since the earliest days and so there are relatively few definite results. The most important halide minerals are cubic in structure. Only halite (NaCl), fluorite (CaF_2) and lithium fluoride (LiF) will be considered here, and the latter only because of early work that was very influential in the study of defects in non-metals. For this reason LiF is briefly considered first.

3.1.1 Lithium Fluoride

Lithium fluoride is unimportant from the geological viewpoint but it has great value for optical components: lenses, prisms, windows, which transmit from the vacuum ultraviolet to the infrared and, when doped, as a laser material. Like halite, the LiF structure is cubic and has two interpenetrating face-centred cubic lattices, one of cations and one of anions. Studies of synthetic lithium fluoride using the etch-pitting method [78, 79] were amongst the first to reveal the behavior of dislocations during plastic deformation. This ground-breaking work proved the main slip system to be $\{110\}\langle 1\bar{1}0\rangle$; it also demonstrated the glide and climb of dislocations, the expansion of surface half-loops under stress as well as the blocking of dislocations on one slip system by an orthogonal one.

3.1.2 Fluorite

The crystal structure of fluorite is most easily visualized as a primitive cubic lattice of fluorine ions with calcium ions at alternate body centers. Granular fluorite aggregate is a source for the chemical industry and large pure crystals have applications in modern optics.
Unlike the main minerals with the rocksalt structure, fluorite cleaves on {111} planes and slips on {100} in the $\langle 01\bar{1}\rangle$ direction [80]. Above 200°C, slip on $\{110\}\langle 1\bar{1}0\rangle$ is also possible. Above

320°C polycrystalline plasticity is observed with the {100} planes providing three independent slip systems and the {110} planes giving two more [81]. Dislocations in fluorite have been studied by etch-pitting methods, and by TEM [82] but the latter is not without difficulty, since the mineral rapidly damages under electron and ion irradiation. A cubic symmetry void superlattice can be formed in TEM if the radiation flux is not restricted [83].

Possible core structures for dislocations gliding during {111} slip have been considered with a view to possible charge effects [84, 85]. A model of jogged dislocations with alternate positively and negatively charged segments to achieve overall neutrality was proposed [86]. Straight and jogged edge dislocations lying in {100} have no intrinsic charge when moving; the anions must move normal to the Burgers vector, i.e. along the dislocation [87, 88]. A core model assumes a uniformly neutral edge dislocation at rest and atomistic movements that could operate to accommodate charge balancing during the glide of various types of dislocation. This has some similarities with the synchroshear mechanism for sapphire [89]. Straight edge and screw dislocations in the {110} planes of the fluorite structure are uncharged [90]. Brantley and Bauer [88] examined various dislocation configurations in the fluorite structure for the presence of long-range electrostatic charge, assuming slip systems of the {001}<110> type. They concluded that neither pure edge or screw dislocations nor jogs and kinks on edge or screw dislocations need necessarily give rise to long-range charge, although it could be produced by adsorption or desorption of anions and cations. They also considered the possible effects on dislocation glide and the likelihood of charge transport by dislocations. Stacking fault energies for the {100}, {110} and {111} planes in CaF_2 were calculated and in all cases the energy was high so that only weak dissociation is to be expected [91].

Further ideas about the behaviour of dislocations in fluorite can possibly be derived from the literature on oxides and oxide fuels [92], because some of these materials have the fluorite structure and they have been more widely researched than fluorite.

3.1.3 Halite

Halite (rocksalt), NaCl, with the same cubic structure as LiF, deforms by slip easily and single crystals can sustain large strains provided failure by cleavage is suppressed. Halite has been studied extensively owing to its importance as a component of fault zones and oil traps in sedimentary basins, nuclear waste repositories, and a pressure medium for high-pressure experiments. Early studies often attributed deformation to twinning or kinking, but Pratt [93] showed that slip was the dominant mechanism. At low temperatures $\{110\}\langle 1\bar{1}0\rangle$ is the principal slip system, with ½<110> as the Burgers vector. Each of the {110} planes contains only one slip direction, so there are only two independent slip systems and the Von Mises [53] criterion for plasticity in polycrystals is not met unless other systems are activated [94]. To a considerable degree, the mechanical properties of KCl (sylvite) are like those of halite.

Deformation and etch-pitting experiments on rocksalt crystals have shown that both {100} and {111} slip can occur although electrostatic considerations make these planes less favoured than {110}. Carter and Heard [95] deformed single crystals with various orientations at temperatures up to 500°C at several strain rates and found that at room temperature {110} slip was greatly favoured but already at 300°C {100} and {111}slip became equally active. The stress-strain curves and hardening behaviour of pure halite resemble those of single crystals of f.c.c. metals, with the three typical distinct stages [54, p225]. Duplex slip, glide polygonization and the creation of deformation bands characterize stage II. Cross-slip and the formation of dislocation tangles occur in stage III. X-ray topography was used to study the nature of

deformation bands formed in stage II [96]. Possible hardening mechanisms have been investigated for several NaCl-type crystals, pure and doped [97]. The finding that the flow stress for the onset of stage III is thermally activated [98] led to the proposal and theoretical evidence that screw dislocations can dissociate in the {110} planes and that cross-slip into {100} requires stress-assisted, thermally activated recombination [99, 100]. This suggests that cross-slip should be favoured by increase in hydrostatic pressure [101].

As mentioned previously, the direct observation of dislocations in NaCl poses problems, although as mentioned in section 1, the very first observations of dislocations were made using halite crystals some 100 years ago. About 50 years later, decorated dislocations in doped and thermally-treated crystals provided much information [102, 15]. Frank [103] studied theoretically the geometries of regular dislocation networks in the rocksalt structure using Thomson's notation [104], while Amelinckx [5] found ways to analyse less regular networks. In the following years most dislocation studies relied on the etch-pitting and stress-birefringence methods, which obviate the need for annealing. Fig.5a shows {110}<1$\bar{1}$0> slip bands in a lightly bent bar of halite, as revealed by the etch-pitting method. The dislocation density is locally very variable but it is approximately 10^6 cm^{-2}. Fig. 5b shows the etch-pit pattern due to edge dislocations arranged in low-angle tilt sub-grain boundaries formed by the annealing of a strongly bent bar of halite. There is evidence for negatively charged dislocations in pure NaCl and positively charged OH-doped NaCl, after deformation by bending [105] with a Bauschinger effect, which is associated with the movement of charged dislocations.

The only report of TEM images of dislocations in deformed alkali halide crystals is by Hobbs and Goringe [106], who used special thin-sample preparation techniques, a TEM fitted with a liquid-He cooled stage and fast-emulsion photographic plates, the latter exposed using very low electron flux densities. Their diffraction contrast images lack any obvious signs of radiation damage and show <110> screw and <100> edge dislocations and tangles in KCl crystals deformed to 15% strain and <110> screws, and dipoles and debris in NaCl deformed to 10%.

3.2 Carbonates

3.2.1 Occurrences and Structures of Carbonate Minerals

Rock-forming carbonate minerals at room temperature are rhombohedral (e.g. calcite, and dolomite) or orthorhombic (e.g. aragonite). Calcite, $CaCO_3$ and the ordered double carbonate, dolomite, $CaMg(CO_3)_2$ predominate. High temperature forms are often associated with rotational disorder of the carbonate groups [107]. Biogenic carbonates are predominately high magnesium calcite, dolomite and aragonite. They importantly occur as very strong but lightweight protective constructions in the phyla *mollusca* and *echinodermata*. The fracture toughness of nacre is more than tenfold that of geological calcium carbonate [108]. Such biological constructions have therefore received attention from scientists interested in designing and making novel synthetic materials. Biogenic carbonates are not considered here because of their diversity of both occurrence and structure and the current evidence that they lack grown-in dislocations and deform in brittle mode (their complex microstructures probably inhibit the nucleation of dislocations and hence their strength).

Calcite has trigonal symmetry, R$\bar{3}$c. The four-digit Miller-Bravais crystallographic indices used for calcite in this section refer to hexagonal axes and a (true) hexagonal structural cell. For this cell the calcite cleavage planes **{r}** have indices {10$\bar{1}$4} and the commonest twin planes **{e}** are {$\bar{1}$018}. Use of a true cell enables one to properly assign all reflections observed in X-ray

and electron diffraction patterns to sets of planes with integer indices. Older literature mostly employs a rhombohedral cell, often the morphological (cleavage) cell containing 2 $CaCO_3$ molecules, which is not a true cell. Dolomite crystallizes in the point group $R\bar{3}$. Aragonite is the orthorhombic (Pcmn) polymorph of calcium carbonate. It is only a stable phase at high pressure, but notwithstanding this, the mineral occurs widely in marine sediments and in marine organisms, both skeletally and as nacre. For an earlier review of microstructures in carbonates see Wenk et al. [109].

3.2.2 Calcite

The plastic deformation of calcite usually involves both slip and twinning; both generate dislocations. Slip and twinning in rhombohedral carbonates have a preferred sense, i.e. a definite direction of shear.

TEM results from the grains in naturally deformed calcites usually indicate that two or more deformation systems have operated, leading to complicated arrangements or tangles of dislocations. Even single crystals experimentally deformed to low strains generally contain complex dislocation configurations that defy analysis. A further handicap is the tendency of most calcite specimens to suffer electron beam damage, making it impossible to analyse dislocation properties from a set of images under various diffraction conditions. The eventual proof that the basal slip system can operate [110], subsequent to a long-held suspicion [111], necessitated the torsion at high temperature of a single crystal orientated to suppress the activation of all other slip systems.

Studies of limestones and marbles from various geological settings [112, 113]) showed a fairly good correlation between the microstructures, metamorphic grade and geologic history. For example, very high dislocations densities ($\sim 10^9$ cm^{-2}) were found in a deformed low grade fine-grained limestone, whereas rocks of high metamorphic grade generally had lower dislocation densities. Greenschist facies samples could be distinguished from those of amphibolite facies on the basis of their microstructures. However, recovery was in evidence even in low grade samples; as a consequence, the densities varied greatly between the grains in a fine-grained mylonite with a complex history. Dislocations in calcitic rocks clearly could move at much lower temperatures than in quartz rocks so that calcite was not suitable as an indicator of conditions in major tectonic events because of ease of subsequent recovery.

Analysis of TEM images of dislocations, together with structural considerations, indicate that the Burgers vectors for **r**, **f** and **c** slip are respectively $\frac{1}{3}\langle 20\bar{2}\bar{1}\rangle$, $\frac{1}{3}\langle 10\bar{1}\bar{1}\rangle$ and $\frac{1}{3}\langle 2\bar{1}\bar{1}0\rangle$. There is no evidence for basal dislocations in calcite and marbles deformed at low temperatures.

Activity on $(0001)\langle 2\bar{1}\bar{1}0\rangle$ in high temperature samples is characterized by many long straight screw dislocations. Slip on **r** in the negative sense occurs over a wide range of temperatures, as shown for single crystals [63] and for polycrystals [64, 114]. Slip on **f** is also important, especially when twinning is less favoured. The dislocations generated by both **r**- and **f**-slip do not have well-defined geometries. Those produced by **r**-slip are not crystallographically controlled; they tend to be strongly curved, are unregimented and seldom adhere strictly to their slip planes or form slip bands (this is in strong contrast to the situation for dolomite). The Burgers vectors are long (0.77 nm for **r**-slip and 0.81 nm for **f**-slip, but only 0.49 nm for **c**-slip).

Despite the theoretical possibility of dissociation in the **r**-planes to partials with $\frac{1}{6}\langle 20\bar{2}\bar{1}\rangle$ Burgers vectors and the creation of a stacking fault in the CO_3 lattice, there is no evidence for it.

Deformation twinning on both the **e** and **r** planes can produce several types of interaction and the generation of microcracks [115]. Twinning in calcite usually creates numerous dislocations, explaining why repeated twinning and de-twinning is not possible [116, 117]. Dislocations typically occur in the twin boundaries, within the twins and also external to them, especially when one twin impinges on another twin or an obstacle. Crossing twins [118] occur readily, producing rhombohedral channels, as first reported by Rose [119], after whom they are named. Stopping twins (these do not taper to a point) are common in polycrystals where many obstacles to propagation exist. Their terminations are important sites for dislocation nucleation and the initiation of microcracks (which themselves may create more dislocations).

In highly deformed calcite rocks **e**-twinning is usually profuse, which is consistent with their thermal history. Stress relief by twinning decreases as the temperature increases and in calcitic marbles deformed under suitable geological conditions it is possible to find grains completely free of twins but with cell-like dislocation microstructures (Fig. 3b), resembling those observed in work-hardened metals.

3.2.3 Dolomite

The characteristics of dislocation configurations seen by TEM in dolomite are markedly different from those for calcite. In comparison, active slip systems for dolomite are more easily identified in deformed and unrecovered samples because dislocations tend to keep to their slip planes and frequently are geometrical in shape. Slip bands are common in experimentally deformed specimens. Because dolomite is an ordered mineral with a superlattice of both cations and anions (CO_3 groups), perfect dislocations in the structure are, *senso strictu*, superdislocations.

Examples of grown-in dislocations are found in ancient calcian dolomites and calcian ankerites. These minerals frequently exhibit fine-scale modulated microstrostructures with wavelengths commonly between 7.5 and 20 nm [120]. The modulations arise directly during growth, have been attributed to compositional or ordering fluctuations and superstructures [121, 122], and are usually associated with a finescale growth banding closely perpendicular to the modulations [120]. The latter is a manifestation of plane concentric zoning and probably reflects small compositional changes during growth [123]. The dislocations in these ancient dolomites and ankerites are oriented perpendicular to the growth zoning and thus roughly parallel to the modulations (fig.10-3 in [120]). They probably nucleated at the growing interface and being unable to terminate, traverse the growth sector.

Metamorphic dolomites can contain quite high dislocation densities, between 10^3 and 10^6 cm^{-2}. Evidence of recovery in the form of dislocation networks is commonly seen (e.g. [124]). Generally speaking, there is a correlation of dislocation density with metamorphic grade: Crevola marble, a medium to high grade amphibolite facies rock [125] has a low dislocation density and is therefore suitable for deformation experiments [126]. To judge both from both experimental specimens and rocks, recovery does not appear to occur as readily as in calcite and so dolomite should be a better indicator of tectonic conditions. Fig. 5 illustrates microstructures in experimentally deformed single crystals. At low temperature dislocations are concentrated in bands (Fig. 6a). At higher temperature climb produces more open microstructures with loops (Fig. 6b).

Dolomite is much less prone to electron damage than calcite and so it is easier to determine Burgers vectors using diffraction contrast methods. The vectors for perfect dislocations are

⅓<2$\bar{1}\bar{1}$0> and ⅓<2$\bar{2}$01>. However, dislocation dissociation is also possible in dolomite; when it

occurs in the basal planes pairs of superpartials separated by region of stacking fault are formed [124, 127]. The Burgers vector of the basal partial dislocations is $\frac{1}{3}\langle 10\bar{1}0\rangle$. Long ribbons of stacking fault can result from this dissociation in experimentally deformed dolomites (Fig. 3a). The basal slip system is considered to be responsible for the unusual increase of strength with temperature demonstrable with single crystals [128, 129]. Strengthening apparently occurs due to inability of basal dislocations to overcome obstacles because a mechanism (e.g. cross slip) is lacking.

Dislocation dissociation accompanying slip on the **f**-planes presents more complex possibilities [127]. The slip directions and Burgers vectors lie along the intersection of two **f**-planes and therefore a superdislocation with a Burgers vector $\frac{1}{3}\langle 2\bar{2}01\rangle$ can glide on two planes simultaneously in a vee-like configuration, or alternatively, as a closed rhombohedron-shaped loop using two planes of each orientation (this is known as pencil glide). If an **f**-slip dislocation dissociates to give partials of type $^{1}/_{6}\langle 2\bar{2}01\rangle$ the passage of such a partial gives a fault in both the cation and CO_3 sublattices, resulting in what is normally called an antiphase boundary (APB). The diffraction contrast properties of such faults in practice, however, are not those expected for APBs. Therefore they have been called complex stacking faults [127]. Usually many dislocation dipoles and small loops result from **f**-slip at moderate temperatures, on account of various interactions and the ease of cross-slip. When **f**-slip can occur, as in most grains in polycrystalline dolomite, it masks the increasing strength-with-temperature behaviour associated with **c**-slip.

3.2.4 Aragonite

There are very few reports of observations of dislocations in either geological or biogenic aragonites although the slip systems are known (see Table 1) and {110} twinning occurs in both types. Studies of the aragonite → calcite transformation have shown that dislocation tangles and twins can serve as nucleation sites for calcite [130]. In an *in situ* TEM study of the transformation [131] there was no evidence of a martensitic mechanism [132] but the moving interphase boundary was seen to sweep away dislocations and twins. Recent interest in biomimetic materials has led to studies of the plasticity and microindentation of nacre. The results have provided new information about aragonite slip systems [133], but to date, no direct data about dislocation behaviour.

3.3. Oxides

Several oxides that occur as significant minerals in nature are also important as ceramics or as components of ceramics, or as technological materials. Such materials are mostly synthesized for reasons of obtaining appropriate volume, mechanical properties or special geometry, control over impurities and crystal defects, achieving functional doping, etc. These aspects of oxides will not be considered here. Bretheau et al. [134] carried out a comprehensive review (in French with English summary) covering the properties and behaviour of several technologically important oxides. The review points out that dislocation glide in oxides is not well documented and that interpretations of observations from different oxides are often contradictory. Dislocation climb is the mechanism of interest at the elevated temperatures that are relevant to ceramics. To test possible theories, data about diffusing species are required and models of dislocation cores and jogs are necessary. Some methods of making core models have been proposed (e.g. [135, 136]), but generally these are lacking.

3.4.1 Corundum

Corundum, aluminum oxide (sapphire), α-Al_2O_3, has a crystal structure in which oxygen ions are close-packed and the aluminium ions occupy two-thirds of the octahedral interstices. The mineral is trigonal ($R\bar{3}c$) and the close-packed oxygen plane is basal, i.e. (0001).

The extreme plastic anisotropy of sapphire was first reported by Wachtman and Maxwell [137] who detected basal creep in tensile specimens at 900°C but found that when specimens with a **c**-axis were stressed in tension, no creep occurred until the temperature exceeded 1600°C. The earliest TEM observations of dislocations in Al_2O_3 [138, 139] used chemically-thinned pure and doped synthetic sapphire imaged grown-in dislocations: sections of low-angle sub-boundaries and regular networks were seen in undeformed specimens while helices and loose networks were seen in specimens deformed in creep. Subsequent optical and TEM results established that slip is in the $<11\bar{2}0>$ close-packed direction and the Burgers vector of the basal dislocations is $\frac{1}{3}<11\bar{2}0>$. It was suggested that basal dislocations would need to glide by a mechanism of synchroshear involving dissociation of dislocations into quarter partials and the cooperative movements of anions and cations [89]. Further work showed that important additional slip systems for high temperatures are $\{11\bar{2}0\}<1\bar{1}00>$ [140, 141] and $\{10\bar{1}1\}<01\bar{1}1>$, with a Burgers vector of $\frac{1}{3}<\bar{1}101>$ [142, 143, 144]). Slip on $\{\bar{1}012\}<10\bar{1}1>$, and possibly on $\{10\bar{1}1\}<1\bar{2}10>$ was also reported. TEM studies of the dislocations arrays around room temperature indentations showed that slip can also take place on the pyramidal planes $\{11\bar{2}3\}$ in the $<1\bar{1}00>$ direction , with the Burgers vector $<1\bar{1}00>$ [145]. Basal twinning [146, 145] and rhombohedral twinning are additional deformation mechanisms [147, 148, 149]. Both can occur at room temperature and rhombohedral twinning has been observed in deformation up to 1700°C. Thermal shock often causes rhombohedral twinning.

Pletka et al. [150] examined various possible strengthening mechanisms in sapphire. The early stage of work-hardening in pure samples deforming by basal slip is due to the formation of obstacles to dislocation glide in the form of many edge dipoles created by the trapping of dislocations on parallel planes (Fig. 7a). As deformation proceeded further the dipoles were seen to break up by climb, forming small loops. When the rate of dipole accumulation became equal to the rate of their annihilation the rate of work hardening became zero. Several studies investigated the role of dislocations in the plastic deformation of Cr- and Ti-doped sapphire [150, 151, 152, 153]. The effect of chromium concentration has little effect on dislocation multiplication mechanisms and dislocation velocities during basal slip between 900 and 1500°C [154].

The slight dissociation possible for some dislocations in Al_2O_3 has been illustrated by several authors; two examples are: a) the two arms of a $[11\bar{2}0]$ dipole are each dissociated into two partials, the adjacent inner partials then annihilate to leave a wider ribbon of stacking fault, bounded by $\frac{1}{3}<10\bar{1}0>$ partials [155]; b) the dissociation of a dislocation with $\mathbf{b} = [01\bar{1}0]$ into three partials that recombine where there is a change in angle [156].

3.4.2. Hematite

Hematite, α -Fe_2O_3, is a major ore mineral. It is isostructural with corundum and it seems reasonable to expect that it would slip on similar systems. There have been few deformation experiments on single crystals, however, and even fewer direct observations of dislocations in hematite.

At room temperature the only easy deformation mechanisms in hematite appear to be twinning on the basal and pyramidal planes, $\{01\bar{1}2\}$. Prismatic slip, $\{11\bar{2}0\}\langle 1\bar{1}00\rangle$, was shown to occur at 200°C and above [157], although brittle fracture can still occur in tension at about 1200°C in the absence of confining pressure [158]. At low strain rates, 25 to 700°C and under confining pressure, hematite tested in compression was made to slip on $(0001)\langle 11\bar{2}0\rangle$ and $\{11\bar{2}0\}\langle 1\bar{1}00\rangle$ [159]. There is TEM evidence for dislocations at twin interfaces and basal slip [160]. High resolution TEM has been used to study symmetry and twinning in hematite [161, 162] and intergrowths of hematite and magnetite [163, 164] (Fig. 8a).

3.4.3. Ilmenite

Ilmenite, $FeTiO_3$, is also isostructural with corundum. Cations are ordered in alternate layers parallel to the close packed oxygen layers, i.e. (0001). Ilmenite is an important ore mineral for titanium. One might expect the same slip systems for ilmenite as with corundum. But similarly, slip on any plane transverse to the basal plane would require a perfect dislocation to have a large Burgers vector. Otherwise such slip would proceed by means of partials, generating regions of antiphase stacking, which would be likely only at high temperature. The mechanisms of plastic deformation of ilmenite have not been studied.

The interfaces between finescale exsolution lamellae of ilmenite in hematite have been investigated and most were shown to be coherent and dislocation free [165]. Due to differences in lattice parameters, dislocation arrays decorate the interface (Fig. 8b). Contrast analysis revealed a hexagonal grid of rhombohedral dislocations [166] rather than dislocations with basal Burgers vectors [167]. The ordering phase transition in ferrian ilmenite from the high temperature $R\bar{3}c$ disordered structure to a $R\bar{3}$ lower temperature ordered structure results in the creation of twin domains [168, 169]. No dislocations were involved.

3.4.4. Periclase and Wüstite (see also 3.8.1.)

Periclase, MgO, has the rocksalt structure. It is rare in the Earth's crust but is thought to be a major component in the lower mantle in a solid solution with FeO (magnesiowüstite). As with NaCl, the easy glide plane at low temperature is the electrically neutral plane, {110} and dislocations in MgO have Burgers vector $\frac{1}{2}\langle 1\bar{1}0\rangle$. At higher temperature glide also occurs on $\{001\}\langle 110\rangle$ and $\{111\}\langle 110\rangle$. Dislocation structures formed during creep of MgO single crystals were investigated by etch-pitting [170, 171]. Later work has relied more on TEM for the interpretation of microstructures [134]. Most of the plasticity of fine-grained polycrystalline MgO above 1000°C was attributed to diffusional processes except for some evidence of dislocation glide [172, 173]. Single crystal MgO shows plasticity due to slip on $\{110\}\langle 1\bar{1}0\rangle$ from below room temperature to moderate temperatures. Above 1200°C the $\{001\}\langle 110\rangle$ system is activated [174].

Wustite, $Fe_{1-x}O$, with x commonly lying between 0.05 and 0.15, occurs as a phase in iron scale. The primary slip system is $\{110\}\langle 1\bar{1}0\rangle$, as in NaCl. A steady state can be attained in

deformation experiments of polycrystalline FeO above 1000°C and strain rates are proportional to the fourth power of stress, indicating that dislocation climb is active [158]. Diffusion creep is observed at yet higher temperatures. High strain experiments were performed in torsion and under confining pressure on magnesiowüstite aggregates by Heidelbach et al [175] to investigate texture development and associated changes in mechanical behaviour. The initial deformation texture was compatible with $<1\bar{1}0>$ dislocation glide on all three possible slip systems: {111}, {110} and {001} and this was confirmed by TEM results. The microstructure evolved into one of subgrains at a relatively low homologous temperature ($<0.5T_m$), which was possibly promoted by cross-slip between the active systems. Rotation of the subgrains ultimately led to a recrystallization texture. Dislocation creep and strain partitioning of olivine-wüstite aggregates deformed to large strains has been studied by Bystricky et al. [176].

3.4.5. Magnetite

Magnetite, Fe_3O_4, crystallizes in the inverse spinel structure (cubic), with Fe^{3+} in the tetrahedral sites and both Fe^{2+} and Fe^{3+} in the octahedral sites (space group Fd3m). Many cationic substitutions occur. It is an important iron ore and occurs in many geological environments, as aggregates, veinlets, and inclusions.

There is relatively little information about dislocations in massive magnetite. Small crystals are usually dislocation-free: magnetosomes in magnetotactic bacteria are perfect single crystals [177]; the magnetites in the carbonates in the Martian meteorite, ALH84001, are also dislocation-free [178, 179]. Preferred orientation measurements on magnetite ores deformed at 300°C suggest the action of $\{111\}<1\bar{1}0>$ slip [180]. This mechanism was shown to be active at least up to 1000°C [158].

3.4.6. Spinel

There is a large range of spinels, including magnetite as discussed above, but the most important, is the magnesium aluminate, $MgO(Al_2O_3)_n$. Slip systems for this mineral have been researched thoroughly [181]. In stoichiometric samples (n = 1, i.e. $MgAl_2O_4$) deformed at high temperature (1800°C), slip occurs on $\{111\}<1\bar{1}0>$ (glide of dislocations on the close-packed plane and direction) as predicted [182], and includes dissociation of <110> dislocations into quarter partials [89]. One can deform spinel at temperatures below $0.5T_m$ if a uniaxial compressive stress is applied in the presence of a confining pressure [183]. Even deformation at room temperature is possible under special conditions [184]. Dislocation configurations associated with indentations made on spinel at room temperature have been studied by TEM [185, 186].

Veyssière and Carter [187] deformed a stoichiometric single crystal of spinel along <110> to cause primary slip on {111} with cross-slip occurring onto a {001} plane. Weak beam imaging indicated that all dislocations associated with the primary slip plane were dissociated out of that plane, no matter what their character (Fig. 7b). Deformation proceeded by gliding of the partials on parallel planes. The accompanying stacking faults have to migrate; this is achieved by a local shuffling of cations. Weak beam images of screw dislocations gave a stacking fault energy of 530 ± 90 mJ m^{-2} for conservative dissociation on {001} at 400°C.

The effect of cation vacancies in alumina-rich samples is to change the slip plane from {111} to {110}, with glide still in the $<1\bar{1}0>$ direction [181, 188, 189, 190]). Dissociation into quarter partial dislocations is again observed but with a larger separation [188].

3.4.7. Perovskite (see also 3.8.5.)

Perovskite, $CaTiO_3$ is one of a large group of minerals with formula AA'BB''O_3 owing to the ease of substitution of the cation species. The structure is unique in having a large cation site in 12-fold coordination. Perovskites have a cubic or cube-octahedral structure but symmetry is often reduced to tetragonal or orthorhombic by ordering or distortion [191]. There are many "perovskites" of scientific curiosity or industrial importance for devices (e.g. the ferroelectric tetragonal oxide $BaTiO_3$ and tetragonal/ rhombohedral $Pb(Ti, Zr)O_3$). The perovskite structure also attracts much attention because of its associations with high-temperature superconductivity in compounds such as $YBa_2Cu_3O_6$. For geosciences, the perovskites $(Mg, Fe)SiO_3$ and $CaSiO_3$ are thought to be the main constituents of the lower mantle and control its rheology. Dislocations in these silicate perovskites will be discussed in the section on high pressure minerals.

The easy glide systems in pseudo-cubic $CaTiO_3$ are $\{110\}<1\bar{1}0>$ and $\{010\}<100>$ [192]. Other slip systems can also be activated under special conditions, e.g. $\{001\}<110>$ and $\{110\}<001>$. There is very little information about dislocations and microstructures in $CaTiO_3$ [193] but a large amount about them in other perovskites such as $SrTiO_3$. Dislocations in perovskites, including $SrTiO_3$, are widely observed to dissociate. Also a very marked flow stress anomaly in $SrTiO_3$ suggests that dislocations in the cubic perovskite structure may possess several core structures [194].

3.4.8. Rutile

The structure of rutile, TiO_{2-x}, is tetragonal, with a pseudo-hexagonal packing of oxygen ions in the (001) plane (space group $P4_2/mnm$). Rutile is commonly oxygen deficient. It is an ore for titanium and occurs in quartz veins in metamorphic rocks and as placer deposits.
The plastic behaviour of rutile is surprising at first sight: (001) is not a slip plane at low to moderate temperatures and does not feature in the primary system at high temperatures, which is $\{101\}<10\bar{1}>$ [195, 196]. The secondary HT system is $\{110\}[001]$. Dissociated $<10\bar{1}>$ dislocations and long stacking faults have been observed [197] but dislocations with [001] Burgers vectors are not dissociated [198]. The amount of dissociation appears to be associated with stoichiometry. Suzuki et al. [199] studied dislocation dissociations in rutile and isostructural SnO_2 by HRTEM and confirmed that [001] dislocations did not dissociate, while <101> dislocations did. Furthermore they observed edge dislocations with **b** = <100>. These were found to dissociate on the $\{10\bar{1}\}$ plane into sessile types by the reaction $[100] \rightarrow \frac{1}{2}[101] + \frac{1}{2}[10\bar{1}]$.

3.4 Quartz

Quartz (SiO_2) is one of the most abundant minerals in the Earth's crust. Owing to its ubiquitous occurrence in zones of high strain tectonic deformation, its rheological properties are commonly used to model the mechanical behaviour of continental regions (e.g., [200]). In addition, dislocation glide mechanics in quartz (specifically double kink nucleation) have been

applied to model the rheological evolution of grain scale asperities on faults during earthquakes [201].

The low-temperature polymorph (α-quartz) is trigonal ($P3_121$). The high temperature polymorph (β-quartz; transition at 573°C, increasing to ~900°C at a pressure of 1.5 GPa) is hexagonal (P622). Low quartz is elastically very anisotropic, with a direction perpendicular to the negative rhomb $\{02\bar{2}1\}$ almost twice as stiff as the direction perpendicular to the positive rhomb $\{20\bar{2}1\}$. High quartz is fairly isotropic.

Dislocation imaging in quartz has a long history, but it was only with the development of ion beam thinning that dislocation microstructures could be quantified with TEM analysis [202]. Dominant slip systems in quartz have been studied by analysis of dislocations in deformed single crystals as well as experimentally and naturally deformed quartz rocks (quartzites). One of the first determinations of Burgers vectors identified $\mathbf{r} = \frac{1}{3}[2\bar{1}\bar{1}0]$ [48]. Contrast analysis is complicated by the fact that quartz undergoes rapid beam damage. Slip takes place mainly in the **a**, **c** and <**c**+**a**> directions on numerous low index planes containing these directions, but dominant under most conditions are (0001) and $\{10\bar{1}0\}$ planes [72]. Creep tests on wet synthetic crystals conducted at room pressure suggest a dominance of **c** slip at low temperatures [203]. Furthermore, extrapolation of the temperature dependence for **c** and **a** slip to higher temperature indicates a transition from **c** to **a** slip (Fig. 9). Evidence for **a** slip in quartz single crystals at lower temperatures has been reported (e.g., [204, 205]) but the data are not unambiguous [203]. Recent high pressure (P = 1.5 GPa) experiments on wet synthetic crystals do suggest that slip on $(0001)\frac{1}{3}\langle 11\bar{2}0\rangle$ is easier than $\{10\bar{1}0\}[0001]$ at 600°C, and that the activity of **c** slip and **a** slip become similar at 900°C, consistent with transitions in texture patterns observed in quartzite [206].

The effect of temperature on the microstructures and dominant slip systems determined from textures are similar for both experimentally and naturally deformed quartzites (e.g., [207, 208, 209, 210]). Inferences about slip systems from textures are not unequivocal, especially because many texture studies rely only on c-axis orientations and not the full orientation distribution. There are very few TEM investigations identifying dislocation geometries in natural quartzites. The newer studies are consistent with the concept that $(0001)\frac{1}{3}[2\bar{1}\bar{1}0]$ slip dominates at lower temperatures, with a transition to $\{10\bar{1}0\}\frac{1}{3}\langle 11\bar{2}0\rangle$ slip at intermediate temperatures (~900°C in the laboratory, 500°C-600°C in the Earth) and finally $\{10\bar{1}0\}[0001]$ slip at temperatures above 600°C-700°C in the Earth [208]. Slip on the rhombohedral planes in the **a** and **c** directions is also observed. The different transition temperatures observed for experiments and rocks recovered from natural settings are interpreted to reflect a kinetic trade-off between the temperature and strain rate. Experimental samples creep at rates 10^5 to 10^7 times faster than deformation occurs in the Earth.

Experimental data suggest that the displacive α-β transition may not strongly influence the dominant slip systems. This is not unexpected because the main basal and prismatic slip systems have “hexagonal” symmetry. However, textures are distinctly trigonal in most natural quartz rocks, with very different orientation distributions for positive and negative rhombs (e.g. [211]). The trigonal textures may arise for various reasons: conceivably rhombohedral slip systems are important. They may be due to mechanical Dauphiné twinning, which is geometrically a 180°

rotation about the c-axis but achieved through slight structural distortions [212, 213, 214]. However, twins are rarely observed in natural quartzites in a wide range of conditions [200]. Interestingly, *in situ* heating experiments in the TEM documented the role of dislocations for the propagation of twins in the vicinity of the α–β transformation [215] (Fig 10a). Most natural quartzites are recrystallized, rather than plastically deformed and recrystallization under stress of this highly anisotropic material may induce the trigonality of the preferred orientation pattern [216, 217, 218, 219].

The stress required for dislocation slip in quartz depends strongly on water fugacity. Under dry conditions, quartz is extremely strong, owing to the strongly covalent Si-O bonding. Dry gem-quality single crystals support stresses in excess of 1.0 GPa at a temperature of 1300^{o}C (~0.8 T/Tm) and confining pressure of 0.3 GPa. At these conditions, strain is accommodated dominantly by microcracking, and dislocation glide is largely isolated to crack tip regions [220]. By contrast, hydrothermally synthesized quartz crystals exhibit yield stresses in the range of 140 MPa at 750^{o}C [221, 222, 203]. The effect of water content on dislocation creep has also been documented for quartz aggregates, where creep rate is observed to increase approximately linearly with increasing water fugacity [223, 224].

While the effects of water are well documented, and further substantiated by measurements of enhanced diffusion and dislocation recovery at high water fugacity [225, 226], the mechanisms by which water (or hydrogen) influence dislocation mobility are still not well understood [227, 228]. Some water is in the form of bubbles associated with dislocations (Fig. 10b) [229]. Microstructural evidence for enhanced dislocation climb, as well as rapid rates of dislocation recovery, suggest dislocation mobility is increased by enhanced diffusion rates under hydrous conditions [230, 231, 224]. However, climb was inhibited in deformation experiments on water-poor quartz, tested under P, T conditions that kept the residual water dissolved in the lattice and only basal and c + a slip were rendered active, glide being aided by dislocation dissociation [232]. Enhanced diffusion rates under hydrous conditions are interpreted to result from an increase in the concentration of H-related defects with increasing pressure [231, 233]. Such a process explains differences in the behaviour of wet quartz at different water fugacities. However, the drastic changes in the behaviour of dry quartz and quartz with ~500 H/10^{6}Si may represent true "hydrolytic weakening", where Si-O-Si bonds are hydrolyzed to form weaker Si-O-H-H-O-Si, lowering the Peierls barrier to dislocation glide [222].

Various TEM studies of quartz rocks illustrate systematic changes in microstructures with metamorphic grade and deformation conditions. Average dislocation densities range from <10^{7} /cm^{2} in high temperature environments to >10^{9} /cm^{2} in heavily deformed cold-worked material (e.g. [58, 234, 210, 235].

3.5 Olivine

Olivine, $(Mg_{1-x}Fe_x)_2SiO_4$, is the primary mineral in Earth's upper mantle with $x \approx 0.1$. The olivine crystal structure is orthorhombic in spacegroup Pbnm. Deformation of olivine has been of longstanding interest, because this mineral is the major component of the Earth's upper mantle and controls its rheology. Furthermore, preferred orientation of olivine attained during mantle deformation by dislocation creep results in high and systematic seismic anisotropy [236, 237], an observation that has been exploited by geophysicists to investigate the dynamics and kinematics of mantle convection.

The dominant slip systems in olivine at high temperatures (low differential stresses) are (010)[100] and (001)[100] with (010)[001] and (100)[001] playing a greater role at lower

temperatures (high differential stresses) [238, 239, 240] (Fig. 11). However, TEM observations have revealed dislocations with [010] Burgers vectors as components of low-angle tilt boundaries [241], and high-resolution lattice fringe images demonstrated their dissociation into three or four partial dislocations [242] (Fig. 12). The transition between [100] and [001] dominated slip also occurs with increasing pressure [243]. At high temperatures, climb provides a portion of the strain as evidenced by analyses of the change of shape of single crystals deformed in compression [244] and by the kinetics of formation of low-angle tilt boundaries [241].

A substantial number of laboratory studies of the rheological behavior of olivine have been undertaken, both on single crystals and on polycrystalline samples [244, 245, 246, 247, 248]. These experiments demonstrate that the strength of olivine is sensitive not only to temperature and pressure but also to Fe content, oxygen fugacity, and water fugacity. In samples deformed under anhydrous conditions, four distinct deformation regimes have been identified: grain boundary diffusion creep, dislocation-accommodated grain boundary sliding, dislocation creep, and lattice friction creep. For samples deformed under hydrous conditions, the dislocation-accommodated grain boundary sliding regime appears to be absent, possibly because of the enhanced role of dislocation climb. In addition to temperature and pressure, 'water' has a major effect on the strength of olivine. The water-weakening effect is associated with the introduction of hydrogen ions into olivine grains, analogous to doping a semiconductor material because olivine can be treated as a wide band gap semiconductor [245, 249, 250].

Transitions between slip systems have also been reported as a function of water fugacity. Five different regimes in stress – water fugacity space have been reported [251]: (010)[100] at low stress, low water content; (001)[100] at low stress, intermediate water content; (100)[001] at intermediate stress, high water content; (010)[001] at high stress, high water content; {0*kl*}[100] at high stress, low water content. The relative roles of stress, water content, temperature, and pressure in the transitions between dominant slip systems is complex as it is not possible to vary one of these parameters without varying another. For example, to reach high water contents, it is necessary to go to high pressures [252]. Deformation at low stresses requires high temperatures, while deformation at high stresses requires high confining pressures and generally low temperatures.

3.6. Other silicates

3.6.1 Garnet (see also 3.8.2.)

Garnets are cubic minerals with a wide range of chemical substitutions that occur in metamorphic rocks from the Earth's crust and as a volumetrically significant fraction of the upper mantle. Some end-members are almandine $Fe_3^{2+}Al_2(SiO_4)_3$, grossular $Ca_3Al_2(SiO_4)_3$, pyrope $Mg_3Al_2(SiO_4)_3$ and majorite $Mg_3MgSi(SiO_4)_3$. Some synthetic garnets are also important technologically. Gadolinium gallium garnet, (GGG) thin films and yttrium aluminium garnet, YAG (the latter with various dopants, e.g. neodymium), have applications in magnetic bubble devices, and optical laser devices and waveguides, respectively. Some reports about growth-induced dislocations in these materials (e.g. [253, 254]) may have relevance to mineral garnets.

One of the earliest reports about dislocations in a natural garnet is that of Carstens [255] who studied Norwegian and Czech pyrope-rich garnets by etching them with hydrofluoric acid. Long etch channels extending from the surfaces, similar to those observed earlier [27], were attributed

to deformation-induced dislocations. Tangled arrangements and cell structures were interpreted as indicators of dislocation creep.

TEM was used to elucidate the characteristics of dislocations in naturally deformed silicate garnets and olivines in garnet-peridotites and silicate garnets in eclogites [256]. It was found that i) dislocation densities in garnets from garnet-peridotites were always almost an order of magnitude less than those in the co-exisiting olivines; ii) dislocation densities of garnets in eclogites that were within garnet peridotites were almost ten times greater than those in the garnets surrounding garnet peridotites. The Burgers vector, **b** was predominantly <100> for garnets with dislocation densities of $10^5 - 10^6$ cm^{-2}, but **b** was ½<111> for dislocation densities of 10^7 -10^8 cm^{-2}.

Two very different but characteristic microstructures were identified in eglogites from the Alps [257]. One is indicative of only local microplasticity but overall brittle behaviour, consisting largely of microfractures. The other, occurring more widely, was a dislocation microstructure that is the result of dislocation creep associated with dynamic recovery in the form of climb. Slip systems found to be operative were $\{1\bar{1}0\}$½<111>, $\{11\bar{2}\}$½<111>, $\{12\bar{3}\}$½<111>, {010}<100> and {011}<100>.

Several analytical methods, including electron back-scatter imaging and diffraction, were used to study elongate natural garnets that were deduced to have deformed at ~700°C [258]. In low strain regions, subgrains with small misorientation between neighbours were observed; boundary misorientations increased when approaching areas of higher strain. A polygonal microstructure was present in high-strain areas.

With HRTEM dissociations in a completely stoichiometric garnet were observed [259], contrary to the notion that dissociation is linked to traces of impurities. Parallel and narrow ¼<111> partial dislocations were separated by stacking faults that corresponded to a low energy configuration resulting from the occupancy of previously vacant dodecahedral and tetrahedral lattice sites.

3.6.2 Orthopyroxene

Enstatite-hypersthene, $(Mg,Fe)Si_2O_6$, the second most abundant mineral in upper mantle rocks, is orthorhombic (Pbca). Pyroxenes are chain silicates, with SiO_3 chains extending along the c-axis. Dislocations with [001] Burgers vectors dominate deformation with glide on the (100) and (010) planes [260, 261, 262, 263, 264, 265]. There are also (100)[010] dislocations with a [100] line direction [275] (Fig. 13a). The critical resolved shear stress for the (100)[001] slip system is significantly smaller than for (010)[001]. With a limited number of slip systems, it is inferred that climb and grain boundary sliding must also be important deformation mechanisms in orthopyroxene rocks [266].

3.6.3 Clinopyroxenes

The clinopyroxenes are monoclinic: diopside $CaMgSi_2O_6$, augite $Ca(Mg,Fe)Si_2O_6$ and spodumene $LiAlSi_2O_6$ crystallize in space group C 2/c, pigeonite $(Ca,Mg,Fe)Si_2O_6$ and clinoenstatite $MgSiO_3$ in space group $P2_1/c$ and omphacite (Ca, Na)(Mg, Fe, Al)Si_2O_6 in P2/n. Based on TEM analyses of experimentally deformed *diopside*, plastic deformation takes place by mechanical twinning on (100)[001] and (001)[100] with dislocation glide on (100)[001], (100)[010] and (010)[100] at temperatures of <500°C [267, 268, 269, 270, 271, 272, 273]. At higher temperatures, slip is activated on (100)[001], $\{110\}$½$<1\bar{1}0>$, {110}[001], (010)[001], (100)[010], and (010)½[101] [273, 274, 275, 269]. The easiest slip system appears to be

(100)[001] at temperatures $500^{o} < T < 800^{o}$C, which alters to {110}½<1 $\bar{1}$0> and {110}[001] for $T > 800^{o}$C [274, 243].

Burgers vector and dislocation line analysis of naturally deformed *augite*-enstatite crystals indicate activation of many slip systems such as (100)[001], {110} ½<110>, {110} ½<112>, (100)[010], (010)[100], (010)<101> and {110}<111>, the first two being the most active [275]. The study demonstrates that most dislocations are dissociated and stacking faults are produced that can be interpreted based on the complex structure of these chain silicates. In naturally deformed augite from a pyroxenite with lamellar exsolution ½ [101] dislocations in (010) combine single to double chains, yielding so-called chain multiplicity faults [276].

An interesting role of dislocations is in the stress-induced phase transformation of orthoenstatite to *clinoenstatite* [277, 278, 279].

As with other nominally anhydrous silicate minerals, the addition of a small amount of hydrogen in clinopyroxene results in a significant decrease in high-temperature viscosity, both in the diffusion creep regime and in the dislocation creep regime [273, 280, 281, 282]. Compared to olivine, the dependence of creep rate on water fugacity is similar to that reported for olivine with an approximately linear relationship between creep rate and water fugacity [282]. However, in the dislocation creep regime, the dependence of creep rate on water fugacity is significantly larger for clinopyroxenes for which creep rate increases roughly as the third power of water fugacity [281].

Omphacite is a clinopyroxene that can be disordered, but is rarely disordered in nature because it typically occurs in eglocite facies (metamorphic) rocks as a main phase with garnet. Mg and Al cations order convergently on the M1 positions of the monoclinic structure, leading to omphacite with the space group *P2/n*. The ½[110] translational symmetry is lost in the ordering transition so that antiphase domains (APDs) with the displacement vector **R** = ½[110] can form [283, 284].

Omphacite samples have been found to contain a range of crystal defects: free dislocations, deformation twin lamellae on (100), chain multiplicity faults parallel to (010), non-crystallographic faults terminating in dislocations, APDs, low-angle grain boundaries, recrystallising grains, exsolution lamellae [285]. Apart from the APDs and exsolution lamellae, all these defects result from deformation followed by or contemporaneous with recovery. The first determinations of the Burgers vectors of dislocations in omphacite were made by TEM by Van Roermund and Boland [286]. They identified the Burgers vectors [001], ½<110> and ½<112> (the latter at dislocation nodes) and concluded from the presence of many sub-boundaries that plastic deformation had been dominated by dislocation creep. These results and conclusions have been investigated in more detail in naturally deformed omphacites [287, 288, 289, 290] and in experimentally deformed disordered (*C2/c*) omphacites [291].

Spodumene the lithium clinopyroxene has a Burgers vector {010] and a glide plane (100) [292]. In addition (100) twinning has been documented.

3.6.4. Amphiboles

Clinoamphiboles are monoclinic (C2/m) hydrous double-chain silicates that are common in metamorphic rocks. Dislocation structures have been studied in hornblende ($(Ca,Na,K)_{2-3}(Mg,Fe,Al)_5(OH,F)_2(Si,Al)_2Si_6O_{22}$) and glaucophane ($Na_2Mg_3Al_2(OH,F)_2Si_8O_{22}$).

Mechanical (-101)[-10-1] twins have been identified in experimentally deformed *hornblende* single crystals, as well as dislocations on the (100)[001] slip system [293, 294]. In hornblendes from naturally deformed rocks dislocations on {hk0} planes were documented, mainly [001]

screws [295, 296, 297, 298]. A systematic investigation of dynamically recrystallized hornblende from a high temperature shear zone discovered microstructures typical of dislocation creep, with subgrain boundaries and free dislocations [299]. The primary slip system is (100)[001] consistent with experimental results. Secondary slip systems are (010)[100] and {110}½<110>. There is evidence for cross slip of [001] screws producing helical microstructures (Fig. 13b). Amphibole structures are intermediate between pyroxenes and sheet silicates and indeed "chain multiplicity faults" have been described [300] and transitional structures may be facilitated by movement of partial dislocations [301].

Studies of *glaucophane* from high pressure-low temperature metamorphic rocks reveal a variety of slip systems: (100)[001], {110}[001], (010)[100], {110}½<110> and (001)½<110> [302].

3.6.5. Mica

Micas are some of the earliest minerals where dislocations have been studied [303, 33] using multiple beam interferometric techniques and imaging screw dislocations in the basal plane (001) of dioctahedral *muscovite* (C2/c) ($KAl_2(OH,F)_2AlSi_3O_{10}$). Burgers vectors were determined with TEM [304, 305]) and X-ray transmission topography [306]: ½[110], ½[-110] and [100]. Dislocation microstructures play an important role in recrystallization of mica [307, 308]) (Fig. 14). Experimental deformation of trioctahedral *biotite* (C2/m) ($K(Mg,Fe)_3(OH,F)_2AlSi_3O_{10}$) confirmed ½<110> and [100] as Burgers vectors [309]. Mica minerals are also of industrial interest because of their unique electrical and thermal properties and dislocations are important [310].

3.6.6. Sillimanite, Mullite

Sillimanite and mullite are silicates with Si-Al tetrahedral chains. They occur in high temperature metamorphic rocks and mullite is an important ceramic material. TEM analyses identify [001] as Burgers vector in sillimanite [311, 312]. Dislocations are generally of screw type in the [001] direction (Fig. 14b) and sometimes are dissociated [313]. Dislocation-assisted high temperature deformation has been documented in mullite [314]. The influence of dislocations and strain on the aluminosilicate phase transformations were investigated for kyanite [315].

3.6.7. Feldspars

Feldspars are the most abundant mineral in the Earth's crust and probably on the crusts of the Moon, Venus and Mars as well. Feldspar compositions vary within two solid solutions, the alkali feldspars ($KAlSi_3O_8$-$NaAlSi_3O_8$) and plagioclase feldspars ($NaAlSi_3O_8$-$CaAl_2Si_2O_8$). Feldspars have two excellent cleavages, (001) and (010); these have also been identified as slip planes. All feldspars have low symmetry: C2/m for the high temperature alkali feldspars high sanidine with complete disorder of Si and Al in tetrahedral sites above approximately 1000^{o}C and partially ordered low-sanidine (orthoclase). Lower temperature alkali feldspars albite and microcline are triclinic in the $C\bar{1}$ space group. (A centered unit cell is chosen to conform with the traditional morphologic unit cell and more or less parallel axes in all feldspar structures. Miller indices in this section all refer to the c= 0.7 nm albite unit cell unless indicated.). The Ca end member of plagioclase (anorthite) is in space group $P\bar{1}$ at temperatures below ~250^{o}C, and transforms to $I\bar{1}$ at higher temperatures due to positional disorder [316]. Feldspar structures of intermediate composition are extremely complex due to the competing forces of ordering (Al-Si) and exsolution (Na-K and Na-Ca). Many feldspars display complex microstructures with fine exsolution lamellae (perthite, peristerite, labradorite, bytownite), antiphase boundaries (anorthite) and pervasive twinning (microcline). There is a large literature on TEM studies of these microstructures. The investigations of dislocations are more sporadic and work has been reviewed by Tullis [317] and Gandais and Willaime [318]. While feldspars are major components of a large majority of igneous and metamorphic rocks they are generally quite undeformed and occur as porphyroclasts in a matrix of highly deformed quartz, calcite and pyroxenes.

Experimental and microstructural studies of granitic rocks demonstrate that feldpars are stronger than quartz [226]. By contrast, plagioclase feldspar becomes a weak and interconnected phase controlling the rheology of more mafic gabbroic rocks [200], which are common in the lower continental crust and oceanic crust.

Analyses of dislocations in experimentally and naturally deformed feldspars by TEM indicate that the dominant slip plane is (010). The (010) plane may be favourable due to its low density of largely covalent Si(Al)-O bonds (2 per unit cell, [317, 318, 319]). With this criterion, other possible slip systems include (001), (110), and $(10\bar{1})$ (with 4 Si(Al)-O bonds per unit cell), (100), and (111) (with 6 4 Si(Al)-O bonds per unit cell). [001] is the dominant Burgers vector, which is supported by TEM analyses of experimentally and naturally deformed samples (e.g., [320, 321, 322] but many other dislocations have also been identified.

In *alkali feldspar* experimental studies on Westerley granite with ordered microcline [323, 324] and disordered sanidine [325, 326, 327, 328] show that $(010)[001]$ slip is active in both. Other dislocations are (010)[101] (Fig. 15a), (001)½[110] and $(1\bar{2}\bar{1})$[101]. In naturally deformed alkali feldspars, subgrain formation was observed, indicative of climb [329, 330, 331, 332]. It has been suggested that shear-induced mechanical Albite and Pericline twinning in potassium feldspar may facilitate ordering [333] but this has been disputed [334]. Dislocations have no effect on diffusion in alkali feldspar [335].

There is a considerable literature on dislocations in *plagioclase* but only few experimental studies. In single crystals deformed in orientations with high Schmid factor for both (010)[001] and (001)<110> slip [336], dislocations from both systems are equally abundant (Fig. 15b). This agrees with work by Marshall and McLaren [337, 338]. High temperature deformation of anorthite aggregates has been conducted at conditions near the transition from diffusion creep to dislocation creep mainly produces microstructures typical of diffusion creep [339, 340, 341];

intriguingly, samples deformed dominantly in the diffusion creep regime develop significant preferred orientation [342].

Many slip systems have been observed in naturally deformed plagioclase: in amphibolite (010)[100], (010)[101], (010)[201], (001) ½ [110], $(\bar{1}1\bar{1})$1/2[110], (001) ½[$1\bar{1}0$], $(1\bar{1}\bar{1})$ ½[$1\bar{1}0$], $(1\bar{1}\bar{1})$ ½ [112], and (110) ½ [$1\bar{1}1$] [320, 343], gabbro (010)[001], (001) ½ [110] [344], albite schist [100] [345]. Similar results were obtained in other studies (e.g. [346, 321]). TEM analysis of Burgers vectors in intermediate $I\bar{1}$ plagioclase (with **c** = 1.4 nm) shows dissociation of [100] dislocations: [100] →½[100]+ ½[100]; these partials would be unit dislocations in the $C\bar{1}$ structure (**c** = 0.7 nm).

Texture analysis and subgrain misorientations in both naturally and experimentally deformed plagioclase feldspar are also consistent with (010)[001] as an easy slip system [344, 342, 346, 322, 319, 347, 348]. Other studies suggested additional (010)[100] and (001)[100] slip (e.g., [349, 350, 351]. Obviously a polycrystalline aggregate cannot deform ductilely on a single slip system and other mechanisms including mechanical twinning, dynamic recrystallization, climb or grain boundary sliding have been observed to occur [352]. Subgrain misorientation axis data in porphyroclasts suggest a dominance of (010)[001] slip in porphyroclasts with dominant slip on (010)[100] and (001)[100] in matrix plagioclase. The relative importance of the [001] or [100] Burgers vectors may be a function of temperature, strain rate, H_2O activity or confining pressure [349, 340]. There is experimental evidence for mechanical twinning on the Albite and Pericline systems in plagioclase [353, 354, 355] but the significance for natural plagioclase is not clear [317].

3.7. Sulphides

Early investigations of the deformation modes of various sulphide minerals observed both plastic and brittle behaviour [356, 357, 358, 359]. Considerable subsequent work established slip and twinning mechanisms in several important sulphide ore minerals [157]. We consider here only what is known about dislocations and related phenomena in the most important sulphides.

3.7.1. Iron Sulphides- General

The crystal structures of iron sulphides are straightforward in principle but various aspects of some structures and their behaviour are still uncertain. We emphasize that iron sulphides and iron oxides in natural rocks are often not in equilibrium.

3.7.2. Pyrite

The structure of pyrite, FeS_2 can be considered as a modified NaCl structure (cubic, Pa3): Fe atoms occupy fcc lattice positions; S-S covalently-bonded pairs are also centred on fcc positions but they alternate in directionality. This alternation destroys the overall face-centred symmetry. Pyrite is stable up to 743°C at which temperature it breaks down to pyrrhotite and sulphur [360]. The phase relationship between pyrite and the orthorhombic (Pmnn) polymorph, marcasite, is still enigmatic [361]. In marcasite, S-S pairs point in the same direction in each layer. This causes a distortion from cubic to orthorhombic. The **b** dimension of the marcasite unit cell is almost identical with the lattice parameter of pyrite. In the transformation of marcasite to pyrite an orientation relationship $\{001\}_P$ // $\{101\}_M$, with $<100>_P$//$[010]_M$ is observed [362]. For the reverse transformation of pyrite to marcasite the similar atomic arrangement in pyrite {001} and marcasite {101} planes was mentioned [363].

Pyrite is usually considered to be hard and brittle, deforming by cataclasis up to 400°C and 600MPa confining pressure [364]. However, glide bands were revealed by metallographic methods on the surfaces of some natural samples [365, 366], indicating plastic deformation. Van Goethem et al. [367] studied by TEM what they believed were translation faults in pyrite and concluded from their diffraction contrast analyses that the glide elements were {100}<011>. Plastic deformation can occur under confining pressure at elevated temperatures, predominately by slip on the {100}<010> system [368, 369, 370]. The resulting dislocations tend to be dissociated into partials with co-linear Burgers vectors of type ½ [010]. Planar defects formed in pyrite during growth lie parallel to the {100} planes [371]. The faults were interpreted either as antiphase boundaries (APBs) with a displacement vector, **R** of type ½[110] [367], or as stacking faults with **R** = ±0.29 [110] [371]. In natural pyrites perfect dislocations with **a**<100> Burgers vectors were identified. The Burgers vectors of partials bordering growth stacking faults are out of the defect plane, with the form **b** = ± **R** ± **a**<100>, where **R**, the fault displacement vector, is **a**[0, 0.27, 0.5] [372].

The growth faults may correspond to marcasite lamellae in the pyrite [372, 373]. Indeed HRTEM and electron diffraction revealed them as single (101) layers of marcasite inserted between (002) layers of pyrite [374]. Dislocation loops formed during the growth of pyrite also have the **a**[0, 0.27, 0.5] fault vector [370]. This translation was predicted as the most probable in a coincidence-site-lattice study [375].

A deformation mechanism map for pyrite in the range 0 – 743°C [376] shows that pressure solution [377] and cataclastic flow are the dominant mechanisms operating at geological strain rates under low-grade metamorphic conditions. Diffusion creep occurs under high-grade conditions. Dislocation glide and power-law creep only occur at higher stresses, above ~ 400°C and at fairly high strain rates. Table 1 lists the known slip systems for pyrite.

3.7.3. Chalcopyrite

Chalcopyrite (ccp) is a common accessory mineral in metamorphic and igneous rocks and is found in many types of ore deposits. It is tetragonal and can be envisaged as an ordered sphalerite structure. Both texture determinations and optical studies of deformed samples (e.g. [378] provided the first information about deformation mechanisms in chalcopyrite. Experimental deformation of chalcopyrite single crystals to low strains at 200°C indicated slip on {112}, {100} and (001) [379, 380, 381].

A comprehensive study of dislocation behaviour established the existence of various slip systems (see Table 1) by applying stresses to crystals in different directions at different temperatures [382]. Deformation twinning according to $\{112\}\langle 11\bar{1}\rangle$ also occurred, with high densities of screw-character twinning dislocation in the boundaries. At 200°C $\{112\}\langle\bar{3}11\rangle$ slip was the main mode of deformation, with perfect dislocations having $\frac{1}{2}\langle\bar{3}11\rangle$ Burgers vectors, whereas at 400°C the main slip system was $\{112\}\langle 11\bar{1}\rangle$, with a Burgers vector of $\frac{1}{2}\langle 111\rangle$ for a perfect dislocation (Fig. 16a). A marked change in slip mechanisms occurs in moving from 200 to 400°C: coarse $\{112\}\langle\bar{3}11\rangle$ slip bands predominated at the lower temperature whereas homogeneously distributed dislocations were characteristic of deformation at 400°C. Dislocations with $\frac{1}{2}\langle 111\rangle$ Burgers vectors were able to cross-slip by means of (110) planes. All the types of perfect dislocation were found to dissociate and many different dislocation reactions were also noted.

3.7.4. Galena

Galena, PbS, crystallizes in the cubic NaCl structure. The deformation of polycrystalline galena has been studied experimentally at temperatures up to 500°C and strain rates down to 10^{-8} s^{-1} [383, 384, 378, 385, 386, 387, 377]. Atkinson [388] derived flow laws and calculated deformation maps for polycrystalline galena. According to the latter, dislocation glide is the predominant mechanism at low temperatures and high stresses. The slip systems are two of those found for NaCl, but unlike for NaCl ,{001}<110> is the primary system for galena whereas the primary system for NaCl, {110}<1$\bar{1}$0>, is secondary for galena. These systems have different CRSSs and very different dependences on temperature up to 400°C [157]. When compression was applied along <111> to achieve non-zero Schmid factors for {001}<110> slip, dislocation glide was activated at low stresses, corresponding to CRSSs of 5-10MPa at room temperature [383]. The strain in deformed polycrystalline specimens is usually distributed inhomogeneously, being largely concentrated in kink and deformation bands [389].

TEM studies of dislocations in deformed natural and synthetic galena show that Burgers vector of perfect dislocations is usually ½<110>, as in NaCl. Up to 200°C, slip on the {001} planes mostly involves edge dislocation dipoles and dislocations lying at 45° to their Burgers vector [390]. The density of dipoles increases as the test temperature is decreased. The numbers of "45° dislocations" is largest at low temperatures, which is consistent with the difficulty of activating {110}<1$\bar{1}$0> slip. Dislocation segments inclined to the planes of the TEM specimens were observed to glide in {001}, {110} and also {111} planes under thermally induced stresses [391], which can be attributed to the commonality of the Burgers vector for all three types of plane. This behaviour is probably confined to elevated temperatures in bulk specimens. That the dissociation of dislocations is possible in galena is suggested by high resolution TEM images of dislocations, lying in both {001} and {110} planes, separated by distances of 1nm and 0.6nm, respectively [392].

Many dislocation interactions occur when multiple slip systems operate, as in milled samples, variously resulting in dislocation annihilation, elimination of dipoles, new segments of dislocation and networks [393]. Some of the complex arrangements observed, e.g. dislocation bundles winding around nodes, were attributed to the special conditions created during milling. Cross-slip was observed on {110} and {111} planes, giving rise to segments in the {001} planes and superjogs. Galena that had been naturally work hardened by tectonic events and then softened by annealing shows that rates of softening (due to both recovery and recrystallization) are temperature dependent and related to the amount of deformation [394].

3.7.5. Sphalerite

Sphalerite (zinc blende) is the cubic polymorph of zinc sulphide, ZnS, a II-VI semiconductor. The sulphur atoms form an f.c.c. array and the zinc atoms fill half of the tetrahedral interstices. Glide and dislocations in sphalerite have been researched both directly and indirectly, the latter because several important semiconductors like GaAs (III-V) and CdS (II-VI) are isomorphous with cubic ZnS. Many studies of defects in the III-V compounds have been carried out and so, by inference at least, various aspects of the behaviour of the mineral sphalerite can be anticipated.

Sphalerite consists of alternate planes of Zn and S, stacked in a sequence represented by AaBbCcAa …., etc. Slip occurs on the {111} planes, which are parallel to the stacking layers of

atoms, and in the close-packed directions <1$\bar{1}$0>. The other deformation mode is {111}<11$\bar{2}$> twinning. Slip on the {111} planes causes a flow of charge in the direction of slip [395], thought to occur because the dislocations are charged. Charged dislocations were predicted in ionic crystals many years ago; the electrical effects associated with dislocation motion in ZnS are strong evidence for such defects.

Sphalerite deformed at temperatures up to 500°C and strain rates between 10^{-3} and 10^{-5} s^{-1} produced no twins in Fe-rich sphalerite [396, 397] but abundant twinning in purer specimens [397], together with slip under all test conditions. The annealing of naturally and experimentally deformed sphalerites suggests that static recovery is possible above 300°C and proceeds rapidly above 500°C [397]. Recrystallization produces new grains with numerous growth twins.
The plastic deformation of ZnS indicates that dislocations glide between planes of aB type stacking and not between planes of Aa type [398]. This was determined from the direction of the current generated by slip in relation to the known absolute orientation of the crystal. Dislocation mobility in covalent semiconductors like ZnS is controlled by the high friction Peierls regime [399]. As a consequence, dislocations with a ½<110> Burgers vector lie along <110> atom rows of the {111} glide planes and a dislocation glide loop consists of two types of segment, screw and 60°. In compound semiconductor one can also identify two types of 60° dislocation, depending on the nature of the atom species ending the associated extra half plane; these are α or β dislocations in the usual semiconductor terminology [400]. Dislocations are usually dissociated into two $^1/_6$<11$\bar{2}$> partials that bound a stacking fault; these partials are either 30° or 90° in character.
Because of the high lattice friction, dislocation glide in compounds like ZnS involves two steps [4]: the nucleation of a kink pair on the dislocation and the migration of these kinks along the line. Thereby the line is able to move smoothly. There are only small differences between the velocities of the various types of dislocations in ZnS [401], which contrasts with the findings for III-V semiconductors [402]. The dislocation mobility in ZnS is found to be greatly enhanced by electron radiation [401] although the Peierls regime still operates [403]. Apparently, the enhancement is due to the non-radiative recombination of charge carriers at electronic energy levels associated with the dislocations. The height of the Peierls barrier and the flow stress depends on the charge on dislocations; the latter is increased by illumination [404]. For this reason ZnS shows a positive photoplastic effect, i.e. there is an increase in the flow stress when the sample is illuminated. An after-effect is also found – the flow stress continues to increase after the illumination ceases [405].

3.7.6. Pyrrhotite

There is little information about dislocations in pyrrhotite, a mineral that can occur in several polymorphs, including monoclinic and hexagonal forms. Deformation experiments [378, 364, 397] at temperatures up to 500°C to establish flow laws and to study textures have incidentally identified basal glide in hexagonal NC pyrrhotite. Fracturing contributes to deformation at low temperatures but decreases with temperature; twinning occurs above 200°C.

3.8. High Pressure Minerals

Samples of the Earth to a depth of about 400km occur at the surface as xenoliths brought up from depth by volcanic eruptions. Minerals in the deeper interior are inaccessible to direct observation, but we know broadly about their conditions from geophysical data. One now can

reproduce the high pressure (>300 GPa) and high temperature conditions (>5000 K) in the laboratory. With multi-anvil equipment we can perform deformation experiments at pressures <25GPa on sample with a volume of about $5mm^3$ and a fair degree of control over the sample environment. At higher pressures, diamond anvil cells are used; and the diamond anvils not only exert pressure but also a compressive stress that deforms the material at pressure. With a resistance furnace or laser heating temperarature can be applied to diamond anvil cells [406]. Some materials can be quenched and investigated *ex-situ* with the TEM. High pressure minerals such as stishovite, majorite and $MgSiO_3$ perovskite have been studied this way. But other minerals such as post-perovskite $MgSiO_3$ (a phase of the lowermost mantle) or ε-iron (composing the Earth's inner core) can only be examined *in situ* by optical, spectroscopic and X-ray diffraction techniques. The determination of slip systems can be inferred from texture patterns that develop during diamond anvil compression [407]. An alternative method is to predict deformation activity from first principles based on the Peierls-Nabarro model [408, 409, 410]. We review here briefly what is known about deformation mechanisms of minerals in the lower mantle [411].

3.8.1 Magnesiowustite (see also 3.4.4.)

Magnesiowustite ($Mg_{0.8}\ Fe_{0.2}O$) is thought to be the second most abundant phase in the lower mantle and probably the weakest. Dislocation creep experiments produced textures consistent with slip on both {001} and {110} slip planes in the $<1\bar{1}0>$ direction [412]. The microstructures formed indicated that recovery rate was fast because dislocations were highly mobile and climbed rapidly. Subsequent high-strain deformation experiments on aggregates to shear strains as large as $\gamma = 15.5$ produced first a deformation texture, compatible with dislocation glide in the $<1\bar{1}0>$ direction on all three probable slip systems {111}, {110} and {001} and then transformed into a recrystallization texture [175]. Study of the dislocation microstructure by TEM confirmed the assignment of slip systems. It appeared that the formation of subgrains at relatively low homologous temperatures ($<0.5T_m$) was promoted by cross slip of dislocations between the different glide planes.

3.8.2. Majorite Garnet (see also 3.6.1.)

$(Mg, Fe)SiO_3$ garnet, i.e. majorite – a high pressure phase of pyroxene, is believed to be a major constituent of the transition zone of the mantle. Majorite also occurs in impact melt veins in heavily shocked ordinary chondrites [413]. Majorite in shocked meteorites is cubic, apparently because they cool very quickly. Synthetic majorite transforms at around 1950°C from the cubic phase to a tetragonal structure during its cooling [414]. Studies of majorite in the Tenham meteorite [415] and in the Acfer 90072 (shock grade S6) meteorite [416] have provided important indications about the origins of dislocations in the majorite grains. Dislocations with ½<111> and <100> Burgers vectors may be largely the results of growth and not plastic deformation. Twin and tweed microstructures seen in synthesized majorite at 20 GPa and 1950-2000°C are believed to form due to the cubic-tetragonal transition during quenching [414].

3.8.3. Wadsleyite

As mentioned previously, wadsleyite (β-Mg_2SiO_4) is a high pressure polymorph of forsterite. In wadsleyite deformed at pressures of 14GPa and 1450°C, dislocations with [100] Burgers vectors were identified, many in tangles, although creep had caused numerous dislocations to

form walls [417]. In wadsleyite synthesized from forsterite in a multi-anvil apparatus and deformed in compression in another multi-anvil apparatus at 15-19GPa and temperatures ranging from room temperature to 1800-2000°C, TEM and LACBED studies identify [100], ½<111>, [010], <101> and [001] dislocations [418], the lattermost resulting from dislocations reactions, not slip. Wadsleyite is elastically almost isotropic but slip occurs predominately on planes that do not break Si-O bonds (e.g. (010) and (001)) and dislocation dissociation is crucial [419].

3.8.4 Ringwoodite

Ringwoodite, γ-Mg_2SiO_4, another high pressure polymorph of olivine with spinel-structure is found in shocked meteorites [420] and believed to be present in the mantle transition zone. Like wadsleyite, β-Mg_2SiO_4, ringwoodite is a high pressure phase of forsterite. Peierls-Nabarro modelling of dislocations at 20GPa and 0°K suggest that the Burgers vector for both {110} and {111} slip is $\frac{1}{2}\langle 1\bar{1}0\rangle$ [421]. This is compatible with *in situ* texture information at 6-10GPa compared with polycrystal plasticity simulations [422]. The curvature of glide dislocations can be used as a method of estimating the resolved shear stress [423] in ringwoodite in multi-anvil deformation experiments.

3.8.5 $MgSiO_3$ Perovskite and Post-perovskite

Two important lower mantle minerals are $MgSiO_3$ perovskite and post-perovskite, the latter being a layered $CaIrO_3$ -structured mineral [424] and thought to be the most important phase in the lowermost region (D"-layer). The slip planes for $MgSiO_3$ perovskite are {010} according to experiment [425] and theory [426]. For post-perovskite theory suggests that the slip plane is {110} [426], but *in situ* experiments suggest that slip on (100) or (110) is dominating [68]. Simulations based on the Peierls-Nabarro model provide models for the structure of dislocations cores in perovskite [427] as well as in post-perovskite [136].

3.8.6 Coesite

Coesite is a monoclinic silica mineral that exists at pressures above a few GPa and transforms to stishovite above about 10GPa. Coesite was first identified as a natural phase at Meteor Crater, Arizona [428] and coesite can assist in the recognition of meteorite impacts. The mineral occurs as a shock-induced phase in meteorites and tektites. It also is found in some high pressure metamorphic rocks as in the Dora Maira massif of the Western Alps. A TEM study found Burgers vectors [100], [001] and [110] which correspond to **a** and **a** + **c** [429]. Twinning occurs on (021) [430].

3.8.7 Stishovite

Stishovite is the tetragonal silica polymorph with a rutile structure, stable at pressures in excess of 10GPa. It was found in both terrestrial and meteoritic shocked samples and studied by TEM (e.g. [431, 432]. In experimentally deformed stishovite, Burgers vectors are <100>, <001>, <110> and <101> [433] comparable to rutile (section 3.4.8). Stishovite experimentally deformed at 14GPa and 1300°C [434] shows evidence for slip in the <100> directions on the (001), 010}, and {021} planes, and slip in the [001] direction (corresponding to the shortest Burgers vector) on {100}, {110} and {210}, and in the direction <110> on $\{1\bar{1}0\}$ [435] (Fig. 16b).

4. Simulations

Most dislocation studies in minerals rely on observations with the transmission electron microscope as described in previous sections. These observations are used to determine the dislocation geometry, slip systems and microstructural configurations. But simulations increasingly complement observations. These simulations are on two levels: To predict slip systems, atomistic simulations of generalized stacking faults (e.g. with density functional theory) are combined with a continuum-based description of the dislocation core within the framework of the Peierls-Nabarro model [408, 409, 436]. To investigate microstructural changes during deformation, e.g. during hardening, a discrete dislocation dynamics model has been developed by metallurgists [437]. Both of these approaches are still restricted to single crystals and do not take dislocation interactions across grain boundaries into account.

The Peierls-Nabarro model has been used to determine properties of dislocation cores, the misfit energy and particularly changes with pressure. This is based on the assumption of a planar core which is the most able to glide. It has direct implications for slip systems. In order to move, a dislocation must overcome an energy barrier under an applied stress. The Peierls- Nabarro model has been used to constrain dislocation core sizes and Peierls stresses in several oxides and silicates relevant to the earth's mantle, particularly periclase [438], olivine [439, 440], ringwoodite [421], silicate perovskite [427] and silicate postperovskite [441]. In olivine the Peierls modeling explained why pressure affects some slip systems more than others [410].

Dislocation dynamics has been recently applied to minerals such as periclase [442] (Fig. 17) to explore the hardening in this material through interactions and reactions between dislocations gliding in non-coplanar slip systems and olivine [410]. Such simulations may in the future become important tools to predict plasticity based on dislocation geometry for a variety of conditions that cannot be explored experimentally.

5. Dislocation densities and strain energy

It is not easy to obtain an accurate estimation of dislocations densities from TEM images. X-ray topography is more reliable but is only applicable to materials with low dislocation densities. Fortunately, X-ray diffraction provides a way of estimating and monitoring dislocation densities and other defining parameters of microstructure. For example, a cellular dislocation microstructure gives an asymmetry in diffraction profiles according to Wilkens [443]. In recent years, analysis of diffraction peak profiles and line broadening [444, 445] has emerged as a powerful tool for the determination of such parameters, although so far mostly applied to metals and composites (e.g. [446, 447]). The effect of dislocation contrast on line broadening has also been investigated [7].

As a result of this research, it is now recognized that various different properties of diffraction peak profiles address several microstructural parameters by modelling crystallite size and strain. These profile properties are peak broadening, asymmetric peak shape, peak shift and anisotropic broadening [448, 449]. The method has been applied to the characterization of diamond/graphite [450] and forsterite [451] and it can be expected to be used increasingly.

The effect of dislocations on the reactivity of minerals has been investigated mainly for quartz with a few studies on feldspar and calcite, both experimentally and theoretically. The strain energy in a crystal lattice caused by dislocations can be described using ideal elastic behaviour [452, 453, 4]. The increase in the internal energy of quartz caused by dislocations can be calculated by the following equation [452]:

$$\Delta E = D(\mu b^2/8\pi K)\ln((r_h^2 + d^2)/r_h^2) \quad (1)$$

with:

$$r_h^2 = \mu b^2 V/8\pi^2 K \Delta H_m$$

and where symbols are (with values for quartz in parentheses):
D = dislocation density (cm^{-2})
μ = shear modulus (44.4 GPa)
ν = Poisson's ratio (0.077)
V = molar volume (22.688 $cm^3\ mol^{-1}$)
ΔH_m = enthalpy of melting (8.159 kJ mol^{-1})
b = magnitude of Burgers vector (0.4913 to 0.7304 nm)
d = mean distance between dislocations $(1/D)^{1/2}$
K = constant related to the Burgers vector orientation, where K = 1 for a screw dislocation and K = 1 - ν for an edge dislocation, where ν is Poissons ratio.

The internal energy is also dependent on the orientation of the dislocation relative to the Burgers vector. The equation assumes that the dependence is small, and is represented by the constant K [454]. Substituting the values into equation (1), one can calculate the increase in energy of quartz caused by a particular dislocation density on a particular slip system containing a certain type of dislocation. This equation indicates, even for a dislocation density as high as 10^{11} cm^{-2}, that the energy contributed to quartz is only 6% of the dissolution energy.

Dislocations may not contribute much to the bulk energy increase of a mineral, but they may nevertheless affect the reactivity by providing favorable areas for chemical processes such as precipitation and dissolution to occur. The local strain energy is more concentrated around the dislocations themselves, and is not distributed through the bulk crystal. Frank [455] has shown that the large amount of energy released locally at a dislocation site during dissolution decreases or eliminates the energy barrier (caused by the change in free surface energy) that prevents the removal of atoms. This may lead to regions where the reactivity is enhanced, potentially allowing also reactions other than dissolution to occur at higher rates [452, 456]. For dissolution it corresponds to etch pits, dissolution spirals or hollow cores at dislocations.

An increase by 2 to 3 orders of magnitude in dislocation density has been shown to increase the dissolution rate by as much as a factor of 3 and this is highly significant for the stability and dissolution of quartz [457, 458], of feldspars [459, 460] and of carbonates [461]. Based on strain energy produced by dislocations in subgrain boundaries, Twiss [462] developed a theory to use the recrystallized grain size as a paleopiezometer.

Dissolution properties of minerals have some significant industrial applications. Concrete produced with highly deformed aggregate rocks such as mylonites, where quartz has high dislocation densities, are subject to the deleterious alkali silica aggregate reaction [463, 235]. As the dislocation density increases by an order of magnitude, the expansion becomes threefold. (Fig. 18). This causes ultimate fracture of the structure.

6. Conclusions

In spite of the enormous structural complexities, from triclinic plagioclase feldspar to piezoelectric trigonal quartz, from plasticity of ice at ambient conditions to post-perovskite deforming at highest pressures and temperatures in the lowermost mantle, from simple salt rocks to a polyphase material such as gneiss, dislocations in minerals are remarkably similar to those in

metals and similar descriptions and interpretations apply. As in metals, dislocations are most relevant in the understanding of deformation processes. They provide the mechanism for deformation by slip that produces on the macroscopic scale preferred orientation and anisotropy. Dislocation microstructures are a driving force for recrystallization. They also play important roles in chemical reactions as well as in dissolution. Minerals compose rocks, and rock deformation is a key ingredient to understanding the dynamic earth, both mountain building and shearing in the crust as well as convection in the deep earth. Similar flow laws apply to metals and rocks because mechanisms are similar, even though time scales are entirely different. Geologic times and slow strain rates compensate for the much slower dislocation mobility in minerals. Based on Orowan's equation, long-term deformation associated with mantle convection and flow in the crust is accommodated by dislocations with velocities in the range of 10^{-12} to 10^{-13} m/s.

But minerals are not just significant in the context of geologic history. They are also important raw materials: most ceramics or their constituents are minerals: alumina, silica, perovskite, spinel. Cement minerals are extremely complex compounds and their strength and stability is of enormous technical importance. We are convinced that a close interaction between materials scientists, mineral physicists and structural geologists will continue as an extremely stimulating endeavour. The investigation of dislocations remains an exciting field of research. Advanced experimental techniques allow for sophisticated imaging at all scales. Modeling of dislocation movements and dislocation interactions has become possible with high-speed computers.

This chapter of the last volume of "Dislocations in Solids" has been dedicated to dislocation in minerals. As we have shown, minerals were among the first materials in which dislocations were observed and with the advent of transmission electron microscopy and sample preparation techniques in the early nineteen-sixties a wide range of studies were undertaken to describe and quantify dislocation microstructures in the wide diversity of minerals. While compiling this review, what was perhaps the most striking revelation is what we still do not know: for example the Burgers vectors in the common mineral - quartz, hardening behaviour while undergoing high strains, the actual mechanism of recrystallization in many deformed rocks and the deformation of polymineralic aggregates, to name just a few. With such a rich background we are sure that future researchers will be inspired to continue investigating the roles of dislocations in minerals.

Mineral	Main slip systems		Known Burge vectors (* is the shorte
	Low temperature	High Temperature	
Carbonates:			
Calcite	**r** $^{-}${10$\bar{1}$4}<20$\bar{2}\bar{1}$>, **f** $^{-}${$\bar{1}$012}<10$\bar{1}$1>	**c** (0001)<2$\bar{1}\bar{1}$0>, **r** $^{-}${10$\bar{1}$4}<20$\bar{2}\bar{1}$>, **f** $^{-}${$\bar{1}$012}<10$\bar{1}$1>	⅓<20$\bar{2}\bar{1}$>, ⅓<10$\bar{1}\bar{1}$> ⅓<2$\bar{1}\bar{1}$0>*
Dolomite	**c** (0001)<2$\bar{1}\bar{1}$0>, **f** $^{-}${$\bar{1}$012}<10$\bar{1}$1>	**c** (0001)<2$\bar{1}\bar{1}$0>, **r** $^{-}$<10$\bar{1}$4}<20$\bar{2}\bar{1}$> **f** $^{-}${$\bar{1}$012}<10$\bar{1}$1>	⅓<2$\bar{1}\bar{1}$0>*, ⅓<20$\bar{2}$ ⅓<10$\bar{1}\bar{1}$>
Aragonite	{100}[001], {110}[001]	{100}[001], {110}[001]	[001]*
Felspars:			
Plagioclase	———	(010)[001], (001)<110>, (001)[100], (010)[100]	[001]*, [100]
Alkali-felspar	———	(010)[001], (010)[101], (001)[110]	[001]*, ½<110>
Halides:			
Halite (rocksalt)	{110}<1$\bar{1}$0>	{110}<1$\bar{1}$0>, {100}<0$\bar{1}$1>, {111}<1$\bar{1}$0>	½<110>*
High P ressure phases:			
Coesite	———	(010) [001]	[001], [100]*, [110
Majorite	———	———	½<111>*, <100>
Magnesio-wustite	———	{001}<1$\bar{1}$0>, {110}<1$\bar{1}$0>	½<110>*
Post perovskite	———	———	———
Ringwoodite	———	{111}<1$\bar{1}$0>, {100}<0 $\bar{1}$1>	½<110>*
Stishovite	———	(001)<100>, {010}<100>, {100}<001>, {110}<1$\bar{1}$0>	<100>, [001]*, <11 <101>
Wadsleyite	———	{101}<111>, (010)[100], {011}[100]	½<111>, [100]*
Olivine	(010)[001], {110}[001]	{0*k*1}[100], (010)[100]	[001]*, [100]

Sulphides: Chalcopyrite	{112}<$\bar{3}$11>, (001)<110>	{112}<11$\bar{1}$>,	½<$\bar{3}$11>, ½<111>*
Pyrite	———	{100}<010>, {100}<011>	<010>*
Galena	{001}<110>	{001}<110>, {1$\bar{1}$0}<110>	½<110>*
Sphalerite	{111}<1$\bar{1}$0>	{111}<1$\bar{1}$0>	½<110>*
Pyroxenes Orthorhombic	———	(100)[001]	[001]*, [010]
Monoclinic	———	(100)[001], {110}[001]	[001]*
Oxides: Corundum	(0001)<11$\bar{2}$0>	(0001)<11$\bar{2}$0>, {10$\bar{1}$1}<0111>	⅓<11$\bar{2}$0>*, ⅓<011
Hematite	(0001)<11$\bar{2}$0>, {11$\bar{2}$0}<1$\bar{1}$00>	(0001)<11$\bar{2}$0>, {11$\bar{2}$0}<1$\bar{1}$00>	⅓<11$\bar{2}$0>*, <1$\bar{1}$00>
Periclase, wustite	{110}<1$\bar{1}$0>	{110}<1$\bar{1}$0>, {001}<1$\bar{1}$0>	½<110>*
Perovskite	———	{110}<1$\bar{1}$0>	½<1$\bar{1}$0>*, [010]
Rutile	———	{101}<10$\bar{1}$>, {110}[001]	[001]*
Spinel	{111}<1$\bar{1}$0>, ({110}<1$\bar{1}$0> when non-stoichiometric)	{110}<1$\bar{1}$0>	½<110>*
Magnetite	———	{111}<1$\bar{1}$0>	½<110>*
Quartz	(0001)<11$\bar{2}$0>	(0001)<11$\bar{2}$0>, {10$\bar{1}$0}[0001], {10$\bar{1}$0}[1$\bar{2}$10], {10$\bar{1}$0}[1$\bar{2}$13]	⅓<11$\bar{2}$0>*

Table 1. The main slip systems and Burgers vectors for major minerals. A dash means that either there is no activity or that there is no reliable data.

Acknowledgements
P. Cordier supplied reference material and reviewed our draft; we thank him for the invaluable help. W. Muller and W. Skrotzki provided micrographs. HRW acknowledges support from NSF (EAR-0337006). We are also indebted to the Editor, John Hirth for thoughtful comments that helped improve the manuscript.

References

[1] J.P.Poirier, Creep of Crystals (Cambridge Univ. Press, Cambridge, UK, 1985).
[2] J.P.Poirier, in: Minerals: Physics and Crystallography – A Handbook of Physical Constants. AGU Reference Shelf 2, (American Geophysical Union, Washington, D.C., 1995), p. 237.
[3] D. Hull and D.J. Bacon, Introduction to Dislocations (Pergamon Press, Oxford, 1984).
[4] J.P. Hirth and J. Lothe, Theory of Dislocations (McGraw-Hill, New York, 1968).
[5] S. Amelinckx, The Direct Observation of Dislocations, Solid State Physics 6 (Academic Press, New York and London, 1964).
[6] A.C. McLaren, Transmission Electron Microscopy of Minerals and Rocks (Cambridge University Press, Cambridge, 1991).
[7] T. Ungár and A. Borbély, Appl. Phys. Lett. 69 (1996) 3173.
[8] H. Seidentopf, Phys. Zeit. 6 (1905) 855.
[9] V. Volterra, Ann. Ec. Norm. Sup. 24 (1907) 400.
[10] L. Prandtl, Zeit. angew. Math. Phys. 8 (1928) 85.
[11] E. Orowan, Z. Physik 89 (1934) 605.
[12] M. Polanyi, Z. Physik 89 (1934) 660.
[13] G.I. Taylor, Proc. Roy. Soc. A145 (1934) 362.
[14] E. Rexer, Zeit. Phys. 78 (1932) 538.
[15] D.J. Barber, K.B. Harvey and J.W. Mitchell, Philos. Mag. 2 (1957) 704.
[16] S. Amelinckx and W. Dekeyser, Acta Metall. 6 (1958) 34.
[17] J.M. Hedges and J.W. Mitchell, Philos. Mag. 44 (1953) 223 and 357.
[18] D.H. Zeuch, Trans.Amer. Geophys. Union 55 (1974) 418.
[19] D. L. Kohlstedt, C. Goetze, W.B. Durham and J.B Vander Sande, Science 191 (1976) 1045.
[20] Y. Guéguen, Tectonophys. 39 (1977) 231.
[21] P.B. Hirsch, R.W. Horne and M.J. Whelan, Phil. Mag. Ser. 8, 1 (1956) 677.
[22] W. Bollmann, Phys. Rev. 103 (1956) 1588.
[23] V.Z. Bengus, Sov. Phys. Cryst. 8 (1963) 322.
[24] M. Paulus and F. Reverchon, in: Le Bombardement Ionique. Proc. Conf. held at Bellevue, France, 1961 (C.N.R.S., France, 1962) p. 223.
[25] D.J. Barber, J. Mat.Sci. 5 (1970) 1.
[26] L.J. Griffin, Phil. Mag. 41 (1950) 196.
[27] A.P. Honess, The Nature, Origin and Interpretation of Figures on Crystals (John Wiley and Sons, New York, 1927).
[28] R. Knipe, Tectonophys. 64 (1980) T11.
[29] J. J.Gilman and W.G. Johnston, in: Report on the Lake Placid Conference on Dislocations and Mechanical Properties of Crystals, ed. R.M. Fisher (John Wiley and Sons, New York, 1957) p.116.
[30] D.J. Barber, J. Appl. Phys. 33 (1962) 3141.
[31] M.W. Wegner and J.M. Christie, Contrib. Mineral. Petrol. 43 (1974) 195.
[32] A.R. Lang, in: Modern Diffraction and Imaging Techniques in Materials Science, eds. S. Amelinckx, R. Gevers, G. Remaut, J. Van Landuyt (North Holland, Amsterdam, 1980) p.407.
[33] S. Amelinckx, Nature 169 (1952) 580.
[34] S. Amelinckx and P. Delavignette, J. Appl. Phys. 31 (1960a) 1691, 2126.

[35] S. Amelinckx and P. Delavignette, Nature 185 (1960b) 603.
[36] S. Amelinckx and P. Delavignette, in: Direct Observations of Imperfections in Crystals, eds. J.B. Newkirk and J.H. Wernick (Interscience, New York, 1962) p.295.
[37] S. Amelinckx and P. Delavignette, Phil. Mag. 5 (1960c) 533.
[38] S. Amelinckx and P. Delavignette, J. Appl. Phys. 32 (1961) 341
[39] S.V. Radcliffe, A.H. Heuer, R.M. Fisher, J.M. Christie and D.T. Griggs, Science 167 (1970) 638.
[40] P.E. Champness and G.W. Lorimer, Contrib. Mineral. Petrol. 33 (1971) 171.
[41] J.M. Christie, J.S. Lally, A.H. Heuer, R.M. Fisher, D.T. Griggs and S.V. Radcliffe, Proc. 2nd Lunar Sci. Conf., Geochim. Cosmochim. Acta, Suppl.2, 1 (1971) 69.
[42] H.-R. Wenk, M. Ulbrich and W.F. Müller, Proc. 3rd Lunar Sci. Conf., Geochim. Cosmochim. Acta, Suppl.3, 1 (1972) 569.
[43] P.R Buseck (ed.) Minerals and Reactions at the Atomic Scale: T ransmission Electron Microscopy. Rev. in Mineral., 27 (Min. Soc. Amer., Washington, D.C.,1992).
[44] H.-R. Wenk and A. Bulakh, Minerals: Their Constitution and Origin (Cambridge University Press, Cambridge, 2004).
[45] D. Stöffler and F. Langenhorst, Meteoritics 29 (1994) 155.
[46] H. Leroux, Eur. J. Mineral. 13 (2001) 253.
[47] P.B. Hirsch, A. Howie, R.B. Nicholson, D.W. Pashley and M.J. Whelan, Electron Microscopy of Thin Crystals (Butterworths, London, 1965).
[48] A.J. Ardell, J.M. Christie and J.W. McCormick, Phil Mag. 29 (1974) 1399.
[49] R. Carpenter and J. Spence, Acta Cryst. A38 (1992) 55.
[50] J.-P. Morniroli, P. Cordier, E.Van Cappellen, Jin Min Zuo and J. Spence, Microsc. Microanal. Microstruct. 8 (1997) 187.
[51] U. F. Kocks and H. Mecking, Prog. Mater. Sci 48 *(*2003*)* 171-273.
[52] D.J. Barber, in: Preferred Orientation in Deformed Metals and Rocks: An Introduction to Modern Texture Analysis, ed. H.-R. Wenk (Academic Press, Orlando, 1985), p. 149.
[53] R. von Mises, Zeit. angew. Math. Mech. 8 (1928) 161.
[54] A. Nicolas and J.P. Poirier, in: Crystalline Plasticity and Solid State Flow in Metamorphic Rocks (John Wiley, London, 1976).
[55] F. Haessner, Recrystallization of Metallic Materials (Riederer, Stuttgart, 1978).
[56] F.J. Humphreys and M. Hatherly, Recrystallization and Related Annealing Phenomena (Oxford. Univ. Press, 1995)
[57] G. Glover and C.M. Sellars, Metall. Trans.4 (1973) 765.
[58] N.A. Liddell, P.P. Phakey and H.-R. Wenk, in: Electron Microscopy in Mineralogy, H.-R. Wenk Edit. (Springer-Verlag, Berlin-Heidelberg-New York, 1976) p 419.
[59] H.G. Avé Lallemant and N.L. Carter, Bull. Amer. Geol. Soc. 81 (1970) 2203.
[60] J.-C.C. Mercier, in: Preferred Orientation in Deformed Metals and Rocks: An Introduction to Modern Texture Analysis, ed. H.-R. Wenk (Academic Press, Orlando, 1985) p.407 .
[61] G.I. Taylor, J. Inst. Met. 62 (1938) 307.
[62] B. Sander, Einführung in die Gefügekunde der Geologischen Körper, Vol. 2 (Springer, Wien, 1950).
[63] F.J. Turner, D.T. Griggs and H.C. Heard, Geol. Soc. Amer. Bull. 65 (1954) 883.
[64] F.J. Turner, D.T. Griggs, R.H. Clark and R.H. Dixon, Geol. Soc. Amer. Bull. 67 (1956) 1259.

[65] L. Ratschbacher, H.-R. Wenk, and M. Sintubin, J. Struct. Geol. 13 (1991) 369.
[66] P. R. Dawson and H.-R. Wenk. Phil. Mag. A 80 (2000) 573.
[67] H.-R.Wenk, S. Speziale, A.K. McNamara and E.J. Garnero, Earth Planet. Sci. Lett. 245 (2006) 302.
[68] S. Merkel, A.K. McNamara, A. Kubo, S. Speziale, L. Miyagi, Y. Meng, T.S. Duffy and H.-R. Wenk, Science 316 (2007) 1729.
[69] H.-R. Wenk, G. Canova, Y. Brechet and L. Flandin, Acta mater. 45 (1997) 3283.
[70] U. F. Kocks, C.N. Tomé and H.-R. Wenk, Texture and Ansiotropy (Cambridge Univ. Press, 2000).
[71] H.-R. Wenk, in: Plastic Deformation of Minerals and Rocks, ed. S.-i. Karato and H.-R. Wenk, Rev. in Mineral. 51 (Mineral. Soc. Amer, Washington, D.C., 2002) p. 291.
[72] J.M. Christie and A.J. Ardell, in: Electron Microscopy in Mineralogy, H.-R. Wenk Edit. (Springer-Verlag, Berlin-Heidelberg-New York, 1976) p 374.
[73] D. Bernaerts and S. Amelinckx, in Handbook of Microscopy, Vol. 3: Applications, in Materials Science, Solid State Physics and Chemistry, eds. S. Amelinckx, D. van Dyck, J. van Landuyt and G. van Tendeloo (VCH, Weinheim, 1997) p.437.
[74] T.E. Mitchell and A.H. Heuer, in: Dislocations in Solids, Vol. 12 (Elsevier, Amsterdam, 2005) p 339.
[75] J.J. Papike Edit., Planetary Minerals, Rev. in Mineralogy Vol. 36 (Min. Soc. Amer., Washington, D.C., 1998).
[76] M. Montagnat, J. Weiss, J. Chevy, P. Duval, H. Brunjail, P. Bastie and J. Gil Sevillano, Philosophical Magazine 86 (2006) 4259.
[77] J. Castaing, Annal. de Phys. 6 (1981) 195.
[78] J.J. Gilman and W.G. Johnston, In Conference on Dislocations and Mechanical Properties of Crystals, eds. J. C. Fisher, W. G. Johnston, R. Thomson and T. Vreeland, Lake Placid, N.Y., 1956 (John Wiley, New York, 1957).
[79] J.J. Gilman and W.G. Johnston, J.Appl. Phys. 30 (1959) 129.
[80] E. Schmid and W. Boas, in Plasticity of Crystals (F.A. Hughes, London, 1950).
[81] A.G. Evans, C. Roy and P.L. Pratt, Proc. Brit. Ceram. Soc. 6 (1966) 173.
[82] E. Schüller and S. Amelinckx, Naturwiss. 47 (1960) 491.
[83] L T Chadderton, E Johnson and T Wohlenberg, Phys. Scr. 13 (1976) 127.
[84] S. Amelinckx, Nuovo Cim. Suppl. 7 (1958) 569.
[85] H. Blank and C. Ronchi, J. Nucl. Mater. 31 (1969) 1.
[86] A.G. Evans and P.L. Pratt, Philos. Mag. 20 (1969) 1213.
[87] K.H.G. Ashbee and F.C. Frank, Philos. Mag. 21 (1970) 211.
[88] W.A. Brantley and Ch.L. Bauer, Phys. Stat. Sol. (b) 40 (1970) 707.
[89] M.L. Kronberg, Acta. Metall. 5 (1957) 507.
[90] P.T. Sawbridge and E.C. Sykes, Philos. Mag. 24 (1971) 33.
[91] R.J. Gaboriaud, M. Boisson and J. Grilhe, J. Phys.C: Solid State Phys. 8 (1975) 3499.
[92] A.H. Heuer, R.J. Keller and T.E. Mitchell, In Deformation Processes in Minerals, Ceramics and Rocks, eds. D.J. Barber and P.G. Meredith (Unwin Hyman, London, 1990) p.377.
[93] P.L. Pratt, Acta Metall. 1 (1953) 103.
[94] G.W. Groves and A. Kelly, Phil. Mag. 8 (1963) 877.
[95] N.L. Carter and H.C. Heard, Amer. J. Sci. 269 (1970) 193.
[96] H. Strunk, Phys.Stat. Solidi (a) 11(1972) K105.
[97] W.Skrotzki and P. Haasen, J. de Phys. C3, suppl. 6 (1981) 119.

[98] J. Hesse, Phys.Stat. Sol. 9 (1965) 209.
[99] G. Fontaine, J. Phys. Chem. Solids 29 (1968) 209.
[100] G. Fontaine and P. Haasen, Phys. Stat. Sol.31 (1969) K67.
[101] L.A. Davis and R.B. Gordon, Phys. Stat. Sol. 36 (1969) K133.
[102] S. Amelinckx, In Report on Conference on Dislocations and Mechanical Properties of Crystals, eds. J. C. Fisher, W. G. Johnston, R. Thomson and T. Vreeland, Lake Placid, N.Y., 1956 (Wiley, New York, 1957) p.3.
[103] F.C. Frank, Report on Conference on Defects in Crystalline Solids (Phys. Soc., London, Bristol, 1954).
[104] N. Thomson, Proc. Roy. Soc. B 66 (1953) 481.
[105] J. E. Caffyn, J. C. de Freitas, T. L. Goodfellow, Phys. Stat. Sol. (b) 9 (1965) 333.
[106] L.W. Hobbs and M.J. Goringe, In Microscopie Électronique (Société Française de Microscopie Electronique, Paris, 1970) p. 289.
[107] R.J. Reeder, in: Carbonates: Mineralogy and Chemistry, ed. R.J. Reeder, Rev. in Mineral. Vol. 11 (Mineral. Soc. Amer., Washington, D.C., 1983), p.1.
[108] M. Sarikaya, K.E. Gunnison, M. Yasrebi and I.A. Aksay, in: Materials Synthesis Utilizing Biological Processes, Mater. Sci. Soc. Symp. Proc. 174, eds. M. Alper, P. D. Calvert, and P. C. Rieke (Mater. Res. Soc, Pittsburgh, 1990) p.109.
[109] H.-R. Wenk, D.J. Barber and R.J. Reeder, in: Carbonates: Mineralogy and Chemistry, ed. R.J. Reeder, Rev. in Mineral. Vol. 11 (Mineral. Soc. Amer, Washington, D.C., 1983) p. 301.
[110] D.J. Barber, H.-R. Wenk, J. Gomez-Barreiro, E. Rybacki and G. Dresen, Phys. Chem. Mineral. 34 (2007) 73.
[111] J.H.P. De Bresser and C.J. Spiers, Tectonophys. 272 (1997) 1.
[112] D.J. Barber and H.-R. Wenk, J. Mat.Sci. 8 (1973) 500.
[113] D.J. Barber and H.-R. Wenk, in: Electron Microscopy in Mineralogy, ed. H.-R. Wenk (Springer, Berlin, 1976) p. 428.
[114] H.-R. Wenk, C.S. Venkitasubramanyan and D.W. Baker, Contrib. Mineral. Petrol. 38 (1973) 81.
[115] D.J. Barber and H.-R. Wenk, Phys. Chem. Mineral. (1979)
[116] R.E. Keith and J.J. Gilman, Acta Metall. 8 (1960) 1.
[117] V.I. Startsev, V.Z. Bengus, FF. Lavrent'ev and L.M. Soifer, Kristallogr. 5 (1960) 737.
[118] R. W. Cahn, Philos. Mag. [Suppl.] 3 (1954) 363.
[119] G. Rose, Abh. Konig. Akad. Wiss. Berlin 23 (1868) 57.
[120] R.J. Reeder, in: Minerals and Reaction at the Atomic Scale: Transmission Electron Microscopy, ed. P.R. Buseck, Rev. in Mineral. Vol. 27 (Mineral. Soc. Amer., Washington, D.C., 1992), p. 381.
[121] R.J. Reeder and H.-R. Wenk (1979) Geophysical Res. Lett., 6 (1979) 77.
[122] K. Reksten, Phys. Chem. Minerals 17 (1990) 266.
[123] R.J. Reeder and J. L. Prosky, J. Sedim. Petrol. 56 (1986) 237.
[124] D.J. Barber, H.C. Heard, M.S. Paterson and H.-R. Wenk, Nature 269 (1977) 789.
[125] V. Trommsdorff and H.-R. Wenk, Schweiz. Mineral. Petrog. Mitt. 45 (1965) 551.
[126] D.J. Barber, H.C. Heard and H.-R. Wenk, Mat. Sci. Eng. A 175 (1994) 83.
[127] D.J. Barber and H.-R. Wenk, Europ. J. Mineral. 13 (2001) 221.
[128] D.V. Higgs and J.W. Handin, Geol. Soc. Amer. Bull. 70 (1959) 245.
[129] D.J. Barber, H.C. Heard and H.R. Wenk, Phys. Chem. Minerals 7 (1981) 271.
[130] S. Frisia-Bruni and H.-R. Wenk, J. Sed. Petr. 63 (1993) 1049.

[131] J. W. McTigue and H.-R. Wenk, Am. Mineral. 70 (1985) 1253.
[132] P. Gillet and M. Madon, Bull. Mineral. 105 (1982) 590.
[133] C. Kearney, Z. Zhao, B.J.F. Bruet, R. Radovitsky, M.C. Boyce and C. Ortiz, Phys. Rev. Lett. 96 (2006) #255505.
[134] T. Bretheau, J. Castaing, J. Rabier and P. Veyssière, Adv. Phys. 28, (1979) 829, 835.
[135] J.D. Gale and A.L. Rohl, Mol. Simul. 29 (2003) 291.
[136] P. Carrez, D. Ferré and P. Cordier, Nature 446 (2007) 68.
[137] J.B. Wachtman, Jr. and L.H. Maxwell, J. Amer. Ceram. Soc. 37 (1954) 291.
[138] D.J. Barber and N.J. Tighe, Philos. Mag. 11 (1965) 495.
[139] D.J. Barber and N.J. Tighe, Philos. Mag. 14 (1966) 531.
[140] D.J. Gooch and G.W. Groves, J. Amer. Ceram. Soc. 55 (1972) 105.
[141] D.J. Gooch and G.W. Groves, Philos. Mag. 28 (1973a) 623.
[142] D.J. Gooch and G.W. Groves, J. Mater. Sci. 8 (1973b) 1238.
[143] R.E. Tressler and D.J. Barber, J. Amer. Ceram. Soc. 57 (1974) 1.
[144] R.E. Tressler and D.J. Michael, in: Deformation of Ceramic Materials, eds. R.C. Bradt and R.E. Tressler (Plenum Press, New York, 1975) p.195.
[145] B.J. Hockey, In Deformation of Ceramic Materials, eds. R.C. Bradt and R.E. Tressler (Plenum Press, New York, 1975) p.167.
[146] K. Veit, Neues Jahrb. Mineral., Geol. Palaeontol., Beilageband, 45 (1921) 121.
[147] E. Stofel and H. Conrad, Trans. AIME 227 (1963) 1053.
[148] R.L. Bertolotti and W.D. Scott, J. Amer. Ceram. Soc. 54 (1971) 286.
[149] W.D. Scott, in: Deformation of Ceramic Materials, eds. R.C. Bradt and R.E. Tressler (Plenum Press, New York, 1975) p.151.
[150] B. J. Pletka, T.E. Mitchell and A.H. Heuer, in: Deformation of Ceramic Materials, eds. R.C. Bradt and R.E. Tressler (Plenum Press, New York, 1975) p.181.
[151] R. Chang, J. Appl. Phys. 31 (1960) 484.
[152] M.V. Klassen-Neklyudova, V.G. Govorkov, A.A. Urusovskaya, N.N. Voinova and E.P. Koslovskaya, Phys. Stat. Sol. 39 (1970) 679.
[153] K.C. Radford and P.L. Pratt, Proc. Brit. Ceram. Soc. 15 (1970) 185.
[154] M.C. Rodriguez, A. Munoz, J. Castaing, P. Veyssière and A.D. Rodriguez, J. Europ. Ceram. Soc. 27 (2007) 3317.
[155] T.E. Mitchell, B.J. Pletka, D.S. Philips and A.H. Heuer, Philos. Mag. 34 (1976) 441.
[156] J.B. Bilde-Sörensen, A.R. Tholen, J.J. Gooch and G.W. Groves, Philos. Mag. 33 (1976) 877.
[157] H. Siemes and Ch. Hennig-Michaeli, in: Preferred Orientation in Deformed Metals and Rocks: An Introduction to Modern Texture Analysis, ed. H.-R. Wenk (Academic Press, Orlando, 1985) p. 335.
[158] Y. Hidaka, T. Anraku and N. Otsuka, Oxidation of Metals 58 (2002) 469.
[159] H. Siemes, B. Klingenberg, E. Rybacki, M. Neumann, W. Schafer, E. Jansen and K. Kunze, Ore Geol. Rev. 33 (2008) 255.
[160] L.A. Bursill and R.L. Withers, Philos Mag. 40 (1979a) 213.
[161] L.A. Bursill and J.L. Peng, Philos. Mag. Lett. A60 (1989) 1.
[162] L.A. Bursill, J.L. Peng and X.D. Fang Austral. J. Chem. 45(1992) 1527.
[163] L.A. Bursill and R.L. Withers, J. Appl. Cryst. 12 (1979b) 287.

[164] L.A. Bursill and P.J. Lin, In Defects and Processes in the Solid State: Geoscience Applications, The McLaren Volume, eds. J.N. Boland and J.D. FitzGerald (Elsevier, Amsterdam, 1993) p.447.
[165] T. Kasama, U. Golla-Schindler and A. Putnis, Amer. Mineral. 88 (2003) 1190.
[166] J.S. Lally, A.H. Heuer and G.L. Nord, in: Electron Microscopy in Mineralogy, ed. H.R. Wenk (Springer Verlag, Berlin, 1976), p.214.
[167] W.M. Cullen, M.J. Marcinkowski and E.S.P. Das, Surface Sci. 36 (1973) 395.
[168] G.L. Nord, Jr., Amer. Mineral.74 (1989) 160.
[169] G.L. Nord, Jr., in: Minerals and Reactions at the Atomic Scale: Transmission Electron Microscopy, ed. P.R. Buseck. Rev. Mineral. Vol. 27 (Miner. Soc. Amer., Washington, D.C., 1992) p.455.
[170] W. Hüther and B. Reppich, Philos. Mag. 28 (1973) 363.
[171] M. Hurm and B. Escaig, J. de Phys. 34, C9 (1973) 347.
[172] J.B. Bilde-Sörensen, J. Amer. Ceram. Soc. 55 (1972) 606.
[173] M. Hurm, J. Phys. Paris 34, C9 (1973) 347.
[174] S.M. Copley and J. Pask, J. Amer. Ceram. Soc. 48 (1965) 139.
[175] F. Heidelbach, I. Stretton, F. Langenhorst and S. Mackwell, J. Geophys. Res.-Solid Earth 108, B3 (2003) #2154.
[176] M. Bystricky, F. Heidelbach and S. Mackwell, Tectonophys. 427 (2006) 115.
[177] S. Mann, R.B. Frenkel and R.P. Blakemore, Nature 310 (1984) 405.
[178] K. L. Thomas-Keprta, D.A. Bazylinski, J.L. Kirschvink, S.J. Clement, D.S. McKay, S.J.Wentworth, H. Vali, E.K. Gibson, C.S. Romanek, Geochim. Cosmocim Acta 64 (2000) 4049.
[179] D.J. Barber and E.R.D. Scott, Proc. Nat. Acad. Sci. 99 (2002) 6556.
[180] P. Müller and H. Siemes, Tectonophys. 23 (1974) 105.
[181] L. Hwang, A.H. Heuer and T.E. Mitchell, in: Deformation of Ceramic Materials, eds. R.C. Bradt and R.E. Tressler (Plenum Press, New York, 1975) p.257.
[182] J. Hornstra, J. Phys. Chem. Solids 15 (1960) 311.
[183] S.H. Kirby and P. Veyssière, Philos. Mag.A 41 (1980) 129.
[184] P. Veyssière, S.H. Kirby and J. Rabier, J. Phys., Paris 41 (1980) C6-115.
[185] P. Veyssière, J. Rabier and H. Garem, Philos. Mag. A39 (1979) 815.
[186] N. Doukhan, J. Phys. Lett., Paris 40 (1979) 603.
[187] P. Veyssière and C.B. Carter, Philos. Mag. Lett. 57 (1988) 211.
[188] M.H. Lewis, Philos. Mag. 17 (1968) 481.
[189] K.C. Radford and C.W.A. Newey, Proc. Brit. Ceram. Soc. 9 (1967) 131.
[190] N. Doukhan, R. Duclos and B. Escaig, J. Physique 34 (1973) C9, 379.
[191] A. Navrotsky and D.J. Weidner (eds) Perovskite: a Structure of Great Interest to Geophysics and Materials Science (Amer. Geophys. U., Washington, D.C., 1989)
[192] J.P. Poirier, S. Beauchesne and F. Guyot, in: Perovskite: A Structure of Great Interest to Geophysics and Materials Science, eds. A. Navrotsky and D. Weidner (Amer. Geophys. Union, Washington, D.C., 1989) p. 119.
[193] Hu Meisheng, H.-R. Wenk and D. Sinitsyna, Amer. Mineral.77 (1992) 359
[194] D. Ferré, P. Carrez and P. Cordier, Phys. Rev. B 77 (2008) 1.
[195] W.M. Hirthe and J.O. Brittain, J. Amer. Ceram. Soc. 45 (1963) 546; 46, 411.
[196] K.H.G. Ashbee and R. E. Smallman, Proc. Roy. Soc. A 274 (1963) 195.
[197] K.H.G. Ashbee, R. E. Smallman and G.K. Williamson, Proc. Roy. Soc. A 276 (1964) 542.

[198] M.G. Blanchin and G. Fontaine, Phys. Stat. Sol. A 29 (1975) 491.
[199] K. Suzuki, M. Ichihara and S. Takeuchi, Philos. Mag. A 63 (1991) 657.
[200] R. Burgmann and G. Dresen, Ann. Rev. Earth Planet. Sci. 36 (2008) 531.
[201] J.R. Rice, N. Lapusta and K. Janjith, J. Mech. Phys. Solids, 49 (2001) 1865-1898,
[202] A.C. McLaren and P.P. Phakey, J. Appl. Phys. 36 (1965) 3244.
[203] M. Linker, S. Kirby, A. Ord and J. Christie, J. Geophys. Res. 89 (1984) 4241.
[204] R.D. Baeta, R. D., and K. H. G. Ashbee, Philos. Mag. 22 (1970) 601.
[205] J.D. Blacic, Tectonophys. 27 (1975) 271.
[206] J. Muto and J. Tullis, *Eos Trans. AGU 88*(52) (2007) T13B-1338.
[207] R. Heilbronner and J Tullis, J. Geophys. Res. 111 (2006) B10202.
[208] V.G. Toy, D.J. Prior and R.J. Norris, J. Struct. Geol. 30 (2008) 602.
[209] G. Hirth, C. Teyssier and W.J. Dunlap, Int. J. Earth Sci. (Geol. Rundschau) 90 (2001) 77.
[210] M. Stipp, H. Stuenitz, R. Heilbronner and S.M. Schmid, J. Struct. Geol. 24 (2002)1861.
[211] J. Pehl and H.-R. Wenk, J. Struct. Geol. 27 (2005) 1741.
[212] A. Schubnikov, K. Zinserling K, Z. Kristallogr. 83 (1932) 243.
[213] J. Tullis and T.E. Tullis, Am. Geophys. U. Monogr. 16 (1972) 67.
[214] H.-R. Wenk, I. Lonardelli, E. Rybacki, G. Dresen, N. Barton, H. Franz and G. Gonzalez, Phys. Chem. Minerals 33 (2006) 667.
[215] D.J. Barber and H.-R. Wenk, Phys. Chem. Minerals 17 (1991) 492.
[216] W.B. Kamb, J. Geophys. Res. 66 (1961) 259.
[217] A.G. McLellan, J. Physics C 11 (1978) 4665.
[218] M.S. Paterson, Rev. Geophys. Space Phys.11 (1973) 355.
[219] I. Shimizu, J. Geophys. Res. 97 (1992) 4587.
[220] J.C. Doukhan and L. Trepied, Bull. Minéral., 108 (1985) 97.
[221] D.T. Griggs and J.D. Blacic, Science 147 (1965) 292.
[222] D.T. Griggs, Geophys. J. Roy. Astr. Soc.14 (1967) 19.
[223] D.L. Kohlstedt, B. Evans and S.J. Mackwell, J. Geophys. Res. 100B (1995) 17587.
[224] G.C. Gleason and J. Tullis, Tectonophysics 247 (1995) 1.
[225] J. Farver and R.A. Yund, Chem Geol 90 (1991) 55.
[226] J. Tullis, Rev. Mineral. Geochem. 51 (2002) 51.
[227] Kronenberg, Rev. Mineral. Geochem. 29 (1994) 123.
[228] D.H. Mainprice and M.S. Paterson, J. Geophys. Res. 89 (1984) 4257.
[229] A.C. McLaren, J.D. Fitz Gerald and J. Gerretsen, Phys. Chem. Minerals 16 (1989) 465.
[230] B.E. Hobbs, in: H.-R. Wenk ed., Preferred Orientation in Deformed Metals and Rocks: An Introduction to Modern Texture Analysis (Academic Press, Orlando, FL. 1985) p 463.
[231] M.C. Paterson, In: S.-I. Karato and M. Toriumi (eds) Rheology of Solids and of the Earth (Oxford University Press, Oxford, 1989) p.107.
[232] P. Cordier and J.C. Doukhan, Phil. Mag. A 72 (1995) 497.
[233] P. Cordier and J.C. Doukhan, Eur. J. Mineral. 1 (1989) 221.
[234] T.G. Blenkinsop and M.R. Drury, J. Struct. Geol. 10 (1988) 673.
[235] H.-R. Wenk, P. Monteiro and K. Shomglin, J. Mater. Sci. 43 (2007) 1278.
[236] H.H. Hess, Nature 203 (1964) 629.
[237] J.P. Montagner and T. Tanimoto, J. Geophys. Res. 95 (1990) 4797.
[238] C.B. Raleigh, J. Geophys. Res. 73 (1968) 369.
[239] N.L. Carter NL and H.G. Avé Lallemant, Geol. Soc. Am. Bull. 81 (1970) 2181.
[240] C.B. Raleigh and S.H. Kirby, Min. Soc. Am. Spec. Pap. 3 (1970) 113.

[241] C. Goetze and D.L. Kohlstedt, J. Geophys. Res. 78 (1973) 5961.
[242] K. Fujino, H. Nakazaki, H. Momoi, S.I. Karato and D.L. Kohlstedt, Phys. Earth Planet. Inter. 78 (1993)131.
[243] P. Raterron, E. Amiguet, J. Chen, L. Li and P. Cordier, Phys. Earth Planet Inter. 172 (2008) 74.
[244] W.B. Durham and C. Goetze, J. Geophys. Res. 82 (1977) 5737.
[245] S.J. Mackwell, D.L. Kohlstedt and M.S. Paterson, J. Geophys. Res. 90 (1985)11319.
[246] Q. Bai, S.J. Mackwell, D.L. Kohlstedt , J. Geophys. Res. 96 (1991) 2441.
[247] P.N. Chopra PN and M.S. Paterson, J. Geophys. Res. 89 (1984)7861.
[248] S.I. Karato, M.S. Paterson and J.D. Fitz Gerald, J. Geophys. Res. 91 (1986) 8151.
[249] S.I. Karato, In Earth's DeepWater Cycle, ed. SD Jacobsen, S van der Lee, (2006) 113. Washington, DC: AGU
[250] D.L. Kohlstedt, In Water in Nominally Anhydrous Minerals, ed. H Keppler, JR Smyth Reviews in Mineralogy and Geochemistry, Vol. 62 (Mineral. Soc. Amer., Washington, DC, 2006) p377.
[251] I. Katayama, H. Jung and S.I. Karato, Geology 32 (2004)1045.
[252] D.L. Kohlstedt, H. Keppler, D.C. Rubie, Contrib. Mineral. Petrol. 123 (1996) 345.
[253] W.T. Stacy, J.A. Pistorius and M.M. Janssen, J. Cryst. Growth, 22 (1974) 37.
[254] C.-Z. Ge, N.-B Ming and D. Feng, Philos. Mag. A 53 (1986) 285.
[255] H. Carstens, Contrib. Mineral. and Petrol. 24 (1969) 348.
[256] J. Ando, K Fujino and T. Takeshita, Phys. Earth Planet. Interiors 80 (1993) 105.
[257] V. Voegelé, P. Cordier, V. Sautter, T.G. Sharp, J.M. Lardeaux and F.O. Marques, Phys. Earth Planet. Int. 108 (1998) 319.
[258] C.D. Storey and D.J. Prior, J. Petrol. 46 (2005) 2593.
[259] F.M. Allen, B.K. Smith, and P.R. Buseck, Science 238 (1987) 1965.
[260] D.L. Kohlstedt and J.B. Vander Sande, Contrib. Mineral. Petrol. 42 (1973) 169.
[261] A.C. McLaren and M.A. Etheridge, Contrib. Mineral. Petrol. 57 (1976) 163.
[262] L. Nazé, N. Doukhan, J.C. Doukhan and K. Latrous, Bull. Minéral. 110 (1987) 497.
[263] J.V. Ross and K.C. Nielsen, Tectonophys. 44 (1978) 233.
[264] J.M. Steuten and H.L.M.van Roermund, Tectonoph. 157 (1989) 331.
[265] J.-C. Van Duysen, N. Doukan and J.-C. Doukhan, Phys. Chem. Mineral. 12 (1985) 39.
[266] S.J. Mackwell, Geophys. Res. Lett. 18 (1991) 2027-2030.
[267] C.B. Raleigh and J.L. Talbot , Am. J. Sci. 265 (1967) 151.
[268] H.G. Avé Lallemant, Tectonophys. 48 (1978) 1.
[269] N. Doukhan, J. Ingrin and J.-C. Doukhan, Terra Abst. 3 (1991) 72.
[270] J.J. Kollé and J.D. Blacic, J. Geophys. Res. 88 (1983) 2381.
[271] S.H. Kirby and J.M. Christie,Phys. Chem. Mineral. 1 (1977) 137.
[272] S.H. Kirby and A.K. Kronenberg, J. Geophys. Res. 89 (1984) 3177.
[273] J.N. Boland and T.E. Tullis, Geophys. Monogr. Amer. Geophys. U. 36 (1986) 35049.
[274] J. Ingrin, N. Doukhan, J.-C. Doukhan, J. Geophys. Res. 96 (1991)14287.
[275] J. Ingrin, N. Doukhan, J.-C. Doukhan, European J. Mineral. 4 (1992) 1291.
[275] W. Skrotzki, Tectonophys. 229 (1994) 43.
[276] W. Skrotzki, Europ. J. Mineral. 13 (2001) 245.
[277] R.S. Coe and S.H. Kirby, Contrib. Mineral. Petrol. 52 (1975) 29.
[278] W. F. Müller, N. Jb. Mineral. 2 (1974) 83.

[279] C.B. Raleigh, S.H. Kirby, N.L. Carter and H.G. Avé Lallemant, J. Geophys. Res. 76 (1971) 4011.
[280] M. Bystricky and S. Mackwell, J. Geophys. Res. 106 (2000) 13443.
[281] S. Chen, T. Hiraga and D.L. Kohlstedt, J. Geophys. Res. 111 (2006) B08203, doi:10.1029/2005JB003885.
[282] S. Hier-Majumder, S. Mei S and D.L. Kohlstedt , J. Geophys. Res. 110 (2005) B07406, doi:10.1029/2004JB003414.
[283] P.E. Champness, Amer. Mineral. 58 (1973) 540.
[284] P.P. Phakey and S. Ghose, Contrib. Mineral. Petrol. 39 (1973) 239.
[285] W.F. Müller and G. Franz, N. Jb. Mineral. Abh. 184 (2008) 285.
[286] H.L.M. Van Roermund and J.N. Boland, Tectonophys. 78 (1981) 403.
[287] H.L.M. Van Roermund and J.M. Lardeaux, Mineral. Mag. 55 (1991) 397.
[288] M. Buatier, H.L.M. Van Roermund, M.R. Drury and J.M. Lardeaux, Tectonophys.195 (1991) 11.
[289] G. Godard and H.L.M. Van Roermund, J. Struct. Geol.17, (1995) 1425.
[290] F.E. Brenker, D.J. Prior and W.F. Müller, J. Struct. Geol. 24 (2002) 1991.
[291] J. Zhang, H.W. Green II and K.N. Bozhilov, Earth Planet. Sci. Lett. 246 (2006) 432.
[292] J.-C. Van Duysen and J.-C. Doukhan, Phys. Chem. Minerals 10 (1984) 125-132.
[293] T.P. Rooney, R.E. Riecker and A.T. Gavasci, Geology 3 (1975) 364.
[294] D.J. Morrison-Smith, Amer. Mineral. 61 (1976) 280.
[295] K.H. Brodie, Tectonophys. 78(1981) 385.
[296] C. Biermann and H.L.M. van Roermund, Tectonophys. 95 (1983) 267
[297] K.H. Brodie and E.H. Rutter, Adv. Phys. Chem. 4 (1985) 138.
[298] R.J. Cumbest, M.R. Drury, H.L.M. van Roermund and C. Simpson, Contrib. Mineral. Petrol. 101 (1989) 339.
[299] W. Skrotzki , phys. stat. solidi (a) 131 (1992) 605.
[300] D.R. Veblen and P.R. Buseck, Amer. Mineral. 66 (1981) 1107.
[301] J.E. Chisholm, J. Mater. Sci. 8 (1973) 475.
[302] B. Reynard, P. Gillet and C. Willaime, Europ. Mineral. 1 (1989) 611.
[303] Tolanski and Morris, Phil. Mag. 28 (1947) 137.
[304] S. Amelynckx and P. Delavignette, Proc. Tech. Conf. on Direct Observations of Imperfections in Crystals, Missouri, 295–356 (1962) ?style, eds? Publishers?
[305] J. Demny, Z. Naturf. A 18 (1963) 1088.
[306] J. L. Caslavsky and K. Vedam, Philos. Mag. 22 (1970) 176, 255.
[307] I.A. Bell and C.J.L. Wilson, Tectonophys. 78 (1981) 201.
[308] M.A. Etheridge and B.E. Hobbs, Contrib. Mineral. Petrol. 43 (1974) 111.
[309] R. Christoffersen and A.K. Kronenberg, J. Struct. Geol. 15 (1993) 1077.
[310] Chang-Lin Kuo, Yue-Hong Huang, Shi-Ji Fan,
[311] H.-R. Wenk, Neues Jahrbuch Mineral. Abh. 146 (1983) 1-14.
[312] D. Menard and J.C. Doukhan, Journ. Phys. 39 (1978) L19-22.
[313] A. Lefevre and J. Paquet, Bull Mineral. 106 (1983) 287-292.
[314] L. Taherabadi, J.E. Trujillo, T. Chen, J.R. Porter and M.L. Mecartney, Journal of the European Ceramic Society 28 (2008) 371-376
[315] D. Menard, J.C. Doukhan and J. Paquet, Bull. Mineral. 102 (1979) 159-162.
[316] J.V. Smith and W.L. Brown, Feldspar Minerals, Vol. 1 (Springer Verlag Heidelberg, 1988)

[317] J. Tullis, in Feldspar Mineralogy, Rev. Mineral. Vol. 2 P.H. Ribbe ed. (Mineral. Soc. Amer., Washington D.C., 1983) p. 297.
[318] M. Gandais and C. Willaime, in Feldspars and Feldspathoids, NATO ASI Series C-137, W.L. Brown ed. (Reidel, Dordrecht, 1984) p. 207.
[319] S. Ji, S., D. Mainprice and F. Boudier, J. Struct. Geol. 10 (1988) 73.
[320] T. Olsen and D. Kohlstedt, Phys. Chem. Miner. 11 (1984) 153.
[321] Y. Montardi and D. Mainprice, Bull. Mineral. 110 (1987) 1.
[322] S. Ji and D. Mainprice, J. Geol. 98 (1990) 65.
[323] J. Tullis and R.A. Yund, J. Geophys. Res. 82 (1977) 5707.
[324] J. Tullis and R.A. Yund, J. Struct. Geol. 2 (1980) 5707.
[325] E. Scandale, M. Gandais and C. Willaime, Phys. Chem. Mineral. 9 (1983) 182.
[326] C. Willaime and M. Gandais, Bull. Soc. Fr. Mineral. Cristallogr. 100 (1977) 263.
[327] C. Willaime, J.M. Christie and M.-P. Kovacs, Bull. Mineral. 102 (1979) 168.
[328] Y. Zheng and M. Gandais, Phil. Mag. A 55 (1987) 329.
[329] G. Bossiere and A. Vauchez, Tectonophys. 51 (1978) 57.
[330] M. Sacerdoti, H. Labernardiere and M. Gandais, Bull. Mineral. 103 (1980) 148.
[331] J.-L. Vidal, L. Kubin, P. Debat and J.-C. Soula, Lithos 13 (1980) 247.
[332] S.K. Hanmer, J. Struct. Geol. 4 (1982) 197.
[333] H.L. Alling, J. Geol. 29 (1921) 193.
[334] R.A. Yund and J. Tullis, Contrib. Miner. Petrol. 72 (1980) 297.
[335] R.A. Yund, J. Quigley and J. Tullis, J. Metam. Geol. 7 (1989) 337.
[336] H. Stünitz, J.D. Fitz Gerald and J. Tullis, Tectonophys. 372 (2003) 215.
[337] D.B. Marshall and A.C. McLaren, J. Mater. Sci. 12 (1977) 893.
[338] D.B. Marshall and A.C. McLaren, Phys. Chem. Minerals 1 (1977) 351.
[339] A. Dimanov, G. Dresen, X. Xiao and R. Wirth, J. Geophys. Res. 104 (1999) 10483.
[340] S. Ji, Z. Jiang, E. Rybacki, R. Wirth, D. Prior, B. Xia, Earth Planet. Sci. Lett. 222 (2004) 377.
[341] Z. Wang, G. Dresen and R. Wirth, Geophys. Res. Lett. 23 (1996) 3111.
[342] J. Gómez Barreiro, I. Lonardelli, H.-R. Wenk, G. Dresen, E. Rybacki E, Y. Ren and C.T. Tome, Earth Planet. Sci. Lett. 264 (2007) 188.
[343] T. Olsen and D. Kohlstedt, Tectonoph. 111 (1985) 107.
[344] D.M. Ague, H.-R. Wenk and E. Wenk, Geophys. Monogr. 56 (1990) 173.
[345] D.B. Marshall and C.J. Wilson, Contrib. Mineral. Petrol. 57 (1976) 55.
[346] S. Ji and D. Mainprice, Tectonophys. 147 (1987) 145.
[347] R. Kruse, H. Stünitz and K. Kunze, J. Struct. Geol. 23 (2001) 1781.
[348] J. Feinberg, H.-R. Wenk, G.R. Scott and P. Renne, Tectonophys. 420 (2006) 345.
[349] S. Ji, R. Wirth, E. Rybacki and Z. Jiang, J. Geophys. Res. 105 (2000) 16,651.
[350] Y. Xie, H.-R. Wenk and S. Matthies, Tectonophys. 370 (2003) 269.
[351] L. Mehl and G. Hirth, J. Geophys. Res. 113 (2008) B05202.
[352] J. Tullis and R.A. Yund, Geol. 15 (1987) 606.
[353] I. Borg and J. Handin, Tectonophys. 3 (1966) 249.
[354] I. Borg and H.C. Heard, Contrib. Mineral. Petrol. 23 (1969) 128.
[355] D.B. Marshall and A.C. McLaren, Phys. Stat. Solidi 41 (1977) 231.
[356] O. Mügge, Neues Jahrb.Mineral. (1898) 71.
[357] O. Mügge, Neues Jahrb.Mineral. (1920) 24.
[358] K. Veit, Neues Jahrb.Mineral. Beilageband, 45 (1922) 121.

[359] M. Buerger, Amer. Mineral. 13 (1928) 1 and 35.
[360] G. Kullerud and H.S. Yoder, Econ. Geol. 54 (1959) 533.
[361] E.H. Nickel, Canad. Mineral. 9 (1968) 311.
[362] M.E. Fleet, Canad. Mineral. 10 (1970) 225.
[363] G. Brostigen and A. Kjekshus, Acta Chemica Scandinavia 24 (1970) 2983.
[364] B.K. Atkinson, Econ. Geol. 70 (1975) 473
[365] A. Mookherjee, Econ. Geol. 66 (1971) 200.
[366] P. Natale, Soc. Italiana Mineralogica Petrologica, Rendiconti, 27 (1971) 537.
[367] L. Van Goethem, J. Van Landuyt and S. Amelinckx, Amer. Mineral. 63 (1978) 548.
[368] J.L. Graf, B.J. Skinner, J. Bras, M. Fagot, C. Levade and J.-J. Couderc, Econ. Geol. 76 (1981) 738.
[369] S.F. Cox, M.A. Etheridge and B.E. Hobbs, Econ. Geol. 76 (1981) 2105.
[370] C. Levade, J.-J. Couderc, J. Bras, M. Fagot, Philos. Mag.A 46 (1982) 307.
[371] M. Fagot, C. Levade, J.-J. Couderc and J. Bras, Philos. Mag. A 38 (1978)
[372] M. Fayard, D. Gratias and R. Portier, Philos. Mag. A, 41 (1980) 125.
[373] M.E. Fleet, P.J. MacLean and J. Barbier, Econ. Geol. Monograph 6 (1989) 356.
[374] I. Dodony, M. Posfal and P.R. Buseck, Amer. Mineral. 81 (1996) 119.
[375] D. Gratias, R. Portier, M. Fayard and M. Guymont, Acta Cryst. A 35 (1979) 885.
[376] K.R. McClay and P.G. Ellis, Mineral Mag. 47 (1983) 527.
[377] K. R. McClay, J. Geol. Soc. London, 134 (1977) 57.
[378] B.K. Atkinson, Trans. Inst. Min. Metall. 83B (1974) 19.
[379] J.-J. Couderc and C. Hennig Michaeli, Phys. Chem. Minerals 13 (1986) 393.
[380] J.-J. Couderc and C. Hennig Michaeli, Philos. Mag. A 57 (1987) 301.
[381] C. Hennig Michaeli and H. Siemes, Tectonophys. 135 (1987) 217.
[382] C. Hennig Michaeli and J.-J. Couderc, in: Deformation Processes in Minerals, Ceramics and Rocks, The Mineralogical Society Series, Vol. 1 (Unwin Hyman, London,1990) p. 391.
[383] K.D. Lyall and M.S. Paterson, Acta Metall. 14 (1966) 371.
[384] H. Siemes, in: Experimental and Natural Rock Deformation, ed. P. Paulitsch (Springer, Berlin, 1970) p.165.
[385] B.K. Atkinson, Econ. Geol. 71 (1976) 513.
[386] B.K. Atkinson, Phys. Chem. Mineral. 2 (1978) 305.
[387] B.C. Salmon, B.R. Clark and W.C. Kelly, Econ. Geol. 69 (1974) 1.
[388] B.K. Atkinson, Geol. Foeren. Stockholm Foerh. 99 (1977) 186.
[389] K.R. McClay and B.K. Atkinson, Tectonophys. 39 (1977) 175.
[390] A. Foitzik, W. Skrotzki and P. Haasen, Phy. Status Solidi A 121 (1990) 81.
[391] A. Foitzik, P. Haasen and W. Skrotzki, Philos. Mag. A 64 (1991a) 29.
[392] A. Foitzik, W. Skrotzki and P. Haasen, Mater. Sci. Eng. A 132 (1991b) 77.
[393] C. Deeb, J. Castaing, P. Walter, P. Penhoud, P. Veyssière and P. Martinetto, Metall. Mater. Trans. A35 (2004) 2223.
[394] R.L. Stanton and H.G. Willey, Econ. Geol. 65 (1970) 182.
[395] Y.A. Osip'yan and V.F. Petrenko, Zh. Eksp. Teor. Fiz. 69 (1975) 1362; Soviet Phys. JETP 42 (1975) 695.
[396] H.J. Saynisch, in: Experimental and Natural Rock Deformation, ed. P. Paulitsch (Springer, Berlin, 1970) p.209.
[397] B.R. Clark and W.B. Kelly, Econ. Geol. 68 (1973) 332.
[398] C.C. Speake, P.J. Smith, T.R. Lomer and R.W. Whitworth, Philos. Mag. A 38 (1978) 603.

[399] C. Levade, J.-J. Couderc and A. Kara, Phys. Status Solidi 112 (1989) 89.
[400] H. Alexander, J. Phys. Colloques 40 (1979) C6-1.
[401] A. Faress, C. Levade and G. Vanderschaeve, Philos. Mag. A 68 (1993) 97.
[402] H. Steinhart and Schäfer, Acta Metall. 19 (1971) 65.
[403] C. Levade and G. Vanderschaeve, J. Cryst. Growth 197 (1999) 565.
[404] V.F. Petrenko and R.W. Whitworth, Philos. Mag. A 41 (1980) 681.
[405] A. Kara, J.-J. Couderc, C. Levade and G. Vanderschaeve, Phys. Status sol. 122 (1990) 545.
[406] P. Cordier, H. Couvy, S. Merkel and D. Weidner, In EMU Notes in Mineralogy, Vol. 7, ed. R. Miletich (Eur. Mineral. Union, 2005) p. 339.
[407] H.-R.Wenk, I. Lonardelli, S. Merkel, L. Miyagi, J. Pehl, S. Speziale and C.E. Tommaseo, J. Phys. Cond. Matter 18 (2006) S933.
[408] R. Peierls, Proc. Phys. Soc. 52 (1940) 34.
[409] F.R.N. Nabarro, Proc. Phys. Soc. Lond. 59 (1947) 256.
[410] J. Durinck, P. Carrez and P. Cordier, Eur. J. Mineral. 19 (2007) 631.
[411] P. Cordier, in Plastic Deformation in Minerals and Rocks, Rev. Mineral. Geochem. Vol. 51, eds. S.-I. Karato and H.R. Wenk (Min. Soc. Amer., Chantilly, VA ., 2002) p. 137.
[412] I. Stretton, F. Heidelbach, S. Mackwell and F. Langenhorst, Earth Planet. Sci. 194 (2001) 229.
[413] B. Mason, J. Nelen and J.S. White, Science 160 (1968) 66.
[414] N, Tomioka, K. Fujino, E. Ito, T. Katsura, T. Sharp and T. Kato, Europ. J. Mineral. 14 (2002) 7.
[415] M. Madon and J.-P. Poirier, Science 207 (1979) 66.
[416] V. Voegelé, P. Cordier, F. Langenhorst and S. Heinemann, Eur. J. Mineral. 12 (2000) 695.
[417] T.G. Sharp, G.Y. Bussod and T. Katsura, Phys. Earth. Planet. Sci. Int. 86 (1994) 69.
[418] E. Thurel and P. Cordier, Phys. Chem. Minerals 30 (2003) 256.
[419] E. Thurel, J. Douin and P. Cordier, Phys. Chem. Minerals 30 (2003b) 271.
[420] D. Stöffler, K. Keil and E.R.D. Scott, Geochim. Cosmochim. Acta 55 (1991) 3485.
[421] P. Carrez, P. Cordier, D. Mainprice and A. Tommasi, Eur. J. Mineral.18 (2006) 149.
[422] H.-R. Wenk, G. Ischia, N. Nishiyama, Y. Wang and T. Uchida, Phys. Earth Planet. Int. 152 (2005) 191.
[423] P. Cordier, E. Thurel and J. Rabier, Geophys. Res. Lett. 29 (2002) 68.
[424] A.R. Oganov and S. Ono, Nature 430 (2004) 445.
[425] H.-R. Wenk, I. Lonardelli, J. Pehl, J. Devine, V. Prakapenka, G. Shen and H.-K. Mao, Earth Planet. Sci. Lett. 226 (2004) 507.
[426] A.R. Oganov, R. Martonak, A. Laio, P. Raiteri and M. Parrinello, Nature 438 (2005) 1142.
[427] D. Ferré, P. Carrez and P. Cordier, Phys. Earth Planet. Inter. 163 (2007) 283.
[428] E. C. T. Chao, E. M. Shoemaker and B. M. Madsen, Science 132 (1960) 220.
[429] F. Langenhorst and J.-P. Poirer, Earth Planet. Sci. Lett. (2002)
[430] D. Jacob, P. Cordier, J.-P. Morniroli and H.-P. Schertl, Eur. J. Mineral. 20 (2008) 119.
[431] S.W. Kieffer, P.P. Phakey and J.M. Christie, Contrib. Mineral. Petrol. 59 (1976) 41.
[432] J.C. White, In Defects and Processes in the Solid State: Geoscience Applications, The McLaren Volume, eds. J.N. Boland and J.D. FitzGerald (Elsevier, Amsterdam, 1993) p.69.
[433] P. Cordier and T.G. Sharp, Phys. Chem. Minerals 25 (1998) 548.
[434] P. Cordier and D.C. Rubie, Mater. Sci. Eng. A309 (2001) 38.
[435] M. Texier and P. Cordier, Phys. Chem. Minerals 33 (2006) 394.
[436] G. Schoeck, Acta Materialia 54 (2006) 4865.

[437] L.P. Kubin, B. Devincre, M. Tang, J. Comput. Aided Mater. Des. 5 (1998) 31.
[438] C.R. Miranda, S. Scandolo, Comput. Phys. Commun. 169 (2005) 24.
[439] J. Durinck, A. Legris and P. Cordier, Amer Mineral. 90 (2005) 1072.
[440] J. Durinck, B. Devincre, L. Kubin and P. Cordier, Amer Mineral. 92 (2007) 1346.
[441] P. Carrez, D. Ferré and P. Cordier, Philos. Mag. 87 (2007) 3229.
[442] P. Carrez, P. Cordier, B. Devincre and L.P. Kubin, Mater Sci Eng. A 400-401 (2005) 325.
[443] M. Wilkens, Phys. Stat. Solidi (a) 2 (1970) 359.
[444] T. Ungár, Acta Metall. 32 (1984) 333.
[445] N. Ji, J. Mater. Sci. 29 (1994) 1553.
[446] N. Ji, J.L.Lebrun, B. Marty, M. Bessiere and B.Chenal, J. Mater. Sci.Lett. 14 (1995) 674.
[447] J. Gubicza, L. Balogh, R.J. Hellmig, Y. Estrin, T. Ungár, Materials Science and Engineering A 400–401 (2005) 334.
[448] T. Ungár, Mat. Sci. Eng A 309 (2000) 14.
[449] I. Groma and A. Borbély, in: Diffraction analysis of the Microstructure of Materials, Springer Series in Materials Science 68 (Springer Verlag, Berlin Heidelberg, 2004) p.285.
[450] C. Pantea, J. Gubicza, T. Ungár, G. Voronin and T. W. Zerda, Phys. Rev. B 66 094106 (2002).
[451] K. Nyilas, H. Couvy, P. Cordier and T. Ungár, Z. Kristall. Suppl. 23 (2006) 135.
[452] A.E. Blum, R.A.Yund and A.C. Lasaga, Geochim. Cosmochim. Acta 54 (1990) 283.
[453] W. Bollmann, Crystal Defects and Crystalline Interfaces (Springer Verlag, Heidelberg, 1970).
[454] A.C. Lasaga and A.E. Blum, Geochim. Cosmochim. Acta 50 (1986) 2363.
[455] F.C. Frank, Acta. Crystall. 4 (1951) 497.
[456] S.L. Brantley, S.R. Crane, D.A. Credar, R. Hellmann and R. Stallard, Geochim. Cosmochim. Acta 50 (1986) 2349.
[457] R.P. Wintsch and J. Dunning, J. of Geophys. Res. 90 (1985) 3649.
[458] M. Liu, R.A. Yund, J. Tullis, L. Topor and A. Navrotsky, Phys. Chem. Minerals 22 (1995) 67.
[459] G.R. Holdren, W.H. Casey, H.R. Westrich, M. Carr, M., Boslough, Chemical Geology, 70 (1988) 79.
[460] R.A. Yund, J. Quigley and J. Tullis, J. Metam. Geol. 7(1989) 337.
[461] J. Schott, S. Brantley, D. Credar, C. Guy, M. Borcsik and C. Willaime, Geochim. Cosmochim. Acta 53 (1989) 373.
[462] R.J. Twiss, Pure Appl. Geophys. 115 (1977) 227
[463] P.J.M. Monteiro, K. Shomglin, H.-R. Wenk and N.P. Hasparyk, ACI Materials Journal 98 (2001) 179.

Figures

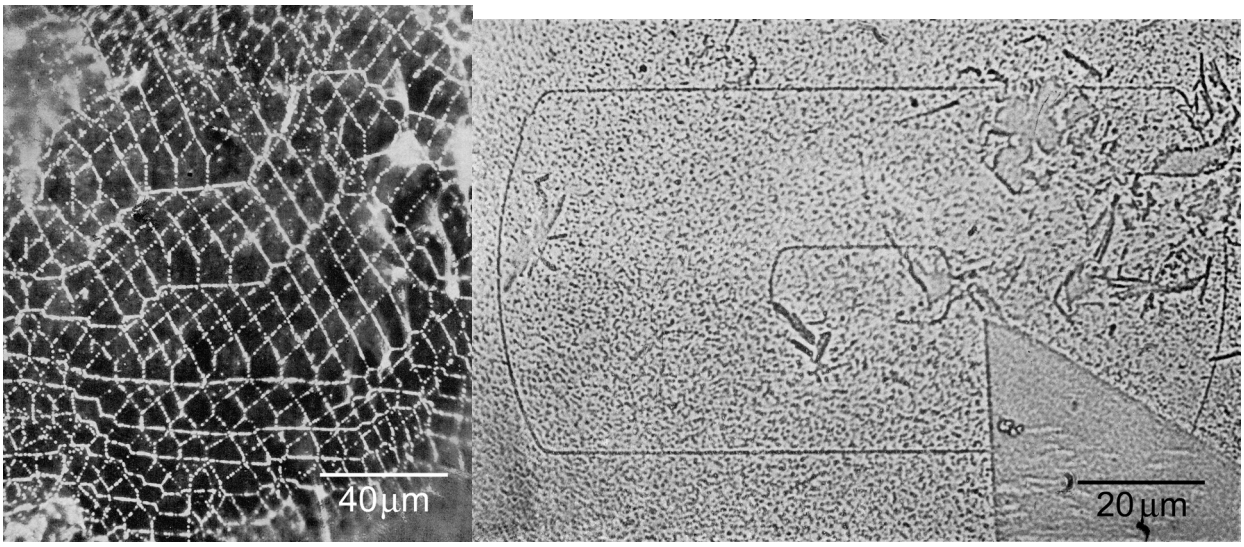

Fig. 1a Darkfield optical micrograph of an extensive dislocation network in halite revealed by the decoration of the dislocations with colloidal silver [16]. (b) Optical phase image of growth steps, one unit cell high (0.79 nm) on the prism surface of a beryl crystal. The inner step joins a pair of opposite-handed screw dislocations, which are imaged as dots. The c-axis is almost parallel to the straight edges [26].

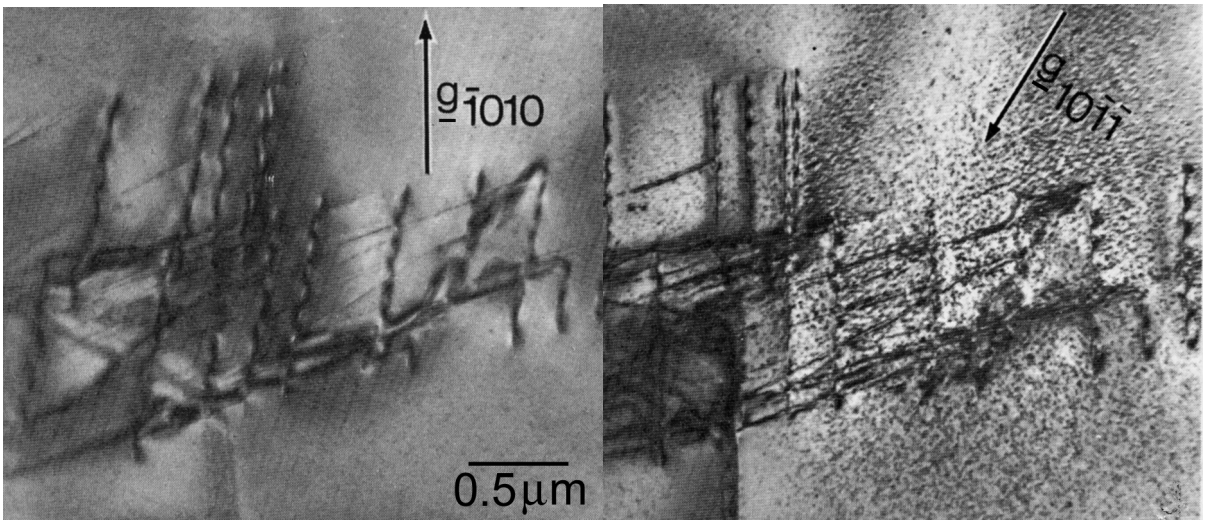

Fig. 2 Transmission electron micrographs of slip dislocations in quartz: (a)all in contrast, (b) some out of contrast (note spotty electron beam damage, typical of ("wet") quartz after irradiation) [48].

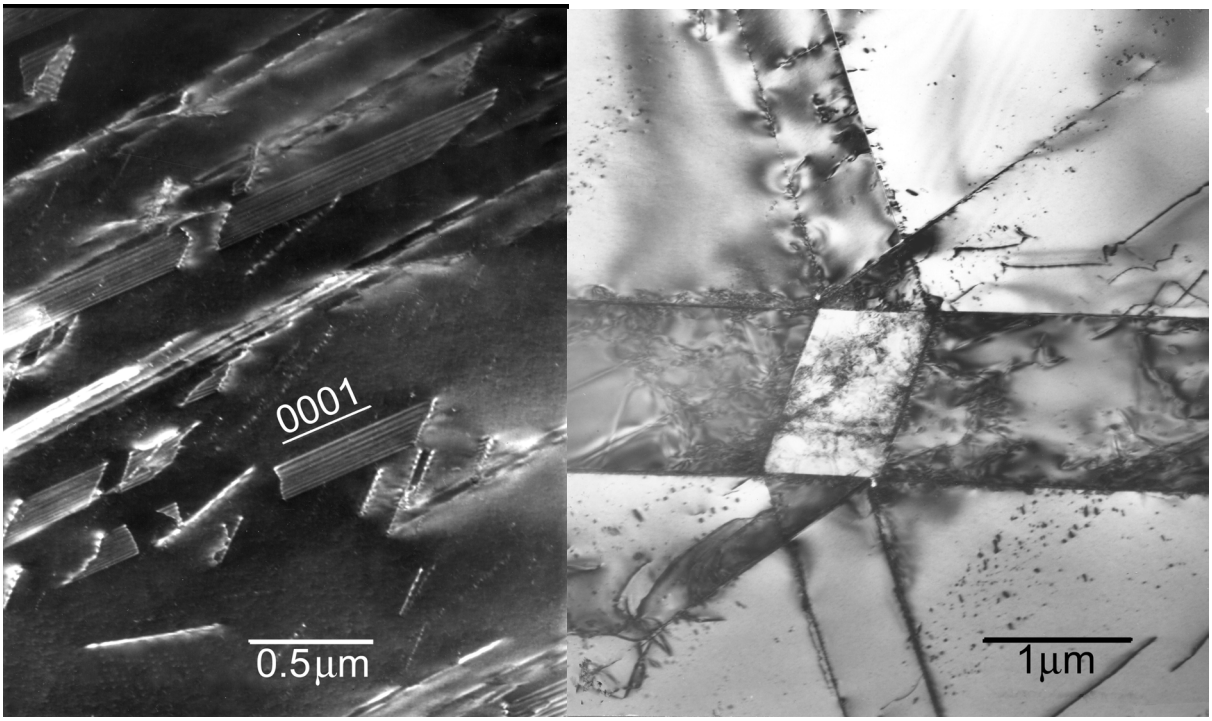

Fig. 3 Dislocations in carbonates: (a) Darkfield TEM image showing dislocations and stacking faults on the <2$\bar{1}\bar{1}$0> planes generated by basal slip in a dolomite single crystal deformed at 420°C [126]. (b) Dislocations associated with crossing mechanical twins in calcite (TEM, bright field) [115].

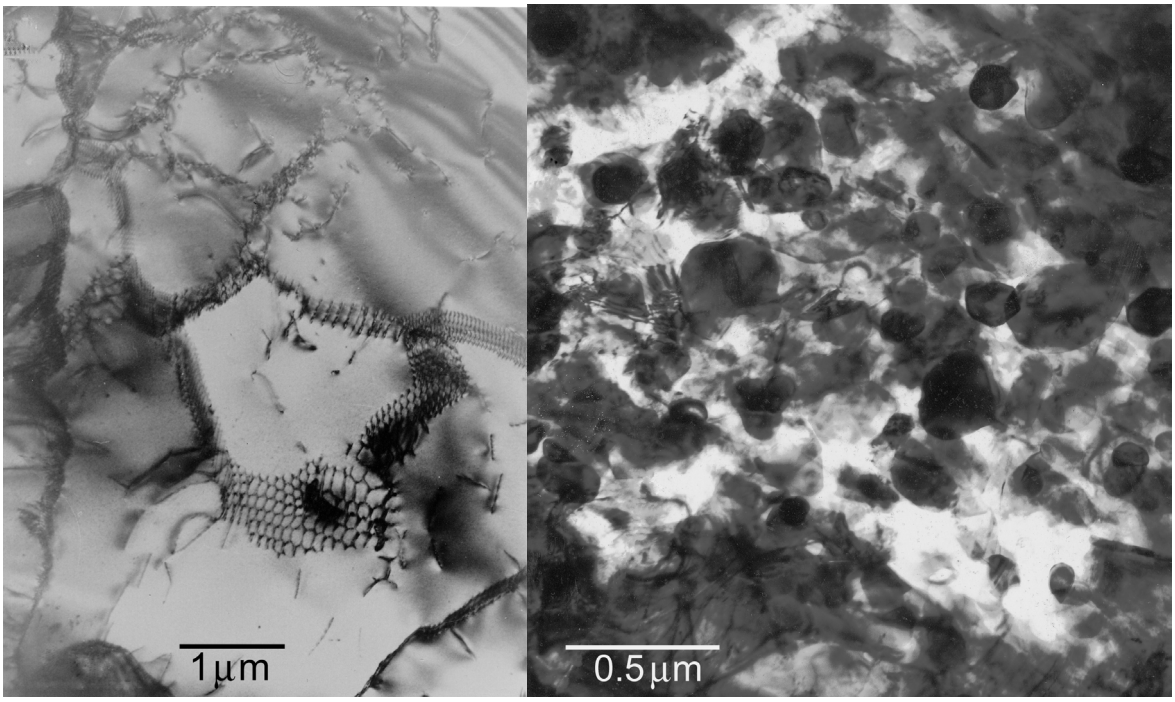

Fig. 4 Dislocations in naturally deformed quartz: (a) Micrograph showing sub-boundaries resulting from dislocation climb [109]. (b) Recrystallization with nucleation in regions of high dislocation density [58].

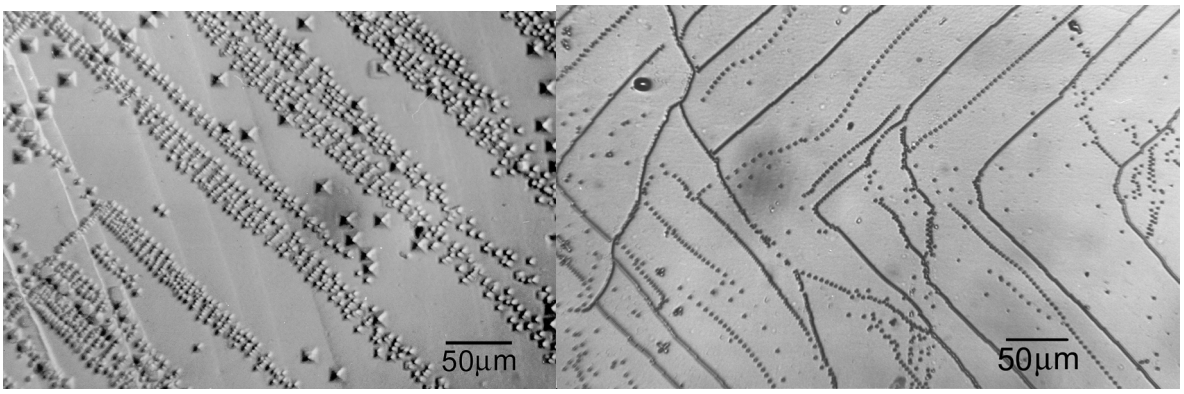

Fig. 5 Etch-pits marking the emergence sites of dislocations in halite: (a) Slip bands in a bent single crystal with glide-polygonization in the bands (i.e. alignment perpendicular to the slip direction). The crystal was etched before and after bending; the larger etch-pits define where grown-in dislocations emerged at the surface. (b) Mostly tilt sub-boundaries formed by the annealing of a bent single crystal. The apices of the "vees" are aligned along the neutral axis of the bar. (Barber, unpublished.)

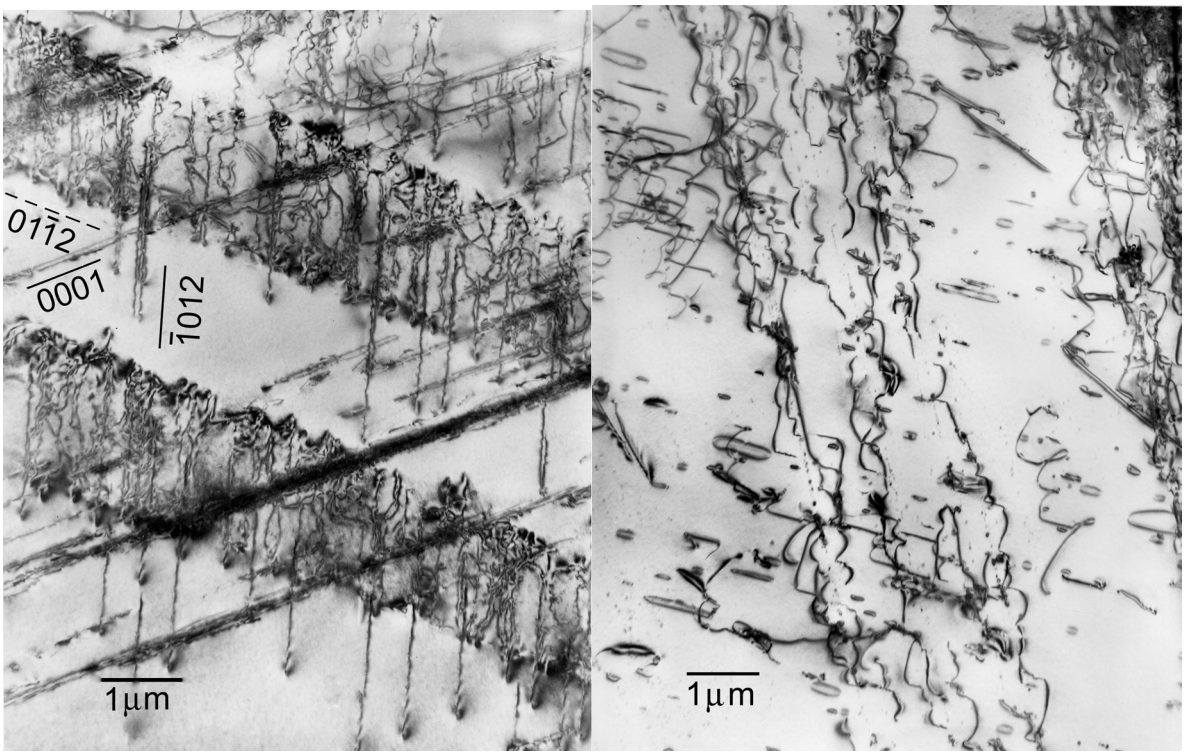

Fig. 6 TEM images of microstructures in experimentally deformed dolomite single crystals [126]: (a) At low temperature dislocations are concentrated in slip bands. (b) At higher temperature climb and dislocation interactions produce dislocation loops.

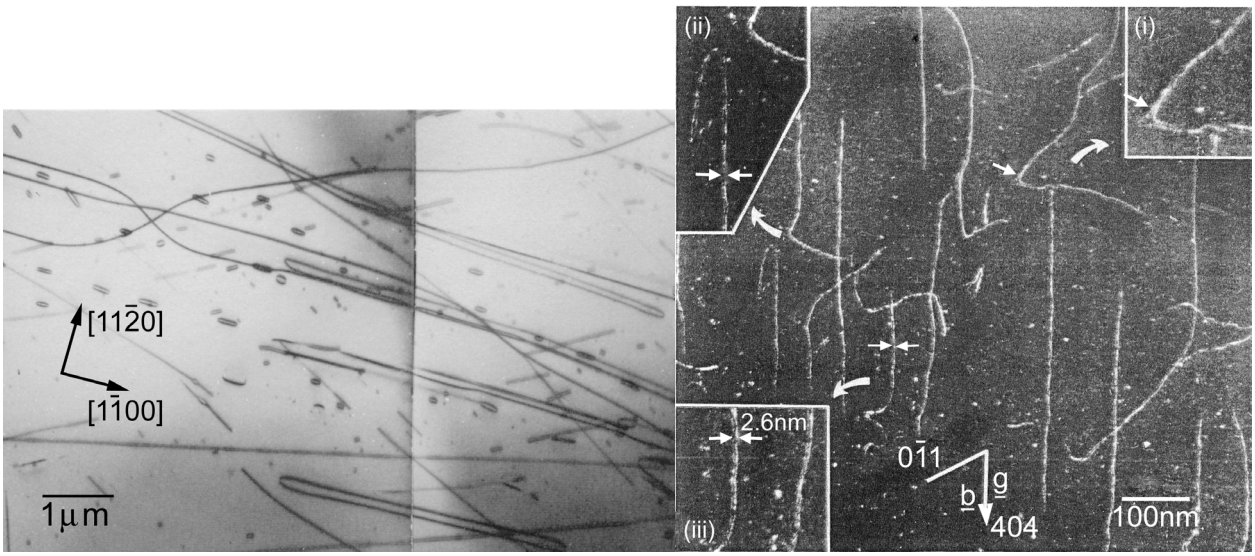

Fig. 7 Dislocation in oxides: (a) Bright fiied TEM image of dislocation microstructure consisting of long ⅓<11$\bar{2}$0> edge dipoles, multipoles and debris of numerous small loops formed at the early stage of work hardening in corundum (sapphire), compressed at 1400°C and deforming by basal slip; basal foil, **g** = 30$\bar{3}$0 [150]. (b) Weak beam dark field TEM image of a region in a spinel crystal deformed at 400°C and slipping on {111} planes. The field is dominated by cross-slip of the ½<101> screw dislocations (vertical) on (010). All the dislocations are dissociated out of the primary slip plane but their widths vary (all the inserts have the same magnification) [187].

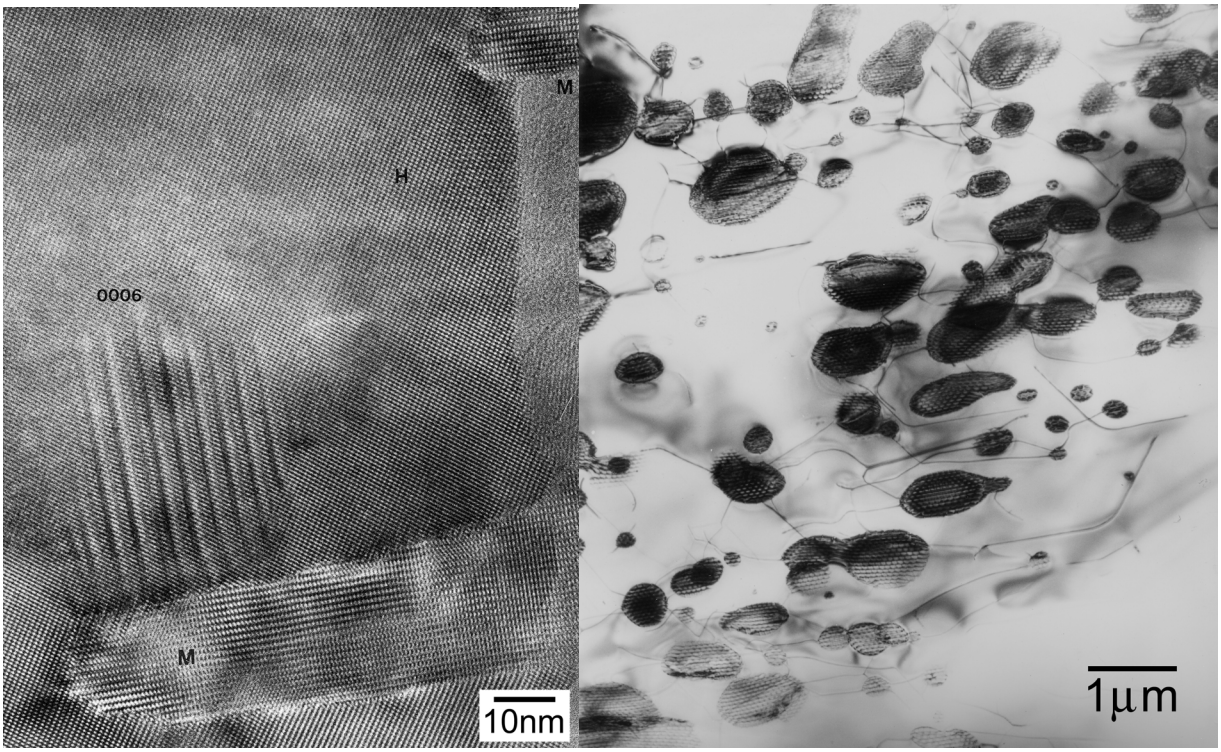

Fig. 8. TEM micrographs of dislocations in hematite intergrowths: (a). Magnetite-hematite intergrowth with zonal dislocation structures [164]. (b)Exsolution of ilmenite platelets in hematite. Ilmenite is decorated with a network of misfit dislocations to account for lattice strain caused by differences in lattice parameters [166].

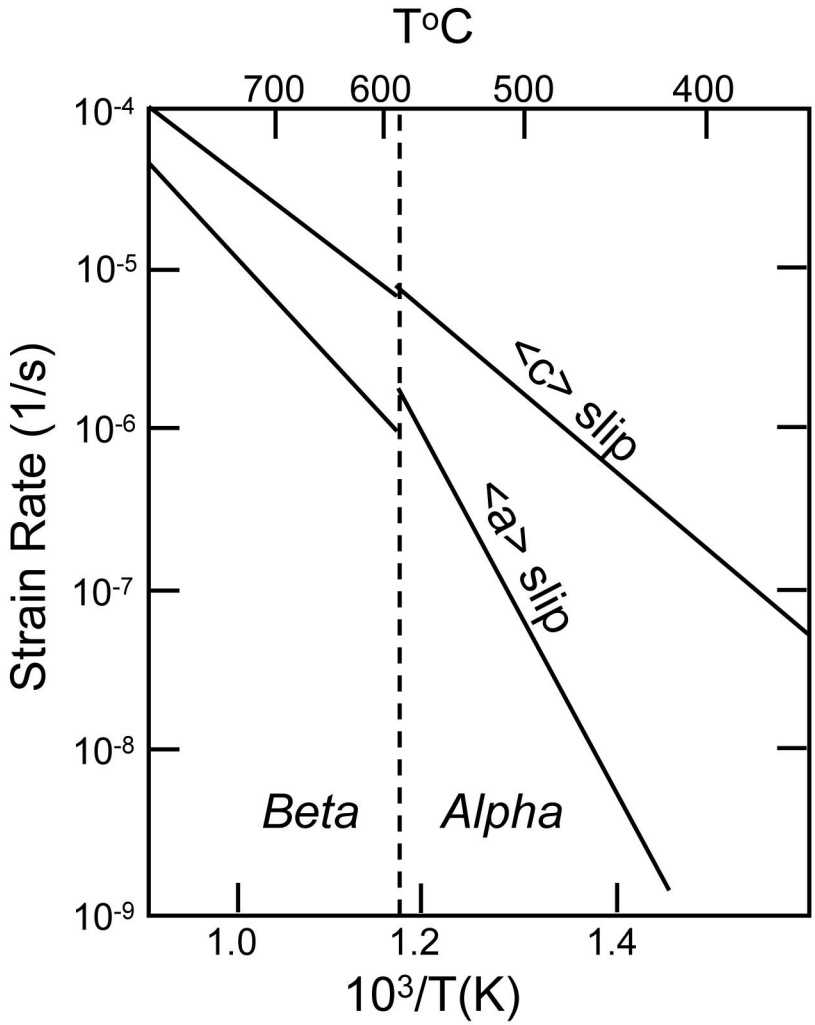

Fig. 9. Axial creep rates for wet synthetic quartz single crystals deformed in orientations to promote prism <c> slip and <a> slip [203].

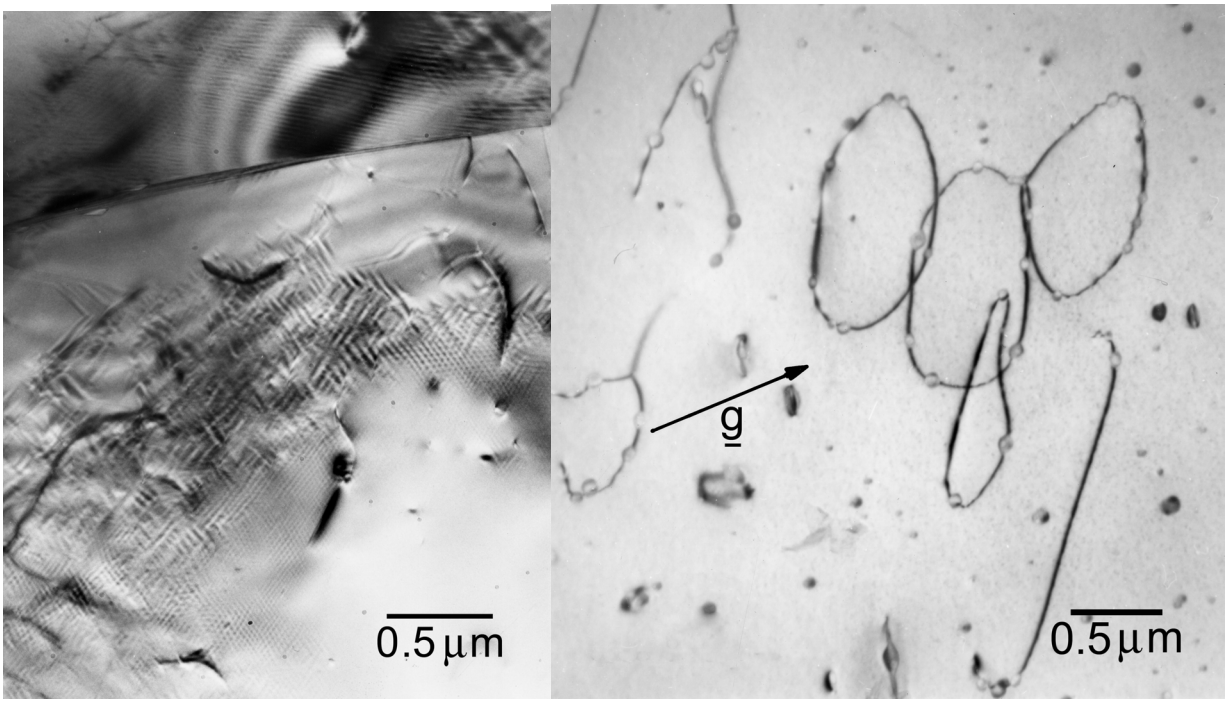

Fig. 10. TEM images of dislocation structures in quartz. (a) *In situ* heating experiment near the α-β phase transition with arrays of Dauphiné twins that are pinned by dislocations [215]. (b) Water bubbles in ("wet") quartz are associated with dislocations, especially loops [229].

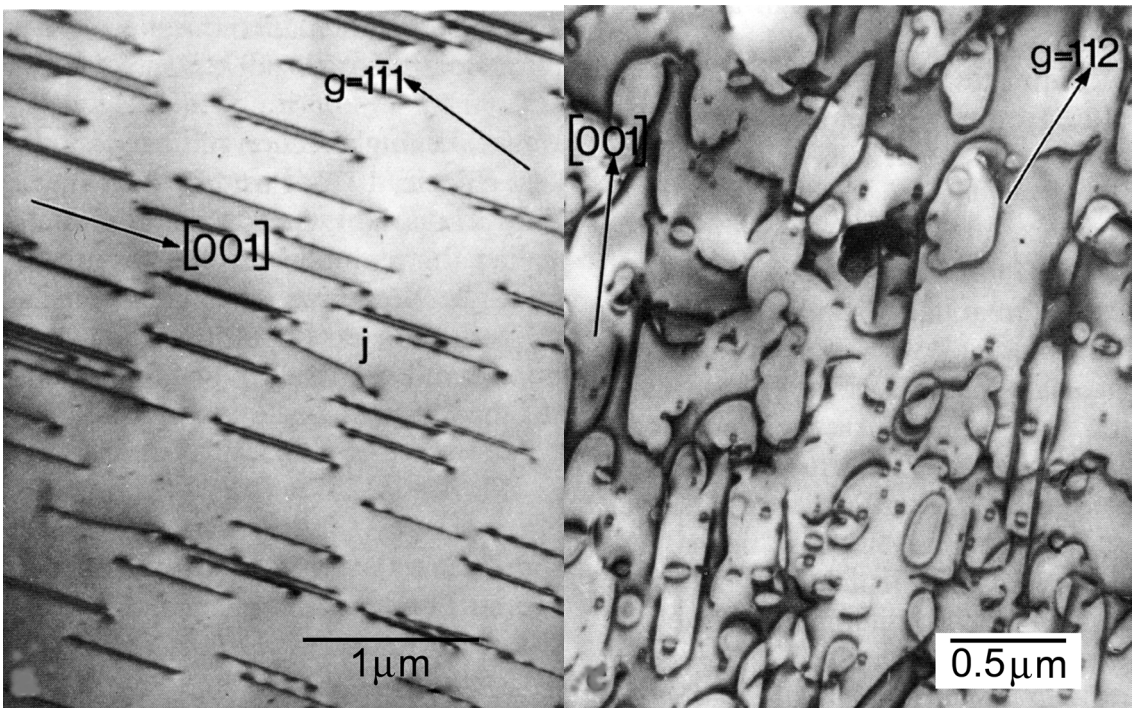

Fig. 11 Dislocation structures in experimentally deformed olivine. (a) Crystal deformed at 800C with [001] screws. (b) Dislocation loops in a crystal deformed at 100C. Also here b=[001] [72]

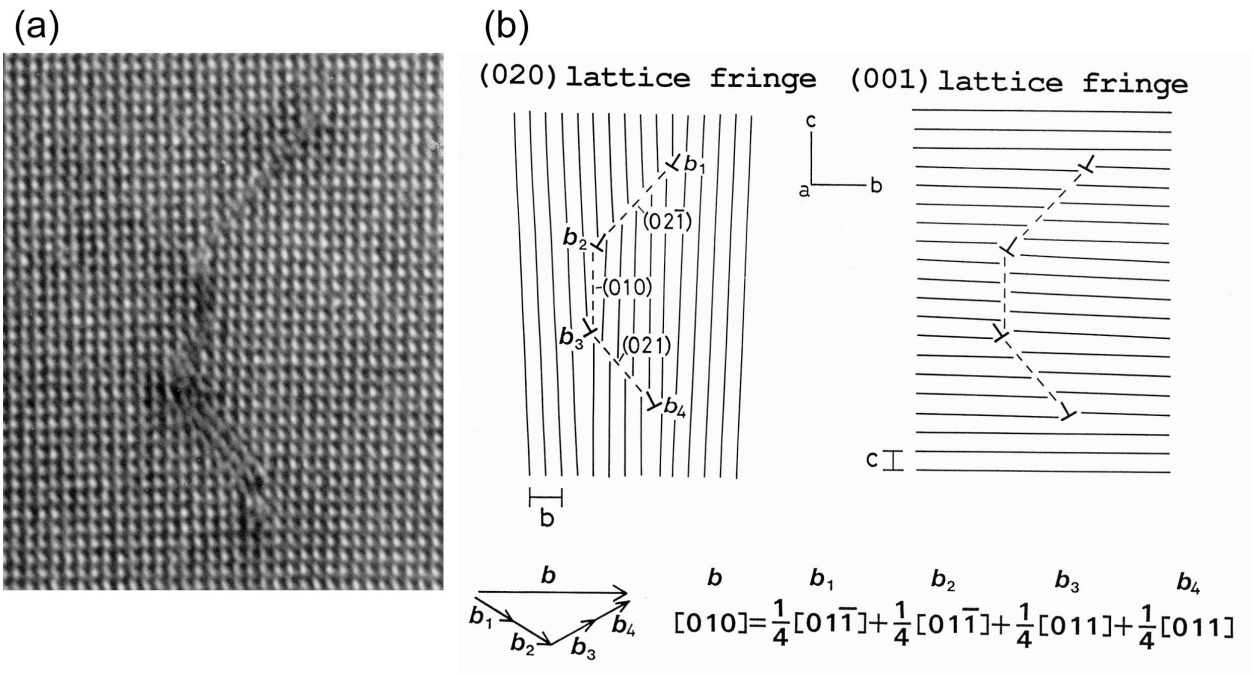

Fig. 12 HRTEM image of a dissociated dislocation with ***b*** = [010] in olivine grain from the Uenzaru peridotite in Japan [242]. The partial dislocations lie along [100]. Offsets in the lattice fringes are best viewed by observing the electron micrograph at an oblique angle. The schematic drawing illustrates (020) and (001) lattice. The stacking faults lie on the (010) and {021} planes. The dissociation reduces the elastic strain energy by a factor of ~3.

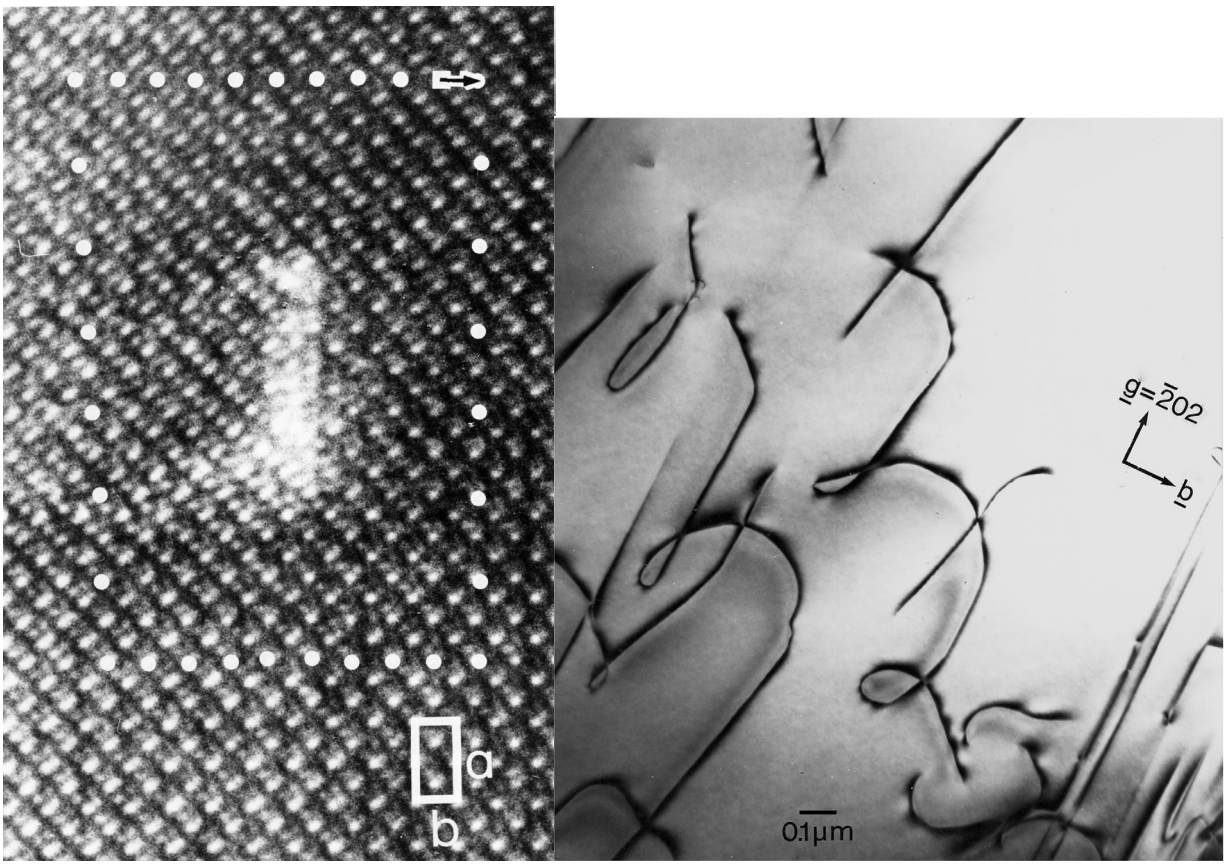

Fig. 13 (a) HRTEM image of a [010] edge dislocation in enstatite [275]. (b) TEM image of helix formation due to cross slip of [001] screw dislocations in hornblende [299].

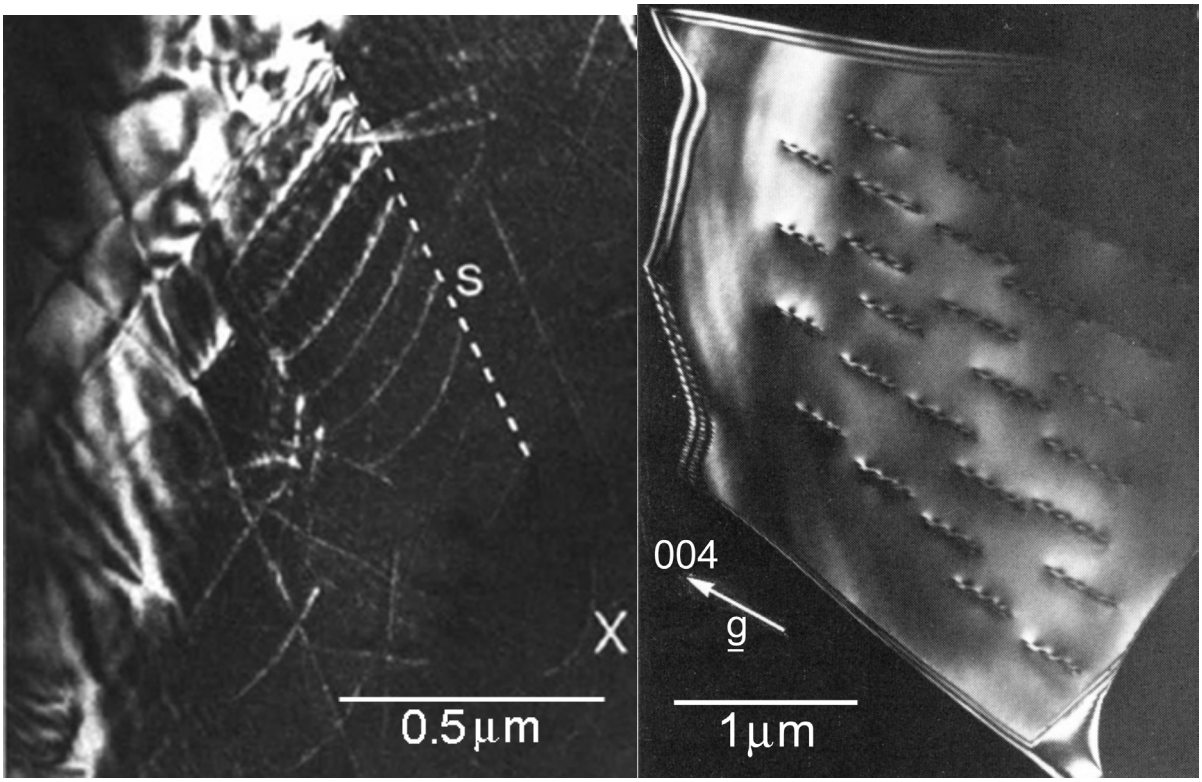

Fig. 14 (a) Weak beam darkfield image of dislocations in biotite. The trace of the slip plane (S) is indicated as well as dislocations bowing out (X). [307]. (b) Darkfield image of screw dislocations in sillimanite [311].

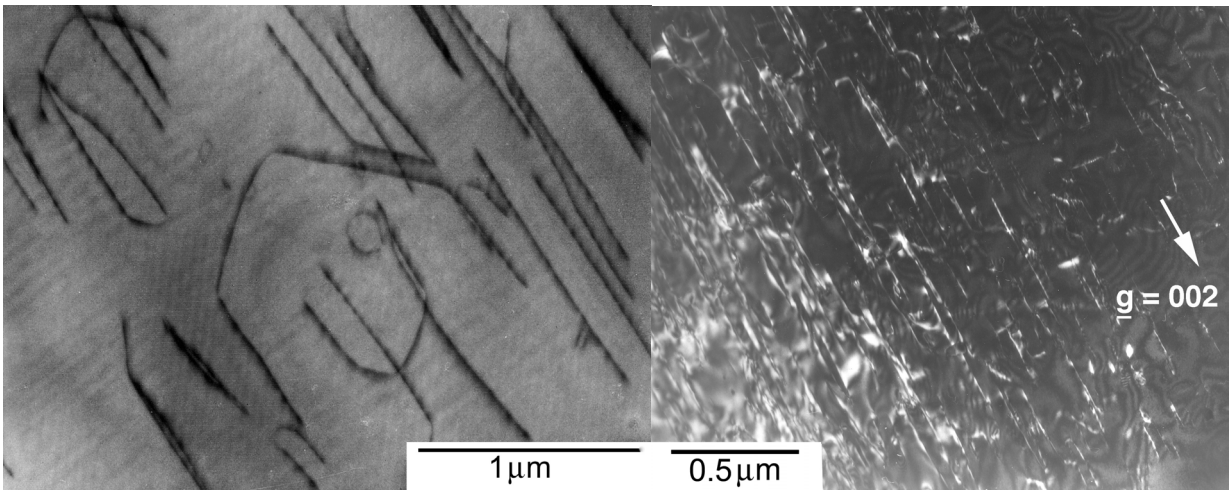

Fig. 15 (a) BF image of (010)[101] dislocations in experimentally deformed sanidine [318]. (b) Weak beam dark field images of dislocations in experimentally deformed plagioclase favourably oriented for (010)[001] slip; **b** = [001] dislocations exhibit long screw components [336].

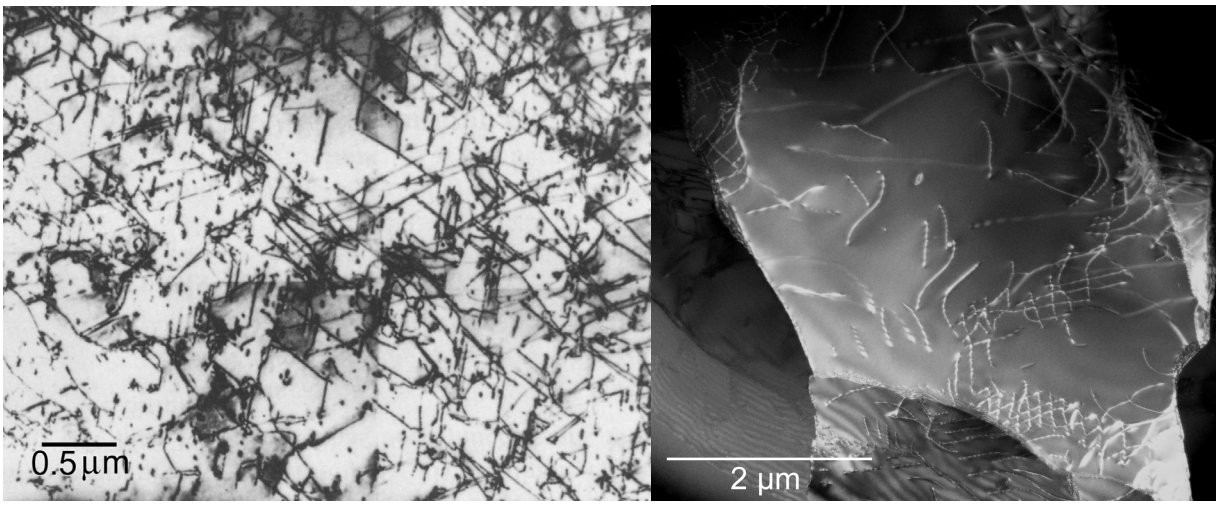

Fig. 16 (a) TEM image of dislocations in experimentally deformed chalcopyrite at 400ºC. Several screw dislocations are in contrast: b=1/2 [-1-1-1] in (11-2) planes (N 45ºW), b=1/2 [-1-11] in (112) planes (N 65ºE) and b=1/2 [1-10] (N 10ºE) [382]. (b) Weak-beam dark field TEM image of [100], [010] and [001] dislocations in stishovite deformed in a multianvil apparatus at 14GPa and 1300˚C [435].

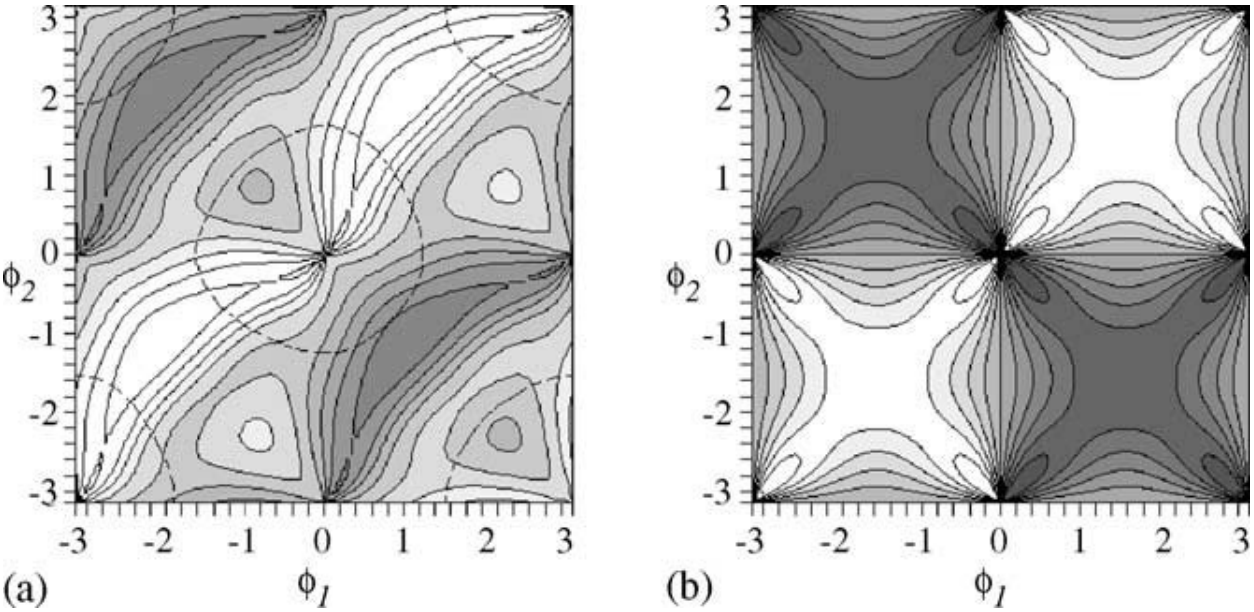

Fig. 17 Map of the interaction between dislocations in MgO as function of angles that define the orientation relative to the intersection of slip planes. Grey shades display interaction force (white attraction, black repulsion. (a) Lomer lock, (b) Hirth lock [442].

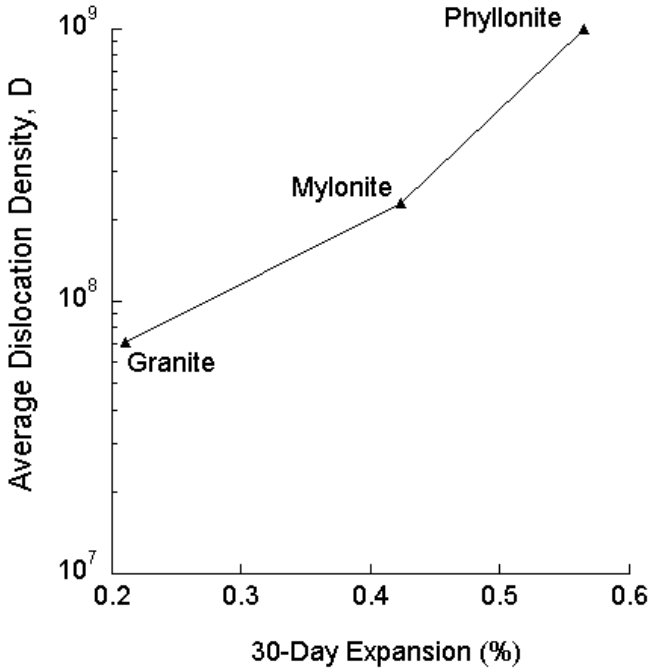

Fig. 18. Plot of the average 30-day expansion value of concrete samples with increasingly deformed granitic rock aggregate as function of average dislocation density in quartz [235].